

QATAR UNIVERSITY

COLLEGE OF ENGINEERING

DEVELOPMENT AND PERFORMANCE EVALUATION OF SMART
POLYMERIC COATINGS FOR CORROSION PROTECTION OF STEEL

BY

ADNAN KHAN

A Thesis Submitted to

the College of Engineering

in Partial Fulfillment of the Requirements for the Degree of

Masters of Science in Mechanical Engineering

January 2020

©2020. ADNAN KHAN. All Rights Reserved.

COMMITTEE PAGE

The members of the Committee approve the Thesis of ADNAN KHAN defended on
08/12/2019.

Dr. Anwarul Hasan
Thesis Supervisor

Dr. Abdul Shakoor
Thesis Co-Supervisor

Prof. Syed Javaid Zaidi
Committee Member

Dr. Bilal Mansoor
External Examiner

Prof. Faris Tarlochan
Examiner

Approved:

Khalid Kamal Naji, Dean, College of Engineering

ABSTRACT

Adnan Khan, Masters:

January: 2020, Masters of Science in Mechanical Engineering

Title: Development and Performance Evaluation of Smart Polymeric Coatings for Corrosion Protection

Supervisor of Thesis: Dr. MD Anwarul Hasan

Co Supervisor of Thesis: Dr. Abdul Shakoor

Most common cause of materials and equipment failure in the oil and gas industry is corrosion. According to one survey, about 1/4 to 1/3 of the total downtime in plants is due to deleterious effects of corrosion. It is, therefore, essential to prevent corrosion to ensure reliability of the assets. Usually, Protection of piping steel against corrosion is achieved by applying thick barrier coatings. These coatings provide decent barrier protection against ageing, mechanical scratches, erosion and other damages. Protection of damaged piping parts requires steel repair and re-coat which is an expensive process. To minimize the impact of damages and subsequent corrosion activity of the steel is essential to act promptly and efficiently, preferably in an autonomous way. Modern trends indicate that smart functional coatings, containing autonomous self-healing species are attractive for prolonged lifetime of materials. These coatings can heal damages at early stage, minimizing corrosion onset and corrosion propagation. Consequently, they are a promising solution for longer durability of coated piping steel and decreased operation expense. If properly designed, smart self-healing coatings also help to reduce the overall thickness of the

coating scheme as well as the investment cost. Altogether, this strategy contributes to economic saves, materials reliability and safety.

The current research work summarizes the synthesis and characterization of polymeric smart coatings developed by reinforcing urea formaldehyde microcapsules encapsulated with linalyl acetate and polyelectrolyte multilayered microcapsules (with two different corrosion inhibitors in the polyelectrolyte layers) into epoxy matrix. In situ polymerization technique was used for the synthesis of urea formaldehyde microcapsules encapsulated with linalyl acetate, whereas layer by layer technique was adopted to develop multilayered microcapsules containing alternative layers of Polyethyleneimine (PEI) and sulphonated polyether ether keytone (SPEEK). Dodecylamine (DOC) and phenylethiourea (PTU) were loaded as corrosion inhibitors in between polyelectrolyte layers of PEI and SPEEK. The prepared microcapsules (each 6.0 wt.%) were uniformly dispersed into the epoxy resin to develop single layer coatings (reinforced with urea formaldehyde microcapsules) and multilayered smart coatings (reinforced with multilayered microcapsules). The anticorrosive performance of the fabricated coatings was evaluated in 3.5 % NaCl solution at room temperature. Experimental results confirm that smart coatings with multilayered microcapsules demonstrate improved self-healing and anti-corrosion properties when compared to other type of coatings. This improvement can be attributed to efficient release of self-healing and corrosion inhibiting species (DOC and PTU) from the multilayered microcapsules. The tempting properties of multilayered coatings make them attractive for oil and gas industries.

DEDICATION

This thesis is dedicated to my beloved father Fazal Wahab and my mother Jano Wahab for their endless efforts, support, prayers and for being on my side in every hard time. They appreciated, supported and motivated me throughout the studies. I believe without them, it would not be possible to achieve this goal.

ACKNOWLEDGMENTS

I am really fortunate that I had kind supervision of Dr. Anwarul Hasan. His exemplary guidance and constant encouragement has been a great influence in my research work and course studies. A debt of gratitude to my co-supervisor Dr. Abdul Shakoor for supervising my research at Center for Advanced Materials Qatar University. His excellent guidance, regular monitoring and encouragement throughout the research made this journey possible. A special thanks to Dr. Zubair Ahmad for his support throughout the research, specifically in the understanding of electrochemical impedance spectroscopy.

Also, I would like to thank Miss Salma Habib and Miss Himyan Muhammad Akber, for helping me with characterizations whenever I needed assistance. I truly appreciate their support and guidance throughout my research.

Special thanks to Center of Advanced Materials (CAM) Qatar University, Gas Processing Center (GPC), Central Lab Unit (CLU), and Environmental Science Center (ESC) for giving me access to their world-class laboratories to conduct my research.

I would like to acknowledge the financial support of the Qatar National Research Fund (a member of Qatar Foundation) through the National Priorities Research Program NPRP9-080-2-039. Without their funding, this research would not have been possible.

I would like to express my very special thanks to the office of VP for research and graduate studies (VPRGS) for supporting my research work with the internal grant (QUCG-CAM-2018\2019-3).

Last but not the least I would extend my gratitude to all the members of Multifunctional Advanced Polymeric Coatings research group at CAM Qatar University.

TABLE OF CONTENTS

DEDICATION	v
ACKNOWLEDGMENTS	vi
LIST OF TABLES	x
LIST OF FIGURES	xi
ABBREVIATIONS	xiv
CHAPTER 1: INTRODUCTION	1
1.1 Background	1
1.2 Microencapsulation	3
1.3 Urea formaldehyde microcapsules	6
1.4 Goal and objectives	8
CHAPTER 2: MATERIALS AND METHODS	10
2.1 Materials	10
2.2 Synthesis of UF microcapsules	10
2.2.1 Pre-polymer preparation	11
2.2.2 Encapsulation process	12
2.3 Synthesis of multi-layered UF microcapsules	13
2.4 Epoxy coating preparation	16
2.5 Characterization of microcapsules and coatings	18
2.5.1 Fourier-transform infrared spectroscopy (FTIR)	18

2.5.2	Zeta Potential particle size analyzer	18
2.5.3	X-ray photoelectron spectroscopy (XPS)	19
	XPS (AXIX Ultra DLD, Kratos, UK) using a monochromatic X-Ray Source - Al K α source was used to further confirm the adsorption of the polyelectrolyte layers of the surface of MLMCs and to detail its chemical composition. The binding energy of C 1s (284.6 eV) was used as reference. The energy resolution was 160 eV and the spatial resolution was 20 eV.	19
2.5.4	Scanning electron microscopy (SEM) and transmission electron microscope (TEM).....	19
2.5.5	X-Ray Diffraction Analysis	20
2.5.6	Thermo gravimetric Analyzer (TGA)	20
2.5.7	UV spectroscopic analysis (UV).....	21
2.5.8	Electrochemical Impedance spectroscopy (EIS)	21
CHAPTER 3: RESULTS AND DISCUSSION.....		23
3.1	FTIR analysis of microcapsules and coatings	23
3.2	Zeta potential measurements of microcapsules.....	27
3.3	XPS analysis.....	30
3.4	FE-SEM/HR-TEM analysis of the encapsulated and multilayered microcapsules	34
3.5	Particle size and XRD analysis of the microcapsules	40
3.6	Thermal stability of the microcapsules and epoxy coatings	43

3.7	Measurement of self- releasing of DOC and PTU from MLUFMCs and PMCs in response to pH change	46
3.8	Self-healing of smart coatings.....	48
3.9	Electrochemical Impedance Spectroscopic (EIS) of DOC samples.....	51
3.10	Electrochemical Impedance Spectroscopic (EIS) of PTU samples	56
CHAPTER 4: CONCLUSIONS AND FUTURE RECOMMENDATIONS		63
4.1	Conclusion.....	63
4.2	Future Recommendations.....	64
REFERENCES		65
APPENDICES		70
APPENDIX A: Poster presentation.....		70
APPENDIX B: Journal article 1.....		71
APPENDIX C: Journal article 2.....		87

LIST OF TABLES

Table 1: The elemental analysis of MLMCs and PMCs.....	33
Table 2: Electrochemical parameters obtained by fitting the measured impedance data shown in Figure 12 of the scratched coated specimens immersed in 3.5 wt.% NaCl solution.....	55
Table 3: Electrochemical Impedance Parameters for different coatings in 3.5% NaCl	59
Table 4: Comparison of the present coatings with the previous results in terms of corrosion impedance values.....	61

LIST OF FIGURES

Figure 1: Schematic diagram, representing the structure of the microcapsules	3
Figure 2: Flow diagram of a typical interfacial polymerization encapsulation technique	6
Figure 3: Schematic diagram for the synthesis of encapsulated UF microcapsules and reaction of urea and formaldehyde to form linear UF chain.....	12
Figure 4: Schematic showing the encapsulation process of the UF microcapsules.....	13
Figure 5: Schematic representation of the structure of as synthesized layered microcapsules with dodecylamine	15
Figure 6: (a) schematic representation of the synthesis of multilayered microcapsules with phenylthiourea (b) profile of multilayers.....	15
Figure 7: Schematic diagrams of smart coatings (a) modified with UFGCs referred to as SLSCs (b) modified with polyelectrolyte multilayered capsules referred as (PMLSCs).	17
Figure 8: Protective mechanism of the self-healing coatings; (a) plain coating (b) layered coating	17
Figure 9: FTIR spectra of the microcapsules and coatings (a, b) as synthesized UFGCs encapsulated with linalyl acetate and pure linalyl acetate (c, d) MLUFGCs and pure dodecylamine (e, f) PMLSCs and SLSCs.....	25
Figure 10: FTIR spectra of the (a) linalyl acetate (b) MLMCs loaded with linalyl acetate (c) and PMCs	27
Figure 11: Zeta potential measurements of microcapsules. Layer number 0: microcapsules encapsulated with linalyl acetate (UFGCs) and layers 1-5, MLUFGCs having various polyelectrolyte layers.	29

Figure 12: Zeta potential value of the microcapsules. Layer 0: as synthesized MLMCs and layer 1-5, the different layers of the PMCs.	30
Figure 13: XPS survey spectra of UFMCs and MLUFMCs samples. Insets show the high resolution XPS spectra C 1s of the both UFMCs (a) and MLUFMCs (b) samples.	32
Figure 14: XPS survey spectra of MLMCs and PMCs samples: (a, b) C1s, (c, d) N1s, (e, f) O1s	34
Figure 15: FE-SEM analysis of microcapsules and smart coatings (a) UFMCs (b) MLUFMCs, (c) SLSCs, (d) PMLSCs and (e, f) HR-TEM of MLUFMCs.....	37
Figure 16: The structural and morphological study of the synthesized microcapsules (a, b) SEM of the UF microcapsules (b, c) the SEM of the multilayered microcapsules (d, e) TEM of the multilayered microcapsules. (f, g, h, i) elemental mapping of MLMCs.....	40
Figure 17: Particle size analysis of as synthesized urea-formaldehyde microcapsules-UFMCs and multi-layered urea-formaldehyde microcapsules-MLUFMCs. Inset shows the XRD of the UFMCs and MLUFMCs.	42
Figure 18: Particle size analysis of MLMCs and PMCs.....	43
Figure 19: Thermal stability of (a) microcapsules-UFMCs, MLUFMCs and (b) developed smart coatings-SLSCs and PMLSCs.	45
Figure 20: Thermal stability analysis (TGA) of (a) MLMCs [27] and PMCs (b) the plain and layered coatings.....	46
Figure 21: UV-vis spectra of the MLUFMCs immersed in 0.1 M NaCl solutions having various pH values after (a) 24 h (b) 48 h and (c) 72 h.	47
Figure 22: UV spectroscopy of polyelectrolyte multilayered microcapsules after (a) 24	

h (b) 48 h (c) 72 h of the immersion in 0.1 M NaCl solution with different pH values.	48
Figure 23: SEM images of the scratched samples (a, b, c) SLSCs after 24, 48 and 72 h. and (d, e, f) PMLSCs after 24, 42 and 72 h.	50
Figure 24: SEM images of the scratched samples (a, b, c) MLMCs and (d, e, f) PMCs after different time intervals.....	51
Figure 25: (a, c and e) Bode and (b, d and f) the corresponding phase angle plots for the scratched coated specimens with PECs (epoxy resin only), SLSCs (epoxy loaded with 5 wt% of the UFMCs) and PMLSCs (epoxy loaded with 5 wt% of the MLUFMCs) after immersion in.....	54
Figure 26: Electrochemical equivalent electric circuit obtained from fitting the impedance data.....	55
Figure 27: Electrochemical equivalent circuit used to fit the impedance data.	56
Figure 28: Nyquist plots for the measured EIS data (symbols) and their fittings (solid lines) using the EC shown in Figure 27 for different epoxy resin exposed in 3.5% NaCl solution for different exposure time a) neat coating, b) plain coating, and c) layered coatings	57
Figure 29: Bode plots for the measured EIS data (symbols) and their fittings (solid lines) using the EC shown in Figure 2 for for different epoxy resin exposed in 3.5% NaCl solution for different exposure time (a, b) pure epoxy resin, (c, d) single layer, and (e, f) multi-layer	60

ABBREVIATIONS

UFMCs	Urea formaldehyde microcapsules
MLUFMCs	Multilayered urea formaldehyde microcapsules
PECs	Pure epoxy coatings
SLSCs	Single layered smart coatings
PMLSCs	Polyelectrolyte multilayered smart coatings
MLMCs	Monolayer microcapsules
PMCs	Polyelectrolyte multilayered microcapsules
SPEEK	Sulfonated polyether ether ketone
PEI	Polyethylenimine
EMA	Ethylene maleic anhydride
DOC	Dodecylamine
PTU	Phenylthiourea
FTIR	Fourier-transform infrared spectroscopy
XPS	X-ray photoelectron spectroscopy
SEM	Scanning electron microscope
EDX	Energy-dispersive X-ray spectroscopy
XRD	X-ray diffraction
TGA	Thermogravimetric analysis
UV	Ultraviolet
EIS	Electrochemical Impedance Spectroscopic
ECs	Equivalent circuits

CHAPTER 1: INTRODUCTION

1.1 Background

In this widely prevailing world, corrosion is considered as the most critical cause of materials failure[1]. This damaging process is mostly accompanied with wear phenomenon[2], [3]. The combined effects of corrosion and wear are immeasurably huge specially when exposed to harsh environment[4]. The global problem of corrosion is very challenging and bothering the humankind since many centuries. In oil and gas, industries about 70% of materials maintenance is caused by corrosion, moreover operational and maintenance (O&M) costs reach to 50-55% out of which 80% are due to corrosion[5], [6]. It is obvious that the engagement of correct anti-corrosion methods can save lot of maintenance cost. In all cases of corrosion, only the surface of a material is directly suffered. Different types of coatings are claimed to be the best solution to safeguard-pipeline surfaces against wear and corrosion. However, defects formed in the coatings such as pores, pinholes, micro scratches and other damages may destroy the protective barrier, exposing the bare metal to the aggressive media. The continuous supply of aggressive species in the presence of oxygen and moisture promotes corrosion. Therefore, it is of utmost relevance to find strategies to repair the damaged areas and to delay the corrosion-induced damages.

In this sense, smart polymeric coatings modified with active agents, either freely dispersed or stored in micro or nano carriers that can impart self-healing ability have been considered attractive options to minimize corrosion damages[7][8]. Moreover,

the use of carriers, sensitive to different stimulus, has to avoid unwanted interactions between the healing species and the host organic matrices. Polymeric coatings modified with carriers where different species can be stored results in a composite coating that works as a smart protective system. Recent literature is fertile in different solutions. For example, polymeric coatings have been modified with capsules loaded with self-healing agents like linseed oil[9], tung oil[10], dicylopetadiene, epoxy monomer, vegetable oil and silanes. These species once released from the smart containers/capsules, where they have been stored, can repair the damaged areas in the coating, hindering the access of aggressive species. In this case, the encapsulation strategy foresees the repair of the polymeric matrices. However, when the damages reach the bare metal, corrosion onset can be very fast and it is relevant to have corrosion inhibitors that heal the corroding areas as well. Therefore, different corrosion inhibitors such as dodecylamine[11], benzotriazole[12], methylthiourea and imidazole[13] have been loaded in different carriers and added into polymeric coatings to confer corrosion healing ability. Different containers, sensitive to different stimulus, like mechanical damage, pH, light, electrochemical potential and others, have been proposed to carry the corrosion inhibitors as reviewed[14]–[17]. Urea formaldehyde microcapsules have been widely used as containers for the storage of active species in polymeric matrices because their shell can be functionalized and made compatible with different host coatings. Furthermore, these materials present high thermal stability and are robust enough to survive the different stages of coating formulation and application. Though, a major limitation is that these are typically used to store only individual healing species, but simultaneous healing of the coating

and inhibition of active metal areas requires the combination of distinct microcapsules or the loading of a certain type microcapsule with different species.

1.2 Microencapsulation

Microencapsulation technique has been widely studied and applied in many areas and applications such as pharmaceutical industries, perfumery and coating as well. One of the most used methods is the microencapsulation which is to impregnate active chemical specie inside the microcapsules, which can be slowly released in a process known as controlled released process. Microencapsulation is a process of coating particles or materials in capsules ranging in size from micrometer to millimeter known as microcapsules, in order to control the releasing character of the core materials.

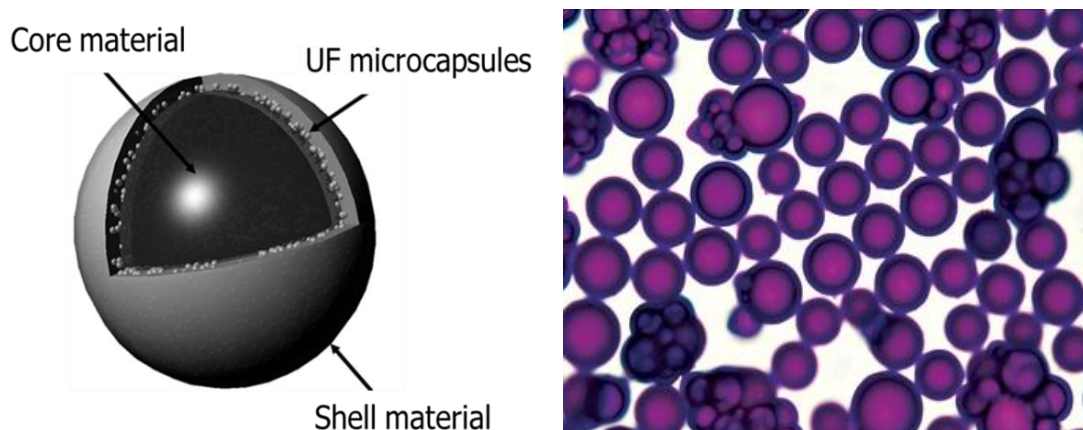


Figure 1: Schematic diagram, representing the structure of the microcapsules

The microencapsulation technique rely on the physical and chemical properties of the core material been used and the process of impregnating the active agents/chemical species in the microcapsules. The preparation methods can be divided into three different categories; 1) Physical process, 2) Physic-chemical process and 3) Chemical process[18]–[20] The Physical preparation process can be further sub divided into six different processing (pan coating, air-suspension coating, centrifugal extrusion, vibrational nozzle, spray drying and solvent evaporation). Further, the Physic-chemical process can also be divided into ionic gelation, coacervation and sol-gel, and interfacial polymerization, suspension polymerization and emulsion polymerization[21]–[23] are the three sub categories of the chemical processes. The two famous methods in the physical process are the pan coating and the air-suspension coating. In all the physical processing techniques, the microcapsule wall is usually applied mechanically around the core materials. The pan coating process is widely used in the pharmaceutical industries for tablets manufacturing. The solid material is mixed with the dry coating substances while the temperature is maintained near the melting point of the coating material. In other alternative methods the coating can be sprayed on the core materials directly, which can save a lot of time and energy[24], [25]. In this technique the temperature must be kept higher than the melting temperature of the shell material.

The air-suspension coating technique has more control and flexibility than other techniques by changing the passing time of the core material[26]. The significant part of this technique is that the core material particles are been coated and dried while been suspended in an upward moving air stream. This technique was developed for

pharmaceutical, food and cosmetics industries[27]–[29]. Other physical preparation techniques are centrifugal extrusion, vibrational nozzle, spray drying and solvent evaporation.

The second preparation technique is the physic-chemical method; consist of ionic gelation, coacervation and sol-gel. In this method stable solid particles are formed and ionic gelation process is heavily used in the drug delivery system. The process depends on the polyelectrolytes that aid in cross linking of the multi-valent counterions such as Al^{3+} , Ca^{2+} and other to form the hydrogels, which can lead to the ionic gelation of the element itself such as calcium alginate (CaAlg) microcapsules[30], [31]. Other techniques are coacervation and sol-gel.

The third microcapsules preparation technique is the chemical method which can be sub divided into suspension polymerization, emulsion polymerization and interfacial polymerization, which are the most common methods of microcapsules preparation[32], [33]. The chemical suspension polymerization techniques are characterized by the suspension of water particles (immiscible mixture) to form droplets in its aqueous phase. As for the emulsion polymerization process, the initiator consists of soluble material in its aqueous phase[34], where the monomer is emulsified with the aid of surfactant in the polymerization process[35]. In the interfacial polymerization technique a rapid polymerization of hydrophilic and lipophilic monomers occurs, which are the two interfaces of an oil-in-water emulsion. The interfacial polymerization technique is used in this study to synthesize microcapsules, illustrated in Fig. 2.

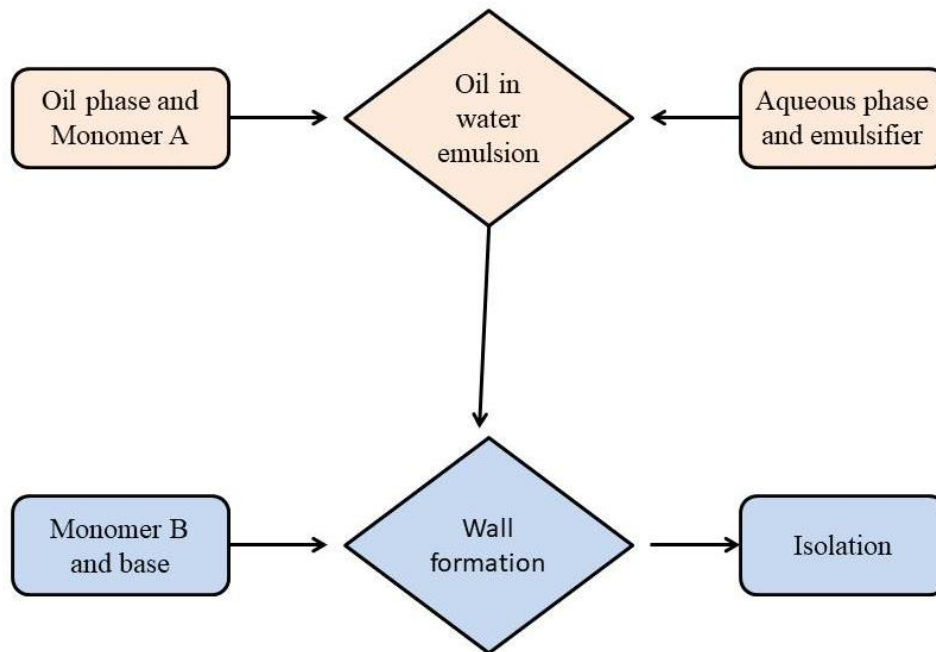


Figure 2: Flow diagram of a typical interfacial polymerization encapsulation technique

1.3 Urea formaldehyde microcapsules

Urea formaldehyde (UF) microcapsules are the most popular microcapsules reinforced in organic coatings for corrosion protection. In urea formaldehyde microcapsules the shell material consists of a linear chain of the urea and formaldehyde[36]. The synthesis and design of UF microcapsule is the major essential step to design an efficient self-healing system. UF microcapsules impregnated with self-healing agents should possess acceptable size, strength and proper bonding type in order to be able to host the core materials. Moreover, the release behavior of the capsules mainly depends on the materials that form the microcapsules shell. The chemical (interfacial polymerization) microencapsulation

procedure, is crucial to acquire the proper type of the microcapsules with suitable features, that can perform their main purpose. Thus, the appropriate choice of the experimental conditions is critical in the synthesis of the microcapsules.

The UF capsules synthesized using interfacial polymerization consist of two parts; the primary step is the emulsion which take place in an aqueous environment, where the urea and formaldehyde reaction take place in water to form low molecular weight compound known as pre-polymer, that have the ability to grow in size with time on the core material. The polymerization mechanism of UF can occur in both acidic and basic median. The other preparation techniques used for the synthesis of the UF microcapsules is one step method that takes place in acidic environment developed by brown. The microcapsules synthesized by this method are more effectively applied as shell material in order to prepare the epoxy loaded microcapsules. Most of the researches done in this field are targeting the UF microcapsules that can be used with epoxy resins for coating.

The epoxy resin is an important material that is usually used as a core material or coating matrix for UF microcapsules, due to the wide variety and compatibility with many curing agent which are compatible with epoxy at different temperatures, that stabilize the thermal decomposition of the epoxy resin and guarantee the miscibility of the healing agent and the epoxy.

1.4 Goal and objectives

The use of smart self-healing composite coatings has been proven to be a promising choice to address the challenges associated with corrosion and wear of steel components, particularly in Oil & Gas industry. It is quite convincing and carries significant novelty that polyelectrolyte multilayered microcapsules smart containers are reinforced into the polymeric matrix to develop high quality smart self-healing composite coatings to mitigate corrosion in the oil and gas industry. The proposed polymeric coatings are expected to deliver superior attributes including: (i) enhanced lifetime (ii) reduced thickness of coatings (iii) enhanced performance towards corrosion protection. The core goals and objectives of the project are presented below:

- Synthesis and characterization of multilayer microcapsules.
- Selection of suitable polyelectrolyte multi-layered polymeric materials.
- Selection of appropriate self-healing agents and corrosion inhibitors.
- Study of self-release of inhibitors from loaded microcapsules.
- Development of smart polymeric coatings.
- Study of structural, thermal, self-healing and anti-corrosive properties.
- Study of self-healing mechanism in developed smart coatings.
- Field exposure testing of developed smart coatings in real environment to check their performance.

- Study of property relationship between coating composition and self-healing capabilities.

In the present study, the concept of multilayered hybrid urea formaldehyde microcapsules has been introduced as a novel strategy to bring different healing functionalities into a single container reinforced into the epoxy matrix to develop novel smart self-healing polymeric coatings[37]–[39]. Linalyl acetate as a self-healing agent and phenylthiourea and dodecylamine as a corrosion inhibitor respectively have been encapsulated into the polyelectrolyte multilayers to form multilayered microcapsules. The so developed multilayered microcapsules are reinforced into a polymeric (epoxy) matrix to form smart self-healing coatings. Furthermore the corrosion inhibition efficiency of both the inhibitors has been evaluated. These novel coatings are expected to play a vital role to mitigate corrosion in the oil and gas industry. To the best of our knowledge, combination of proposed self-healing agent (linalyl acetate) and inhibitor (phenylthiourea and dodecylamine) in the polyelectrolyte multilayered microcapsules have not been reported so far.

CHAPTER 2: MATERIALS AND METHODS

2.1 Materials

Urea, ammonium chloride, resorcinol, hydrochloric acid, sodium hydroxide, formaldehyde (37 wt%) , ethylenemaleic anhydride copolymer (EMA) and ethanol were used to synthesize UF microcapsules (purchased from sigma-Aldrich). And, Sulfonated polyether ether ketone (SPEEK) and polyethylenimine (PEI) (purchased from BDH Chemicals Ltd) were used as polyelectrolyte layers on the surface of UF microcapsules. In order to compare corrosion inhibition for carbon steel in epoxy matrix, we used Dodecylamine and Phenylthiourea as corrosion inhibitors in this study. Linalyl acetate used as self-healing specie, Epofix resin along with diethylenetriamine employed as hardener for the resin and sodium chloride to provide the corrosive environment to the epoxy coating was also purchase from BDH Chemicals Ltd. Cleaned and polished carbon steel samples were used as substrates from the epoxy coatings. The samples were ground with the help of sand papers to improve the adhesion of the epoxy with the steel surface and reduce the delamination property.

2.2 Synthesis of UF microcapsules

In situ polymerization technique was used to synthesize urea-formaldehyde (UF) microcapsules. The preparation method of UF microcapsules consists of mainly two experimental phases; the pre-polymerization and the encapsulation process. In the

first phase, pre-polymerization step the urea and formaldehyde polymerize in an acidic medium to form a linear and discontinuous chain of urea-formaldehyde. In the second phase of microencapsulation; oil based self-healing specie is used to introduce to the urea-formaldehyde acidic solution. The high stirring speed of the impellers in the in situ polymerization cut the self-healing agents into small droplets (depending on the speed of the impeller). The uniform heating rate (55C°) and stirring of the solution make a continuous thin UF layer around each droplet. As the reaction proceeds, it results in the thick walled UF microcapsules with the encapsulated self-healing specie. The thickness of the wall of microcapsules mostly depends on the time of the reaction. The details of both the experimental phases are given below.

2.2.1 Pre-polymer preparation

In situ polymerization (oil-in-water) the microcapsule is prepared at a temperature of 55 °C. 50ml of aqueous solution containing 2.5wt% of ethylene maleic anhydride (EMA) and 100ml of deionized water were mixed in a beaker with the help of mechanical stirrer. The beaker was placed in a controlled temperature (55 °C) water bath under slow stirring. The solution mixture was agitated at slow speed (300 rpm) with a mechanical digital mixer that has three blades propeller.

Under the influence of agitation 5g of urea, 0.5g of resorcinol and 0.5g of ammonium chloride were added in the beaker to dissolve in the solution. The pH was maintained at around 3 by adding drops of sodium hydroxide (NaOH) and hydrochloric acid

(HCl). The whole reaction mechanism and the schematic of the experimental setup for UF microcapsules synthesis is illustrated in Fig.3.

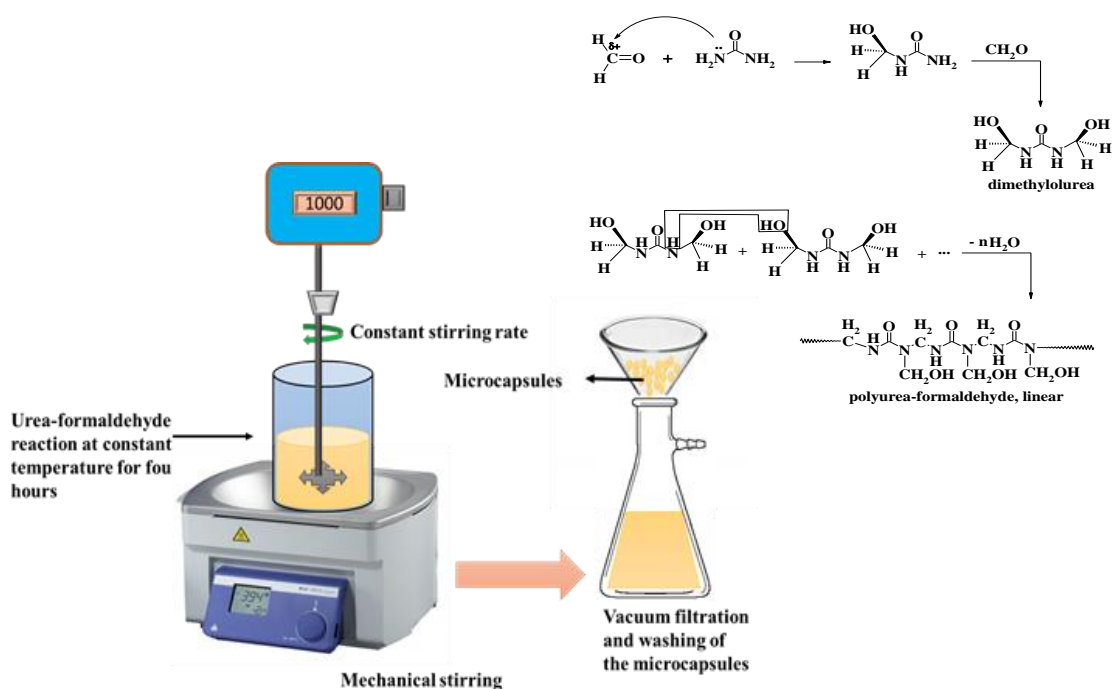


Figure 3: Schematic diagram for the synthesis of encapsulated UF microcapsules and reaction of urea and formaldehyde to form linear UF chain

2.2.2 Encapsulation process

The impregnation of the self-healing specie into the capsules usually takes place in the encapsulation process. Different self-healing materials such as dicyclopentadiene (DCPD), polydimethyl sioxane (PDMS), diglycidylether bisphenol (DGEPI), linseed

oil (LO), tung oil (TO) and 5-ethyidene-2-nor-bomene (EB) are added as a core material based on the core material of the microcapsules type and applications. A 50ml slow addition (drop by drop) of the linalyl acetate (self-healing agent) was added to the beaker to form oil and water emulsion. The solution was then allowed to stabilize for 10-15 minute. The reaction process was then followed-up with the addition of 37wt% (13.0g) of aqueous solution of formaldehyde. The mixture was then stirred on the faster rate of 1000rpm and heated for 4 h at 55°C. After the constant heating rate of 55°C and stirring speed of 800rpm for 4 h, the mixture was allowed to cool down and the microcapsules were separated by vacuum-filtration, the product is allowed to dry for 24-48hrs. The schematic in figure 4 shows the detail of the microcapsule encapsulation process.

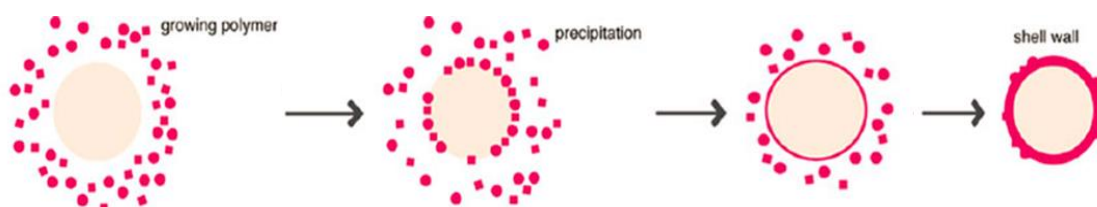


Figure 4: Schematic showing the encapsulation process of the UF microcapsules

2.3 Synthesis of multi-layered UF microcapsules

Two different inhibitors (dodecylamine and phenylthiourea) were loaded in the polyelectrolyte layers (PEI and SPEEK) on the surface of UF microcapsules in order to synthesize two different types of multilayered microcapsules. The corrosion

inhibition properties of the two newly designed multilayered microcapsules reinforced in epoxy matrix were studied. Layer by layer technique was used to coat the polyelectrolytes (SPEEK and PEI) on the surface of the UF microcapsules encapsulated with linalyl acetate. The positively charged polyelectrolyte PEI was first, coated on the surface of the microcapsules by mixing 40 ml microcapsules suspension with 60 ml of PEI solution (2mg/ml) for 10 minutes. The mixture is stirred for 10 minutes. To remove the excess of PEI from the suspension, the mixture was centrifuged first and then washed three times with distilled water. The second layer assembled was a negatively charged polyelectrolyte SPEEK. It was assembled by the addition of 40 ml suspension of the microcapsules (microcapsule + PEI) to the 60 ml solution (2 mg/ml) of the SPEEK (the PEEK was dissolved in the dimethylacetamide at room temperature to make a homogeneous solution) and stirred the mixture for 10 minutes to absorb the SPEEK completely. The excess of the SPEEK was removed in the same way as the first layer. The third layer was the coating of positively charged dodecylamine/phenylthiourea that was prepared by adding the 40 ml solution of the microcapsules (microcapsules + PEI + SPEEK) with the 60 ml solution of dodecylamine/phenylthiourea (10mg/ml), adjusting the pH to 3 and stirred the mixture for 20 minutes. The fourth layer, the SPEEK, and the fifth layer, the PEI, were coated on the shell of the microcapsules using the same procedure. So, the final expected structure, after the assembly of all coated layers on the outer surface (shell) of the microcapsules; was (microcapsules + PEI + SPEEK + dodecylamine/phenylthiourea + SPEEK + PEI). The detail design of the multilayered microcapsules with dodecylamine and phenylthiourea is illustrated in figure 5 and 6. The nomenclature for the multilayered microcapsules with phenylthiourea is as follow; UF

microcapsules = MLMCs (mono layered microcapsules), PTU= phenylthiourea,
 PMC= (polyelectrolyte multilayered microcapsules).

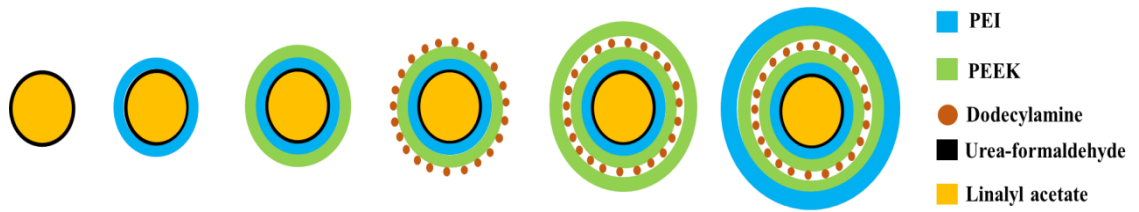


Figure 5: Schematic representation of the structure of as synthesized layered microcapsules with dodecylamine

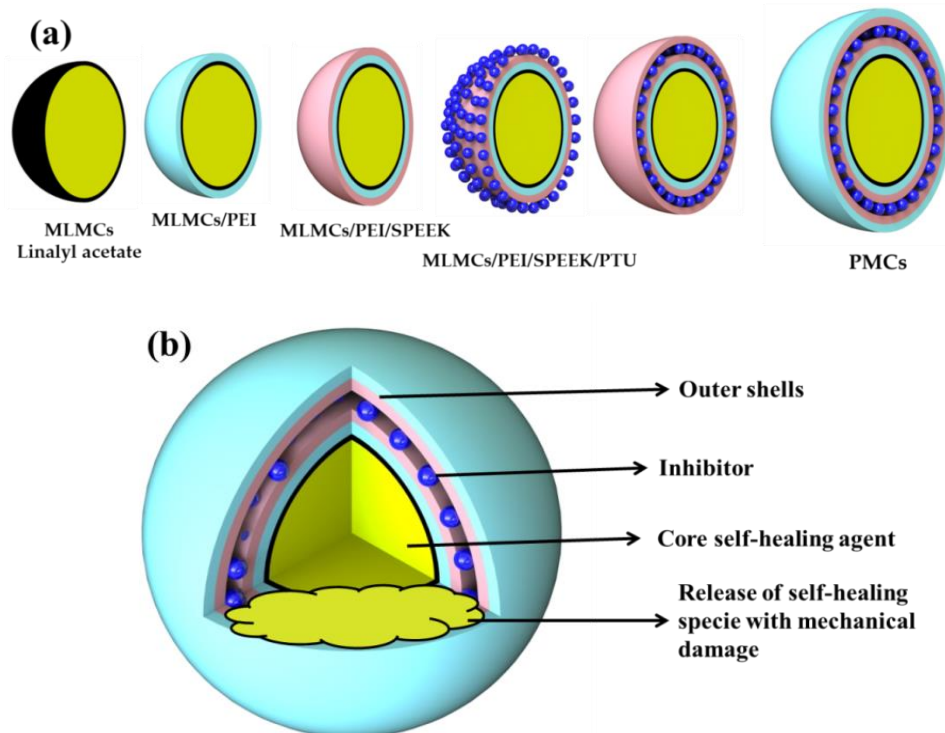


Figure 6: (a) schematic representation of the synthesis of multilayered microcapsules with phenylthiourea (b) profile of multilayers

2.4 Epoxy coating preparation

Cleaned carbon steel specimens were used as a substrate for epoxy coatings. The specimens were grinded using different grits of the abrasive papers, up to 1200 grits, washed with water, degreased in acetone, washed again with water and dried with air. Three types of epoxy coatings were prepared for each set of the microcapsules. In the first set, three types of coatings were developed, 1) the control sample was only epoxy coated sample without microcapsules, and will be referred to as pure epoxy coating. The epoxy coating reinforced with UF microcapsules containing linalyl acetate will be referred to as Single layered smart coatings (SLSCs). Finally, the epoxy coating with the multilayered microcapsules, which has UF microcapsules containing linalyl acetate and polyelectrolyte layers entrapping dodecylamine (DOC) on their shell will be referred to as polyelectrolyte multilayered microcapsules coating (PMLSCs). For the second set of coatings, pure epoxy were named neat coatings, The monolayer UF microcapsules reinforced epoxy coatings were named plain coatings and the multilayered microcapsules reinforced epoxy were named layered coatings. To create each type of coating, 5 wt.% of each type of microcapsules were dispersed in epoxy, stirred for 5 minutes, mixed with the hardener in a stoichiometric ratio and finally the reinforced epoxy mixture was sonicated for 10 minutes to remove the air bubbles. Then the prepared coatings were applied on the cleaned carbon steel specimens for a thickness of 300 μm using doctor blade. The coated specimens were left for 48 hours at room temperature to cure. According to ASTM D1654 standard, a manual scratch was produced along the different coatings (of both the sets) using a scalpel. The scratches are mechanical stimuli to observe the release of the linalyl

acetate that will self-heal the coatings and the corrosion inhibitors release (dodecylamine and phenylthiourea) will stop the initiation of further corrosion process. Figure 7 and 8 further explain the schematics of the coatings for both the sets of capsules.

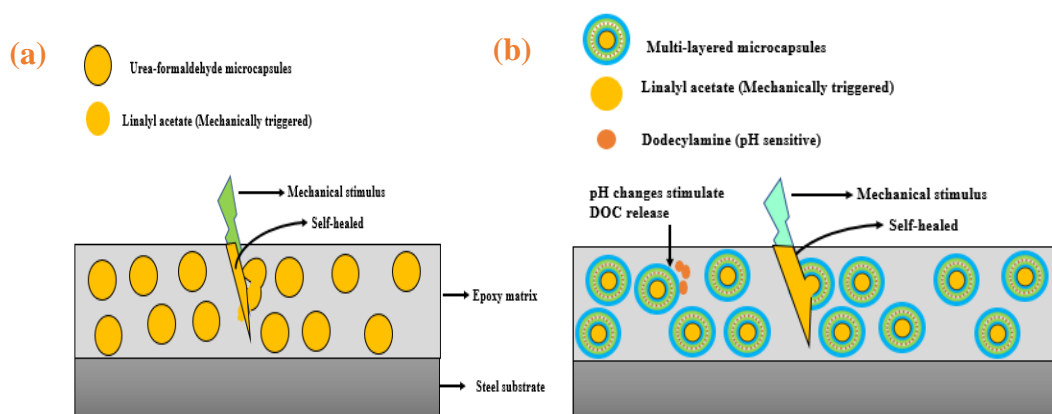


Figure 7: Schematic diagrams of smart coatings (a) modified with UFMCs referred to as SLSCs (b) modified with polyelectrolyte multilayered capsules referred as (PMLSCs).

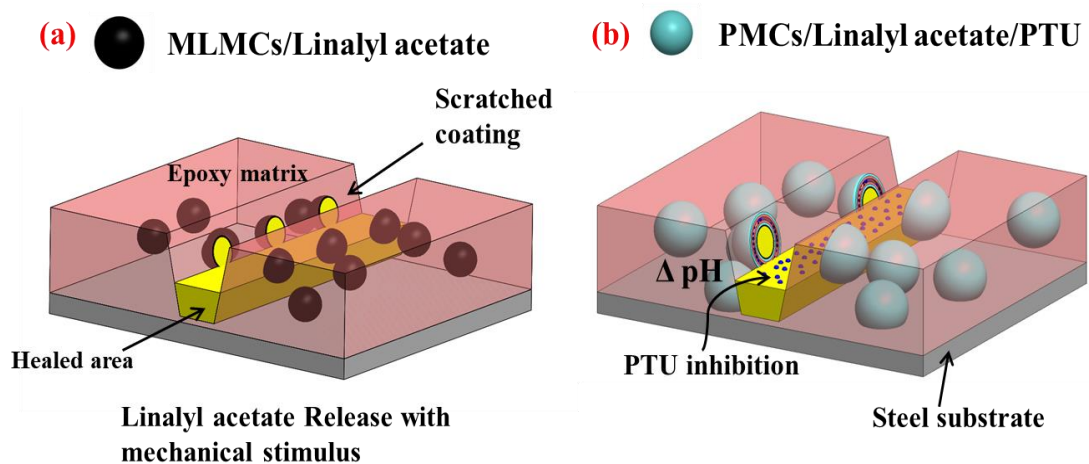


Figure 8: Protective mechanism of the self-healing coatings; (a) plain coating (b) layered coating

2.5 Characterization of microcapsules and coatings

2.5.1 Fourier-transform infrared spectroscopy (FTIR)

Using FTIR spectroscopy the chemical composition of the UF microcapsules loaded with linalyl acetate was carried out and compared with the XRD pattern of the pure linalyl acetate in order to compare the successful loading of the core material (linalyl acetate) in the UF microcapsules. FTIR spectra of the UF microcapsules encapsulated with linalyl acetate, pure linalyl acetate, pure inhibitors (DOC and PTU) and all the multilayers on the surface of the UF microcapsules were observed. Moreover the successful adsorption of the layers on the surface of the UF microcapsules was studied with the FTIR spectra. The spectra were determined over a frequency range of 500-2000 cm^{-1} . It was recorded with a resolution of $\pm 4 \text{ cm}^{-1}$ and a scanning frequency of 32 times at room temperature.

2.5.2 Zeta Potential particle size analyzer

Zeta potential and particle size analyzer were used to analyze the size and the surface charge of the microcapsules. Surface charge confirms the deposition of the polyelectrolyte layers while the change in the size is also evidence the adsorption of the additional layers on the surface of the microcapsules. Zeta potential equipment (Malvern, Zeta sizer, Nano ZSP, USA) was used to confirm adsorption of PEI and SPEEK layers with the inhibitors, by determining the surface charge during layer by

layer process. The sample surface charge was determined after each layer deposition. The variation in the charge confirms the successful deposition of the layers.

The size distribution of synthesized microcapsules, including the single layered microcapsules and layered microcapsules was studied using a particle size analyzer (Malvern, Master sizer 2000, Panalytical, USA). The increment in the size of the microcapsules also confirms the synthesis of the multilayer microcapsules.

2.5.3 X-ray photoelectron spectroscopy (XPS)

XPS (AXIX Ultra DLD, Kratos, UK) using a monochromatic X-Ray Source - Al K α source was used to further confirm the adsorption of the polyelectrolyte layers of the surface of MLMCs and to detail its chemical composition. The binding energy of C 1s (284.6 eV) was used as reference. The energy resolution was 160 eV and the spatial resolution was 20 eV.

2.5.4 Scanning electron microscopy (SEM) and transmission electron microscope (TEM)

A scanning electron microscope is a powerful tool and is being widely used for material characterization in recent years. It is an electron microscope that scans the surface of the material using electron beam to produce images of the surface. The surface morphology of UF microcapsules and layered microcapsules (both with DOC and PTU) was observed using Scanning Electron Microscope (SEM). Furthermore

Transmission Electron Microscope (TEM) was used to analyze the layers deposited on the surface of UF microcapsules. Both the UF microcapsules and layered microcapsules samples were placed (in a very small amount) on the table of the scanning electron microcapsules. A thin layer of gold (6nm) was then coated on the samples to avoid discharging of the electron. The samples were observed using a secondary electron detector under an accelerating voltage of 20kv.

2.5.5 X-Ray Diffraction Analysis

X-Ray diffraction (XRD) is an analytical technique used for the chemical composition analysis. XRD pattern of the UF microcapsules loaded with linalyl acetate were carried out and the multilayers on the surface of the UF microcapsules were also been verified by the changes (addition of extra peaks) in the XRD pattern with the additional layers. Dried UF microcapsules samples and multilayered microcapsules of 2 mg were placed into the specimen holder of XRD at room temperature (40 KV voltage, 30 mA current scanning scope of 2θ was range from 00 to 600 scanning rate of 50/min to 110 with a step size of 0.0320) and the resultant patterns were analyzed.

2.5.6 Thermo gravimetric Analyzer (TGA)

In order to examine the weight loss with respect to time as temperature changes, the thermal degradation behavior of UF microcapsules loaded with linalyl acetate, layered

microcapsules and the developed coatings were studied with TGA analyzer. Dried samples of 1 mg were heated from room temperature to 600°C at a heating rate and a flow rate of 5°C/min.

2.5.7 UV spectroscopic analysis (UV)

UV spectroscopy analysis was used to study the release of the stored inhibitors in the layered microcapsules. UV-vis spectroscopic analysis (LAMBDA 650 UV/Vis Spectrophotometer, PerkinElmer, USA) was used to analyze the release of inhibitor from the MLMCs and PMCs. Various solutions with different pH were prepared and a small amount (0.1 g) of both the layered microcapsules were added to determine the release of the DOC and PTU at different pH and after different times.

2.5.8 Electrochemical Impedance spectroscopy (EIS)

EIS is the technique used to measure the impedance of the developed coatings to corrosion. The two sets of the developed coatings were subjected to a controlled mechanical damage following ASTM D1654 standard procedure and were immersed in the 1 molar NaCl solution to study its anti-corrosion behavior. The EIS study was performed at open circuit potential (OCP) within frequency range 10 mHz to 100 KHz, with rms of 50 mV, using a GAMRY 3000 potentiostat (Gamry, Warminster, PA, USA). The coated steel plates were used as working electrodes, with an exposed

area of 0.5 cm² and a platinum wire was used as counter electrode. An Ag/AgCl electrode was employed as reference. All electrochemical tests were carried out at controlled room temperature. Two scratches with 5 cm length were made on the cured epoxy coatings to study the self-healing effect. The coated specimens were exposed to a 3.5% NaCl solution for 60 minutes before the electrochemical tests. Tests were carried out after different exposure time 24, 48 and 72 h respectively. To ensure reproducibility each test was repeated three times in coated samples with similar scratched.

CHAPTER 3: RESULTS AND DISCUSSION

3.1 FTIR analysis of microcapsules and coatings

FTIR analysis confirmed encapsulation of linalyl acetate in UF microcapsules and the loading of dodecylamine in the polyelectrolyte layers. FTIR spectra of the first set of capsules and its coatings (with the inhibitor dodecylamine), is shown in figure 9.

Figure 9 (a, b) shows the FTIR spectra of UFMCs and pure linalyl acetate. The broad absorption band at 3320 cm^{-1} shows overlapping of the O-H bond and N-H bonds and can be ascribed to urea-formaldehyde. The O-H bond is shifted to the right side due to the strong C=O dipole force of encapsulated linalyl acetate in the UFMCs. The small sharp peak at 3090 cm^{-1} represents the C-H bands, while peaks at 2970 cm^{-1} and 2930 cm^{-1} show the presence of C-H₃ and the sharp peak at 1740 cm^{-1} represents the carbonyl C=O bands, which can be associated with linalyl acetate and urea formaldehyde. All these bands confirm the presence of linalyl acetate. However, there is a new peak at 1542 cm^{-1} representing the N-H band and it accounts for the presence of urea-formaldehyde. Moreover, the peak at 1366 cm^{-1} also represents a C-H band with different vibration, while the peak at 1250 cm^{-1} corresponds to the C-N band. It can be noticed that the C-H and C-N vibrations are present in both UFMCs and pure linalyl acetate. The presence of corresponding distinctive absorption bands of N-H at 1542 cm^{-1} (urea formaldehyde), C=O at 1740 cm^{-1} ((linalyl acetate)) and C-N at 1250 cm^{-1} (linalyl acetate) in the UFMCs confirms efficient storage of linalyl acetate.

Figure 9 (c, d) shows the FTIR spectra of pure dodecylamine (DOC) and MLUFMCs. The broad peak at 3315 cm^{-1} in the MLUFMCs spectrum and a minor sharp peak in the spectrum of pure DOC correspond to the N-H bonding. The two sharp peaks at 2925 cm^{-1} and 2850 cm^{-1} represent the C-H bonds in DOC and MLUFMCs, however, the peak intensity is high in DOC because of the long C-H chain in the structure of DOC. The peaks present at 1550 cm^{-1} and 1187 cm^{-1} represent C=C and C-O bonds respectively which confirms the presence of SPEEK layer on the surface of MLUFMCs. Similarly, the peak at 1250 cm^{-1} can be ascribed to C-N band, which clearly demonstrates the existence of a PEI layer on the MLUFMCs. The presence of corresponding distinctive absorption bands of N-H at 3315 cm^{-1} (DOC), C=C at 1550 cm^{-1} and C-O band at 1187 cm^{-1} (SPEEK) and C-N at 1250 cm^{-1} (PEI) confirms the formation of MLUFMCs and efficient encapsulation of DOC. It is pertinent to note that C-N band at 1250 cm^{-1} overlaps with linalyl acetate as reported previously.

Figure 9 (e, f) indicates the FTIR spectrum of PMLSCs and SLSCs. A comparison of FTIR spectra of PMLSCs, SLSCs, UFMCs and MLUFMCs confirms their identical nature. The multiple small peaks present at 2924 cm^{-1} represent the C-H bond and associated with DOC and MLUFMCs. The C=O bond at 1750 cm^{-1} represents the carbonyl C=O group which can be associated to linalyl acetate and urea form aldehyde. Moreover, the sharp peak at 1250 cm^{-1} represents the C-N bond that can be ascribed to urea form aldehyde, DOC and PEI. A small intensity peak at 3500 cm^{-1} indicates N-H bond, which can be associated to urea form aldehyde, DOC and PEI. A close comparison of the FTIR spectra confirms encapsulation of linalyl acetate in UFMCs and DOC in MLUFMCs. Furthermore, FTIR spectra also confirm the

presence of UFMCs and MLUFMCs in SLSCs and PMLSCs without evident side reactions.

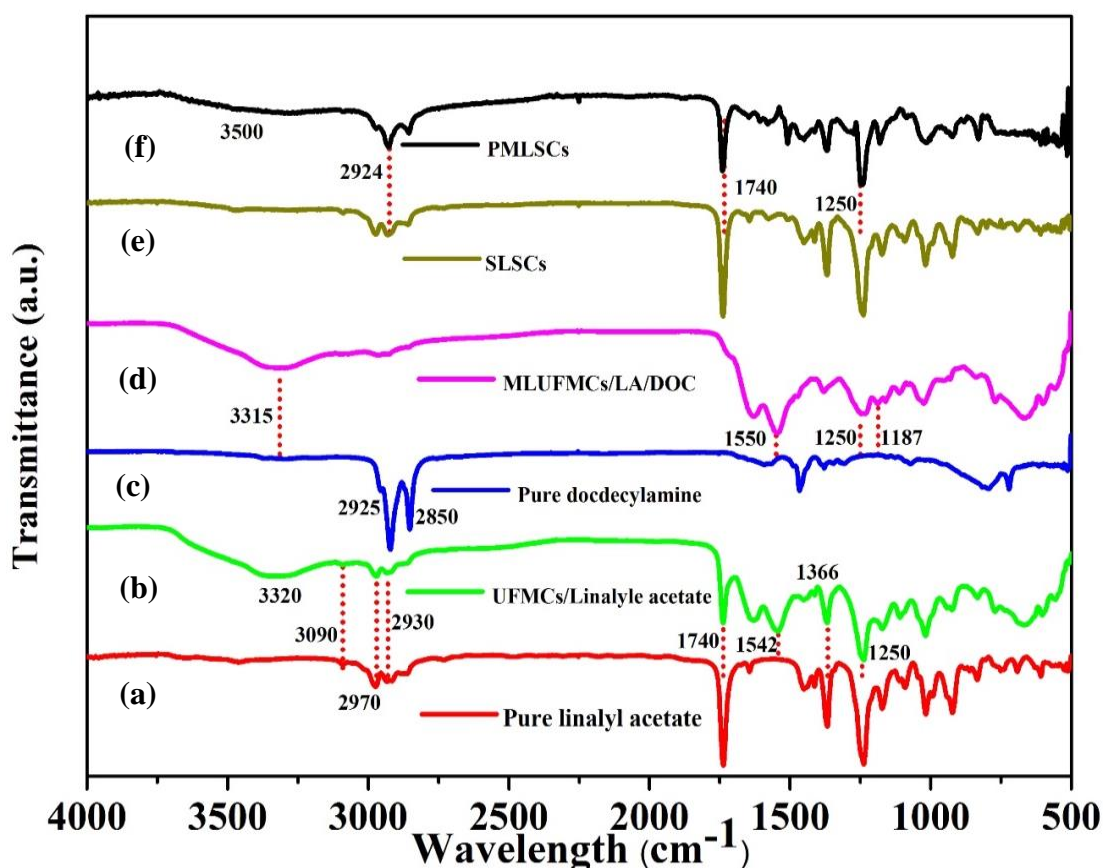


Figure 9: FTIR spectra of the microcapsules and coatings (a, b) as synthesized UFMCs encapsulated with linalyl acetate and pure linalyl acetate (c, d) MLUFMCs and pure dodecylamine (e, f) PMLSCs and SLSCs

Furthermore, the FTIR spectra of the second set of the microcapsules (with phenylthiourea as a corrosion inhibitor) are shown in figure 10. Figure 10 depicts the FTIR spectra of (a) pure linalyl acetate, (b) MLMCs and (c) PMCs. Linalyl acetate spectrum shows several absorption peaks including the C-H bond stretching at 2972

cm^{-1} , and C=O ester bond at 1736 cm^{-1} , as well as the C=C bond at 1646 cm^{-1} and C-O-C ester at 1250 cm^{-1} . The MLMCs spectrum presents the O-H peak around 3303.6 cm^{-1} , C-H stretching peak around 2964.76 cm^{-1} , as the amide C=O peak was observed at 1623.63 cm^{-1} . Finally the C-N and N-H peaks were found around 1232.43 cm^{-1} and $1541\text{-}1631 \text{ cm}^{-1}$ respectively, and were assigned to bond formation in the MLMCs.

The mechanism behind MLMCs formation is the reaction of the acetate group with the hydroxyl methylene group of urea formaldehyde, which leads to the formation of an ester/ether bond. The formation of the ester/ether bonds is evidenced in the FTIR spectrum by the shift in the urea formaldehyde amide group to $1541\text{-}1631 \text{ cm}^{-1}$. The change in the amide group is due to the change in polarity between the linalyl acetate and the urea formaldehyde bonds, confirmed by the shift in the N-H bond. The spectrum (c) representing the PMCs is similar to the one for MLMCs. The major differences can be observed in the frequency region where the C=O stretching peak responds. First, the elimination of the C=O in PMCs indicates the formation of new bonds, which can be explained by the successful layering with PEI, SPEEK and PTU. Other significant changes are the contents of O-H and the N-H peak intensity; the peak intensity of N-H after addition of polyelectrolyte layers to the MLMCs is clearly high. As for the hydroxyl content, the O-H content in the MLMCs is much lower than the O-H content in the PMCs, due to the consumption of hydroxyl after addition of the polyelectrolyte layers (SPEEK and PEI).

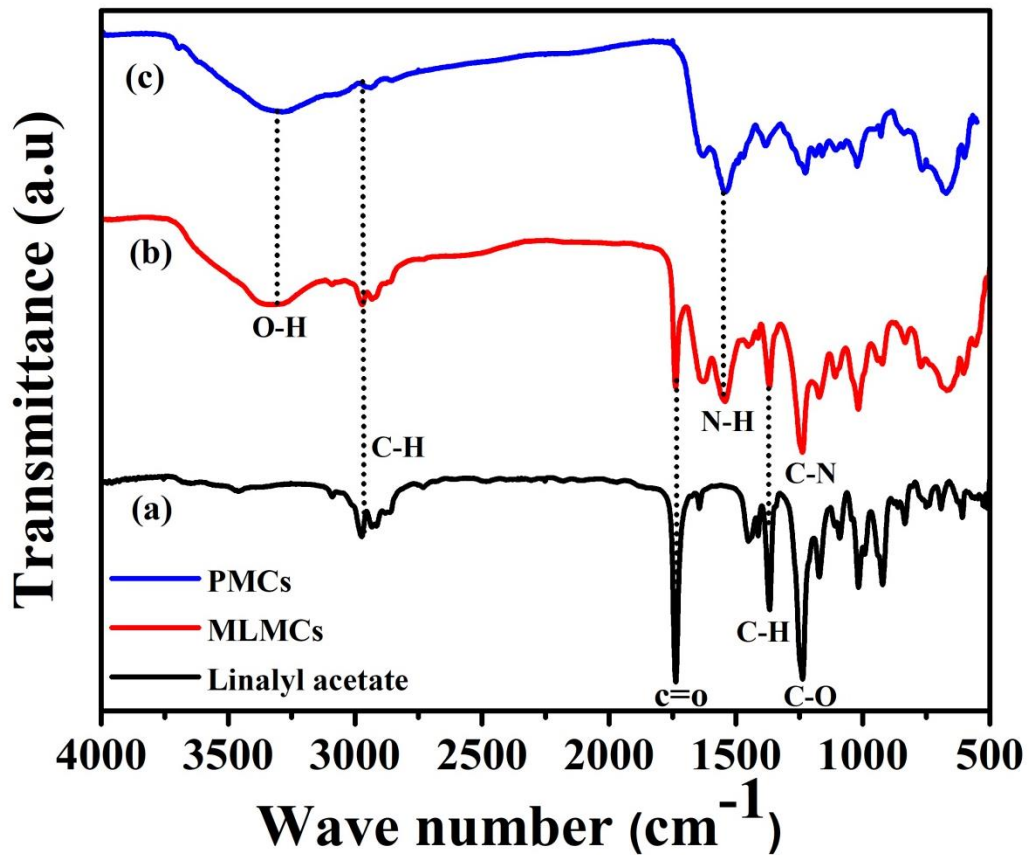


Figure 10: FTIR spectra of the (a) linalyl acetate (b) MLMCs loaded with linalyl acetate (c) and PMCs

3.2 Zeta potential measurements of microcapsules

To confirm the polarity of layers on the MLUFMCs, zeta potential of each layer was determined, and the results are presented in Figure 11. It can be noticed that the zeta potential of the UFMCs is negative ($\sim -1.84\text{mV}$). However, when a PEI layer is formed on UFMCs the value of charge shifted to positive value ($\sim +20\text{ mV}$) which indicates that the PEI layer carries a positive charge and thus can be easily bonded to the UFMCs. Furthermore, adsorption of SPEEK layer on PEI shifts the charge towards negative value ($\sim -10.0\text{ mV}$) confirming its negative polarity. Owing to

negatively charged (from the $-\text{SO}_3$ group), the SPEEK layer can be easily bonded to the positively charged underneath PEI layer. Finally, shifting of the potential towards positive value ($\sim +1.0$ mV) due to DOC indicates that it can be easily encapsulated between the SPEEK layers. It can be noticed from Figure 4 that the surface charge varies according to the deposited layer (PEI, SPEEK, DOC) confirming the adsorption of the corresponding layer. Furthermore, zeta potential is increased by the addition of PEI (cation) on the surface and it decreased with the deposition of SPEEK (anion). A slight increase in zeta potential is observed after the addition of DOC leading to the successful adsorption of DOC. The obtained zeta potential results are consistent with results reported elsewhere.

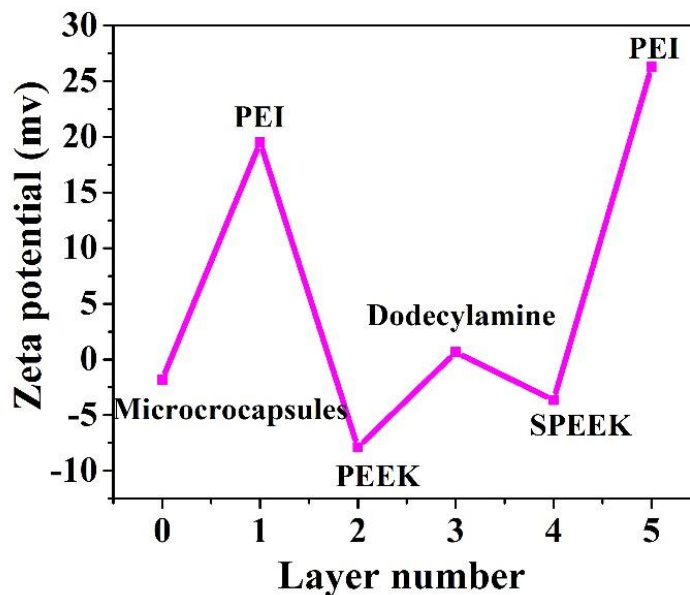


Figure 11: Zeta potential measurements of microcapsules. Layer number 0: microcapsules encapsulated with linalyl acetate (UFMCs) and layers 1-5, MLUFMCs having various polyelectrolyte layers.

The surface charge of the second set of the microcapsules was also studied to confirm adsorption of the polyelectrolyte layers and the layer by layer design of the PMCs. Figure 12 presents the zeta potential of each layer of the PMCs. It is noticed that the zeta potential of the as synthesized MLMCs is negative (~ -6.7 mV). After deposition of PEI the zeta potential shifted to positive values (~ 19.3 mV), which confirmed the bonding of the MLMCs with the polycation PEI. Furthermore because of the sulphonic group in SPEEK, the zeta charge shifted to the negative value (~ -25.5 mV). In addition due to the difference in the specific charge and molar mass of PTU compared to the polyanion SPEEK, the zeta potential slightly increased (~ -20 mV) after adsorption of the PTU layer. The valence electrons in PTU hold the $-\text{SO}_3$ group

of the SPEEK and thus ensure the loading of PTU between the two polyanion layers. Finally the zeta potential was dramatically shifted to positive values (~ 33.2 mV) after the deposition of the new PEI layer. The results are in agreement with results reported elsewhere.

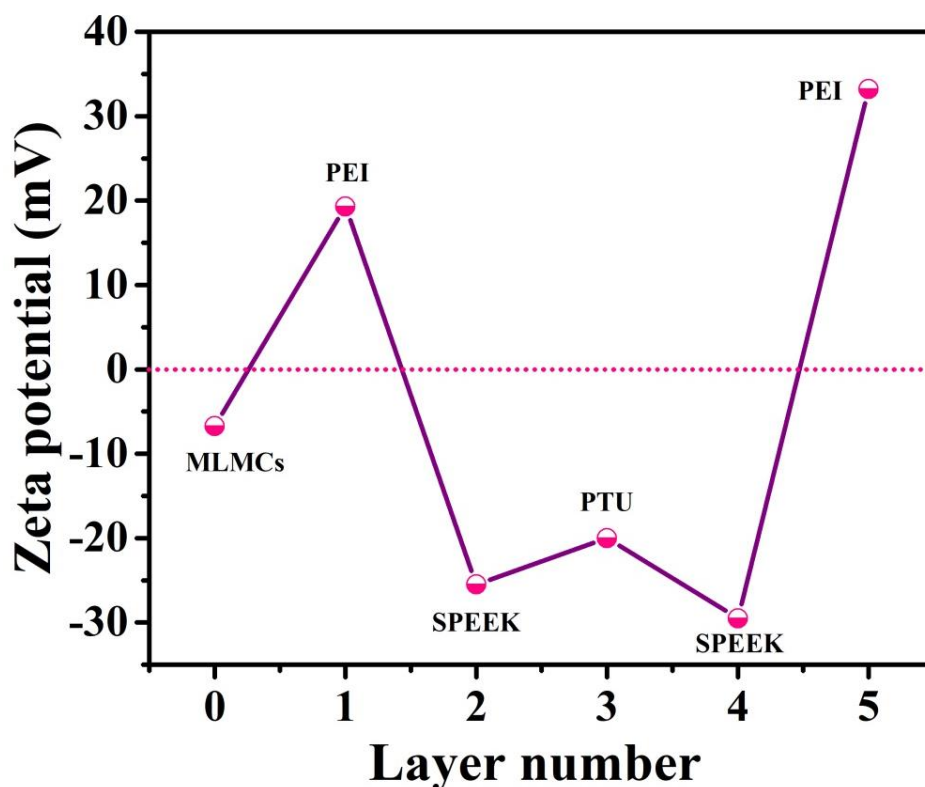


Figure 12: Zeta potential value of the microcapsules. Layer 0: as synthesized MLMCs and layer 1-5, the different layers of the PMCs.

3.3 XPS analysis

The XPS analysis was carried out in order to verify the adsorption of the polyelectrolyte layers on surfaces of the UF microcapsules. The XPS survey spectra

(for the first set of capsules) were recorded in the binding energy range of 250 to 800 eV is shown in Figure 13. XPS measurements with probe depths of up to 10 nm were performed. The major identified elements in the samples are carbon, oxygen and nitrogen. The presence of carbon, oxygen and nitrogen were expected from the chemical composition of the urea formaldehyde and polyethylenimine (PEI) in UFMCs and MLUFMCs, respectively. The high resolution XPS spectra (C 1s) for the UFMCs and MLUFMCs samples are also presented in inset (a) and (b) of Figure 6, respectively. In C1s spectrum for the both type of samples, the peaks at 284.6 and 286.3 and 288.3 eV refer to C-C bond, C-O bond and C=O bond, respectively. The intensity of C-O and C=O bonds peaks in C1s spectrum have significantly been reduced after the adsorption of PEI on the surface of the microcapsules. The positions of the C-O and C=O are not very distinguishable in the encapsulated samples due to the widening of the peaks. This indicated that the microcapsules have been encapsulated by the coated materials. As it is obvious from the molecular structure of the PEI (inset c), it mainly consists of C-C chains and there is no clear existence of C-O and C=O bonds when compared to the urea formaldehyde.

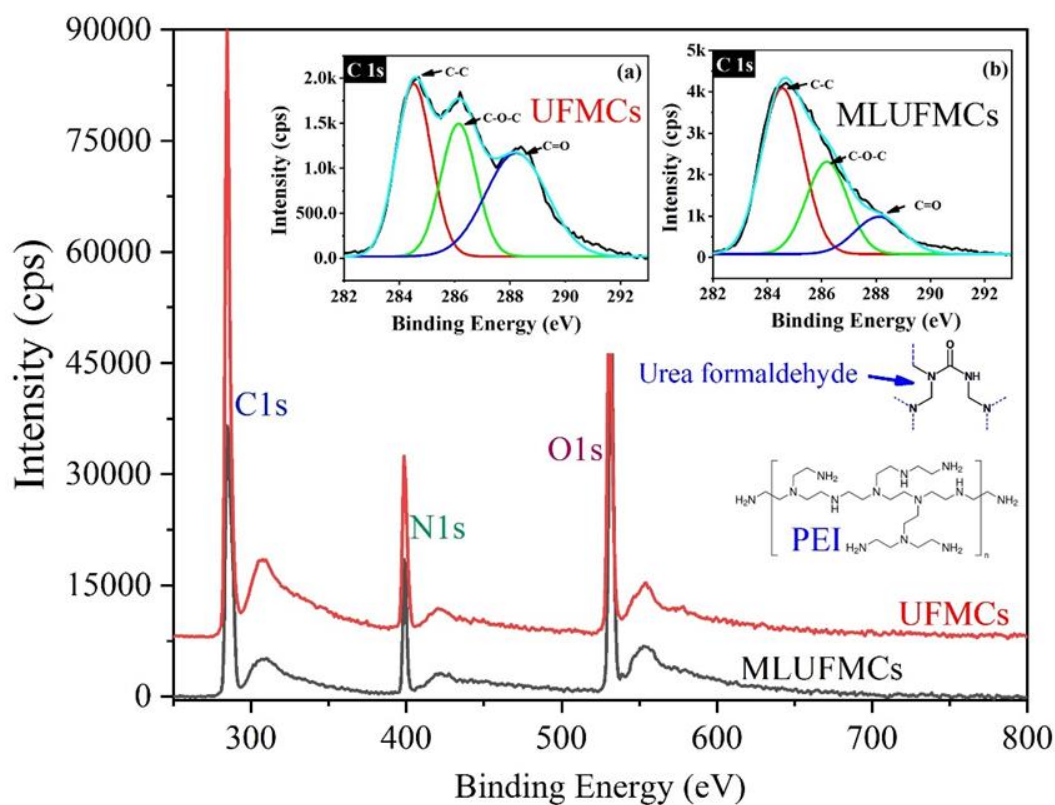


Figure 13: XPS survey spectra of UFMCs and MLUFMCs samples. Insets show the high resolution XPS spectra C 1s of the both UFMCs (a) and MLUFMCs (b) samples.

Molecular structures of the urea formaldehyde and PEI are also given in the Figure.

To confirm the adsorption of the polyelectrolyte layers on the surface of the MLMCs, also XPS characterization was carried out as shown in the figure 14. The XPS spectra of the MLMCs and PMCs show the presence of carbon, nitrogen and oxygen which correspond to the structure of the urea-formaldehyde and PEI+SPEEK (outer layer in PMCs) and the respective quantification is depicted in table 1.

Table 1: The elemental analysis of MLMCs and PMCs

Elements	MLMCs (%)	PMCs (%)
C 1s	55.52±2%	69.22±2%
N 1s	23.25±2%	19.64±2%
O 1s	21.24±2%	11.24±2%

The XPS spectra of C1s on the surface of microcapsules (MLMCs and PMCs) is shown in figure 14 (a,b). For MLMCs the main peak was fitted with three peaks placed at 284.9 eV, 286.6 eV and 288.5 eV assigned to the binding energies of C-C, C-O-C and C=O on the surface of MLMCs. In PMCs the fitting peaks are shown at 284.8 eV, 286.3 eV and 288.0 eV which were assigned to the same species observed for the MLMCs surface. Since XPS is a surface analysis technique, there is a clear difference in the concentration at the surface of the microcapsules which accounts for the adsorption of polyelectrolyte layers on the MLMCs. The XPS results showed only the outer small portion of the PMCs layers (mainly consist of PEI and SPEEK) because of the short mean free path of photoelectrons. The contents of carbon increased in the PMCs surface (PEI + SPEEK) from 55.2% to 69.19 %, which reflect the complex carbon chain structure of PEI and SPEEK. Nitrogen and Oxygen showed a decrease in the PMCs. Figure 14 (c, d) represents the nitrogen peak and both MLMCs and PMCs showed only the binding energy of C-NH₂. Moreover O1s is shown in figure 14 (e, f) for both microcapsules. The O1s spectra showed that the binding energy of C-O and C=O were dominant.

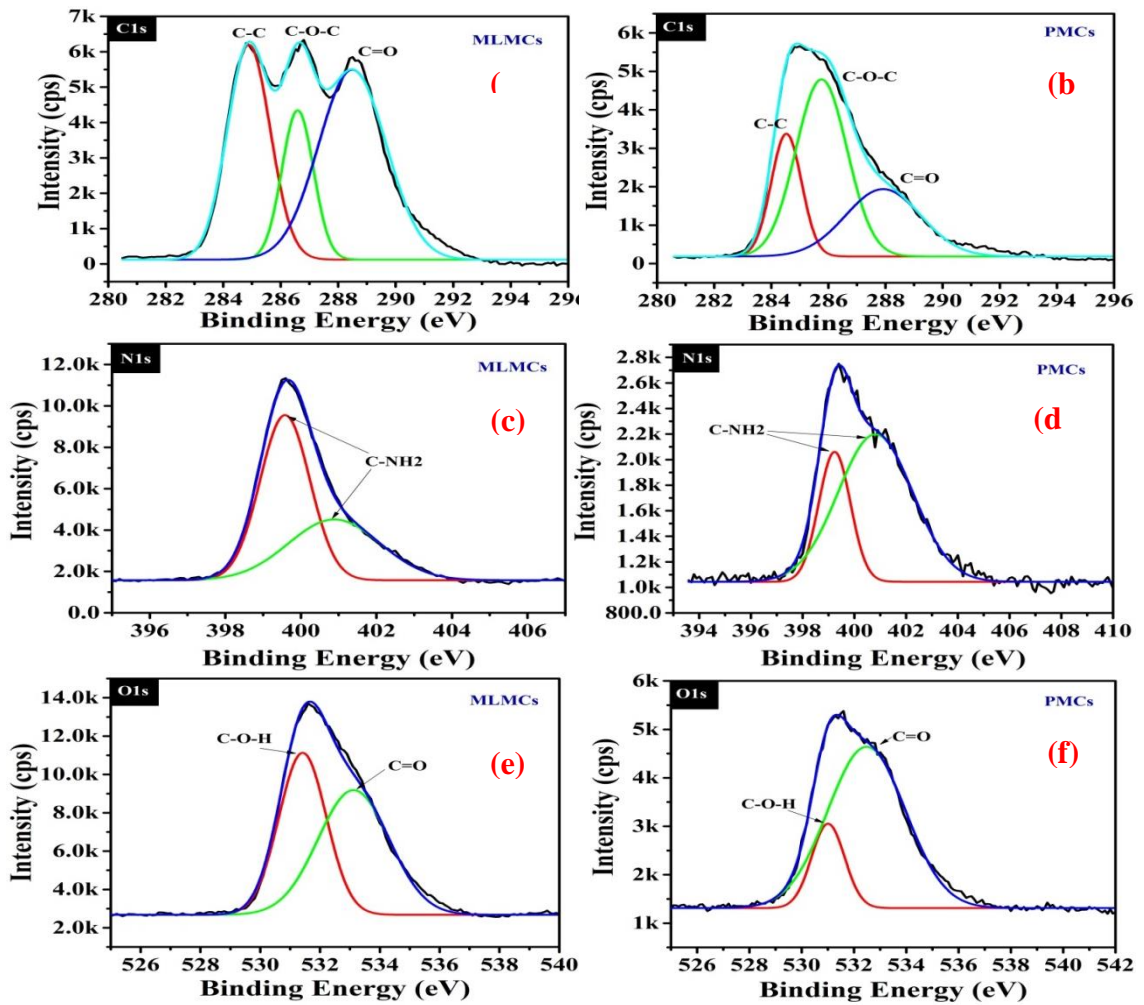


Figure 14: XPS survey spectra of MLMCs and PMCs samples: (a, b) C1s, (c, d) N1s, (e, f) O1s

Field Emission Scanning Electron Microscopy (FE-SEM) and High-Resolution Transmission Electron Microscopy (HR-TEM) analyses were conducted to study the morphology of the microcapsules (UFMCs, MLUFMCs) and the respective smart coatings (SLSCs, PMLSCs). Figure 15(a) shows the FE-SEM image of UFMCs. A spherical morphology of the UFMCs with mean diameter 36 μm is observed without any crack and porosity. Moreover, a rough surface and variation in the size of

microcapsules can also be noticed. In the *in-situ polymerization*, the size of the microcapsules depends on the stirring rate and it becomes finer with increasing stirring rate due to high shear force. The rough exterior surface improves the adhesion of the microcapsules to the coating matrix. The complete dryness, high tensile strength and low water absorbing capability of the urea-formaldehyde has led to the formation of more visible and isolated UFMCs. Figure 15(b) shows the morphology of the MLUFMCs. These multilayered capsules have similar nodular morphology as UFMCs. A significant variation in the size of the MLUFMCs capsules can also be noticed. A change in color may be related to the deposition of polyelectrolyte layers on the encapsulated UFMCs. However, a denser and more diffused structure is achieved in MLUFMCs as compared to UFMCs due to existence of multiple layers of polyelectrolyte materials. Figure 15 (c, d) represents the structure of PMLSCs and SLSCs. It can be noticed that a dense, uniform, crack free and homogeneous structure is preserved in both kind of coatings. It can also be noticed that there are no pore and pin holes present in the coatings.

In order to have more insight of the developed MLUFMCs microcapsules, HR-TEM analysis was under taken and the results are presented in Figure 15 (e, f). It can be clearly noticed that well defined multilayered nodular structure is preserved. The encapsulation of linalyl acetate and the presence of polyelectrolyte multilayers in MLUFMCs can be clearly noticed. The average core is ~350 nm and the average thickness of polyelectrolyte multilayer is ~206 nm. The TEM analysis clearly confirms the formation of MLUFMCs. In TEM analysis, only smaller size microcapsules were focused to study morphological features. However, it is pertinent

to note that the average particle size of the synthesized MLUFMCs is 65 μ m as confirmed by our particle size analysis and discussed in the proceeding section.

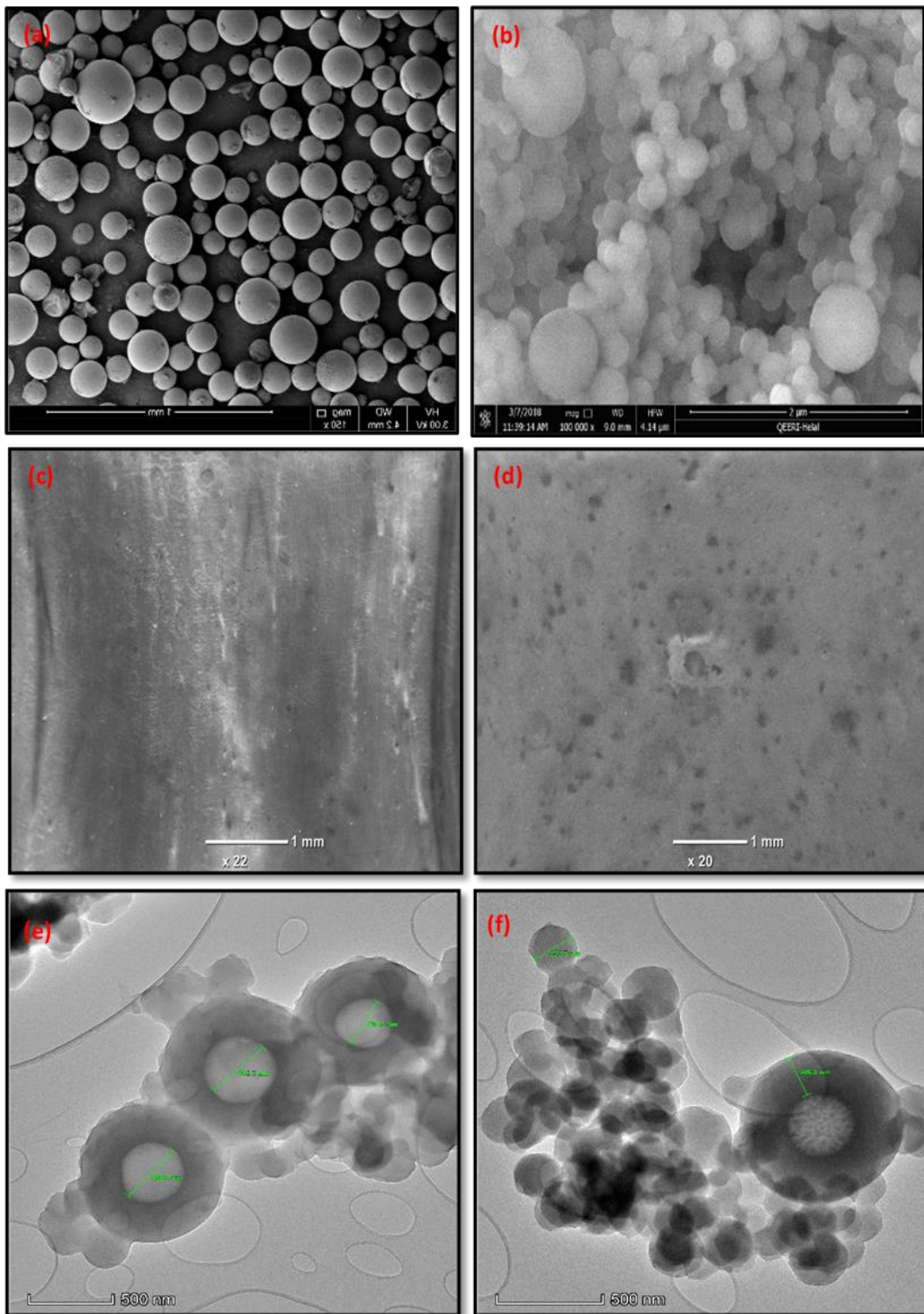
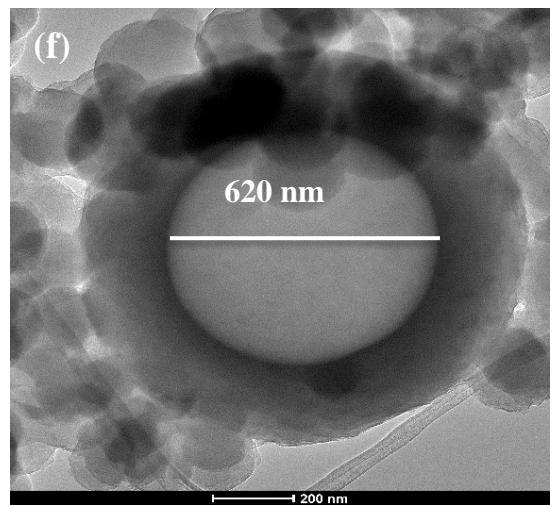
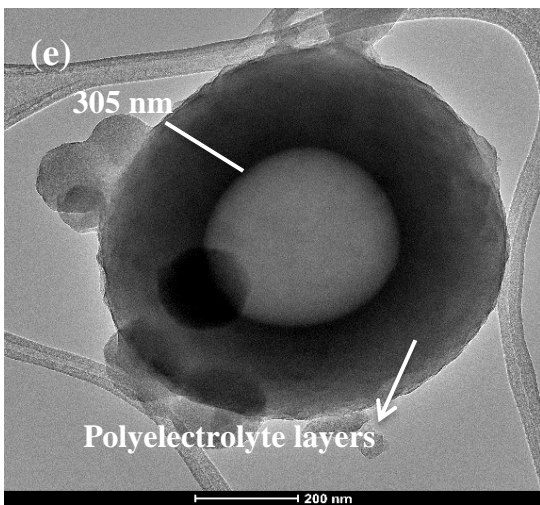
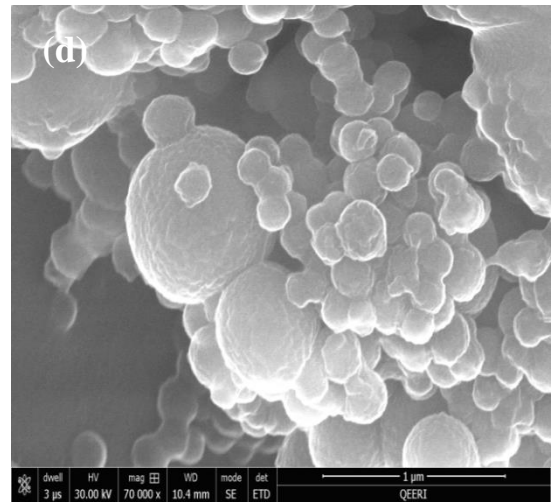
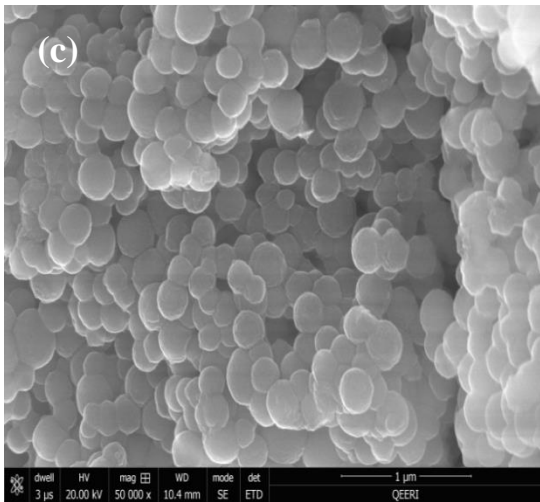
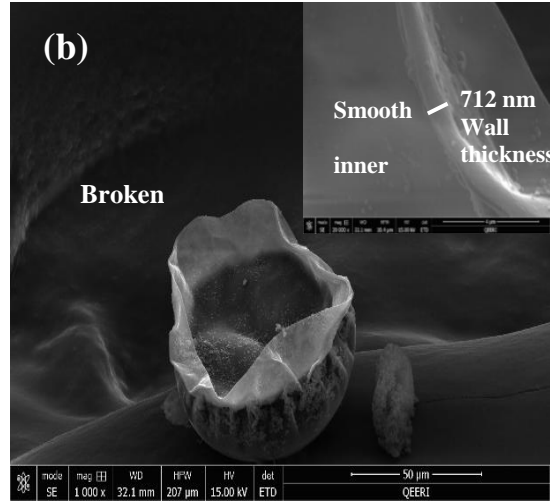
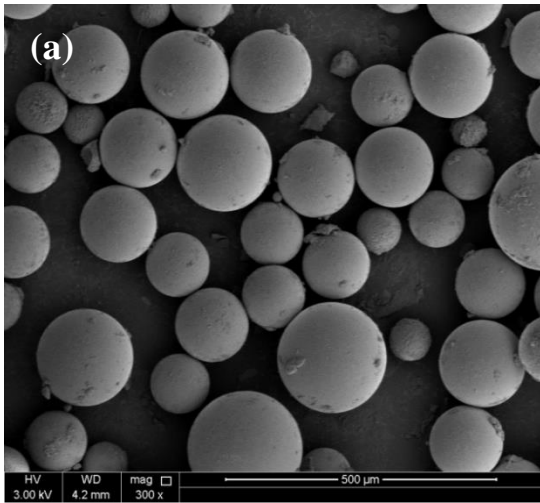


Figure 15: FE-SEM analysis of microcapsules and smart coatings (a) UFMCs (b) MLUFMCs, (c) SLSCs, (d) PMLSCs and (e, f) HR-TEM of MLUFMCs.

Figure 16 depicts the structural and morphological study of the as synthesized MLMCs and PMCs. Figure 16(a) shows the MLMCs and reveals the presence of micro sized spherical beads with a slightly rough outer surface, according to previous results. Figure 16 (b) is the wall thickness of the broken MLMCs. The average wall thickness is about 712 nm with a smooth inner surface. The thickness of the wall depends on the stirring rate and the time of polymerization reaction during the syntheses of the MLMCs. By prolonging the time of polymerization reaction it is expected to achieve thicker wall microcapsules with higher mechanical strength.

Figure 16 (b, c) depict the SEM images of PMCs, that present various sizes, in line with the particle size analysis. The morphology of the PMCs is also spherical with more compaction compared to MLMCs. The surface morphology of the PMCs was also studied by TEM to clarify the presence of the multilayers (polyelectrolyte and inhibitor) on the surface of MLMCs. Figure 16 (e, f) depicts the TEM analysis, which clearly showed the deposited polyelectrolyte layers on the surface of the MLMCs in agreement with previous results. The average thickness of the deposited polyelectrolyte is about 350 nm. The images clearly demonstrate the core microcapsules with an average size of about 620 nm. The detail discussion about the size distribution of the microcapsules is made in the proceeding sections. Figure 16 (g, h, i, j) represent the elemental mapping of the surface of MLMCs which showed that carbon, nitrogen and oxygen are the primary elements present in the MLMCs.



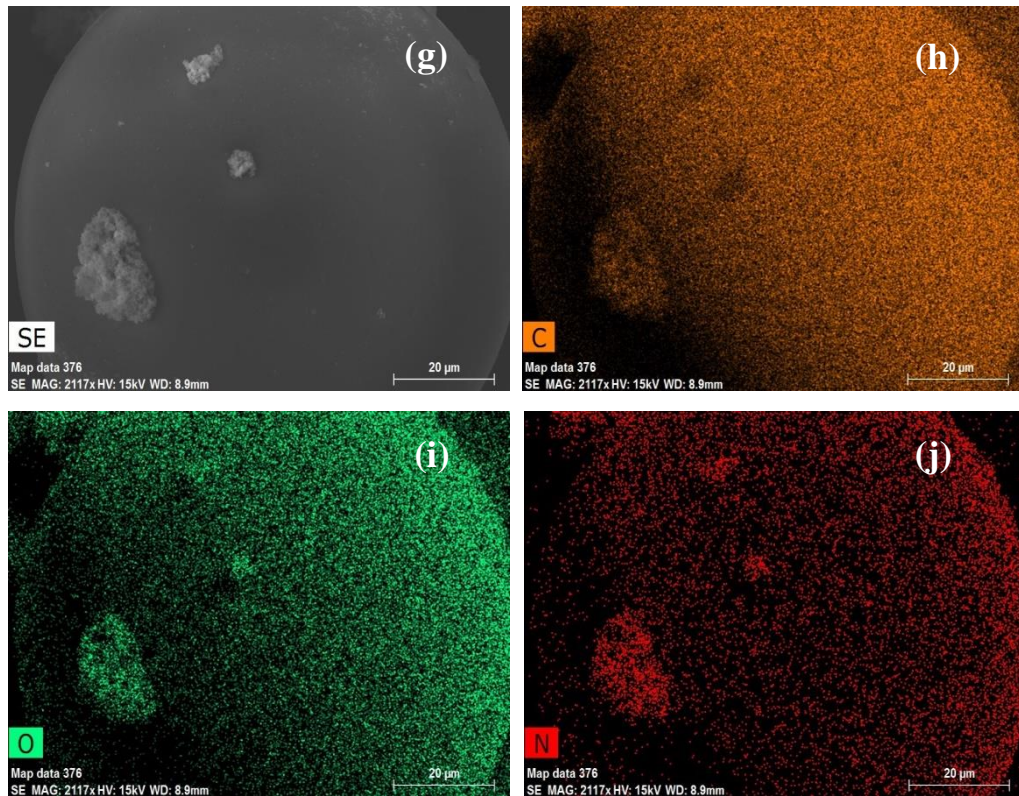


Figure 16: The structural and morphological study of the synthesized microcapsules (a, b) SEM of the UF microcapsules (b, c) the SEM of the multilayered microcapsules (d, e) TEM of the multilayered microcapsules. (f, g, h, i) elemental mapping of MLMCs

3.5 Particle size and XRD analysis of the microcapsules

The particle size distribution of the microcapsules is further confirmed with particle size analyzer and the results are shown in Fig .17. It can be seen that the particle size of the UFMCs ranging from 0.01 to 500 μm . The majority of the UFMCs are made up of 10~63 μm and the mean diameter of the UFMCs is found to be 36 μm . Our analysis indicates that the stirring rate of 1000 rpm has resulted in UFMCs having average size of 36 μm . Fig. 17 also shows the particle size distribution of MLUFMCs. It can be seen that the mean diameter of MLUFMCs is about 65 μm . The increase in

the diameter of MLUFMCs indicates the deposition of polyelectrolyte layers and the inhibitor on the surface of the UFMCs. Furthermore, size variation in MLUFMCs can also be noticed and it is found that majority of the MLUFMCs are made up of size in the range of 10 to 125 μm . The mean diameter of MLUFMCs is found to be 65 μm . These results are consistent with our TEM analysis.

In order to study the effect of polyelectrolyte layers and the surface of microcapsules and the structural analysis of UFMCs and MLUFMCs, XRD analysis was also conducted. Fig. 17 inset shows the XRD spectra revealing the amorphous behavior of the UFMCs and MLUFMCs. The peak at 17.5° accounts for the presence of urea-formaldehyde present as the shell material of UFMCs encapsulated with linalyl acetate. Another peak at 22° is observed, with higher intensity, which can be attributed to the deposited polyelectrolyte layers on the surface of UFMCs.

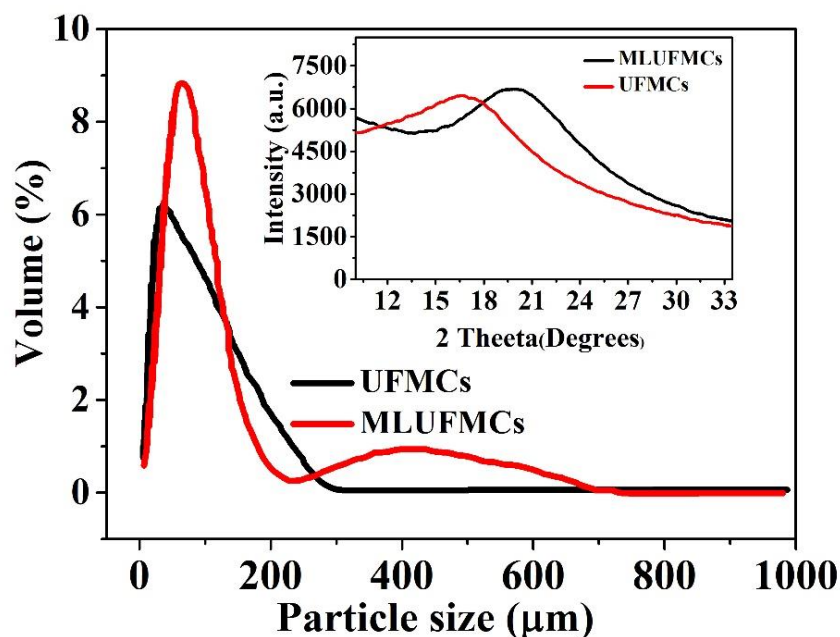


Figure 17: Particle size analysis of as synthesized urea-formaldehyde microcapsules-UFMCs and multi-layered urea-formaldehyde microcapsules-MLUFMCs. Inset shows the XRD of the UFMCs and MLUFMCs.

Figure 18 indicate the particle size study of MLMCs and PMCs, using particle size analyzer. The MLMCs were in the range of 0.01 μm to 500 μm . The average size of the capsules observed was 37 μm . The majority of the particle lies in the range of 4 μm to 63 μm (volumes %) while there was only 10 volume % of capsules in the size range of 125 μm to 250 μm . The analysis indicates that most of the particles are in the lower range which reflects the high stirring rate which further split the linalyl acetate into smaller pieces resulting in smaller microcapsules. Fig. 18 also shows the particle size distribution of the PMCs. The mean size observed was about 68 μm . The particles are in the range of 0.01 to 2000 μm but the majority of the microcapsules

were present in 4 to 125 μm (77.79 volume %). Only 4.39 volume % of the PMCs lies in the range of 1000 to 2000 μm . The increase in the mean diameter of the PMCs indicates the successful adsorption on the surface of MLMCs. The insets in figure 18 present the variation in the size of microcapsules. It is worth to note that the TEM images shown above focuses only the smallest PMCs.

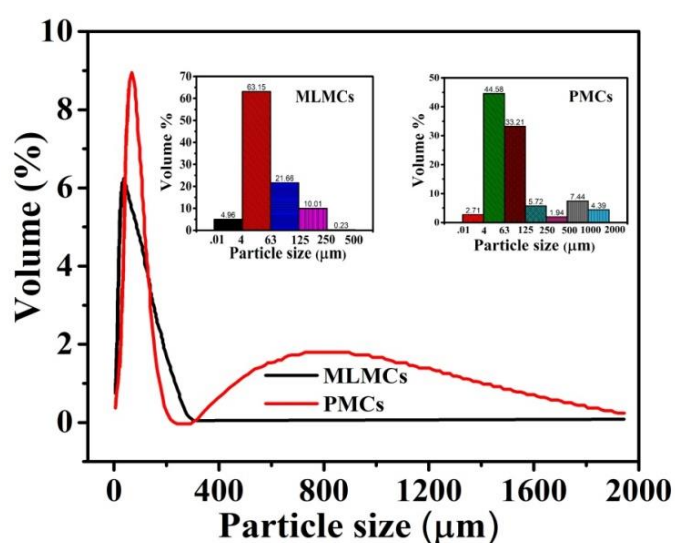


Figure 18: Particle size analysis of MLMCs and PMCs

3.6 Thermal stability of the microcapsules and epoxy coatings

Thermal stability of encapsulated UFMCs, MLUFMCs, SLSCs and PMLSCs was analyzed using TGA and the results are presented in Figure 19 (a, b). It is seen that both UFMCs and MLUFMCs experience a gradual weight loss with increasing temperature up to 600 $^{\circ}\text{C}$ (Figure 19(a)). The initial weight loss (50 $^{\circ}\text{C}$ to 80 $^{\circ}\text{C}$) may be associated to the removal of the absorbed moisture in the microcapsules. In the

next region, the UFMCs shows complete weight loss up to 200°C due to encapsulated linalyl acetate (B.P, 220°C). However, the MLUFMCs exhibit better thermal stability which can be associated with the presence of high thermally stable polymeric structure (PEI and SPEEK) and dodecylamine. The drop around 200°C could be due to the loss of sulfonic acid group of the SPEEK. These findings are consistent with previous studies. Figure 19(b) shows the TGA spectra of the SLSCs and PMLSCs. Like microcapsules, there is small weight loss at the first stage (50°C to 80°C) for only the SLMCs, attributed to the presence of moisture in the coating. A comparison of Figure 19(a) and Figure 19(b) indicates that SLSCs and PMLSCs demonstrate better thermal stability compared to UFMCs, MLUFMCs which could be linked to the presence of polymeric matrices of the PEI and SPEEK and the long chain of dodecylamine.

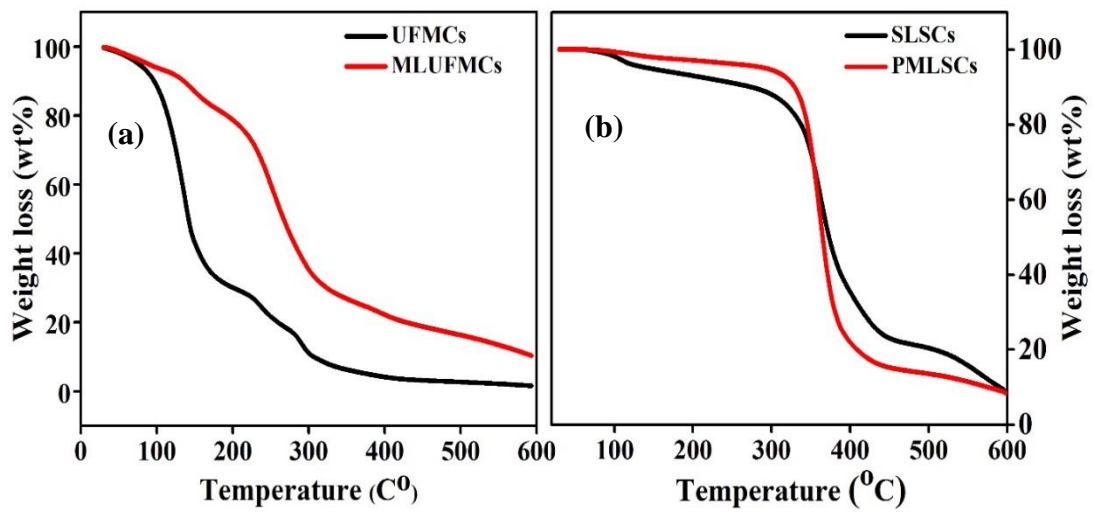


Figure 19: Thermal stability of (a) microcapsules-UFMCs, MLUFMCs and (b) developed smart coatings-SLSCs and PMLSCs.

Moreover, the thermal stability of the MLMCs and PMCs added into the epoxy coatings were analyzed by TGA (Fig.20 (a, b)). Figure 20 (a) indicate that there is a gradual weight loss in both the MLMCs and PMCs with the increasing temperature (up to 600 °C). The complete weight loss in the MLMCs spectra observed was from 130 °C to around 270 °C which can be associated with the shell of urea-formaldehyde (200 °C) and the encapsulated linalyl acetate (B.P 220 °C). The PMCs display improved thermal stability because of the highly thermally stable polyelectrolyte materials (PEI and SPEEK). The first stage (100 °C to 230 °C) showed a minor weight loss which can associate with the decomposition of impregnated phenylthiourea (157 °C) and core linalyl acetate (220 °C). The second stage (270 °C to 420 °C) was attributed to the adsorbed polyelectrolyte materials. The inset in figure 20(a) shows the peaks of the derivative weight loss of both the MLMCs and PMCs. Figure 20(b)

shows the TGA spectra for the plain and layered coatings. Like the microcapsules, the layered coating exhibited better thermal stability compared to the plain coating. Both the coatings are thermally stable and showed negligible weight loss till 400°C, which can be attributed to the highly thermally stable epoxy resin matrix. The peaks of the derivative weight loss of the coatings can be seen in the inset of figure 20(b).

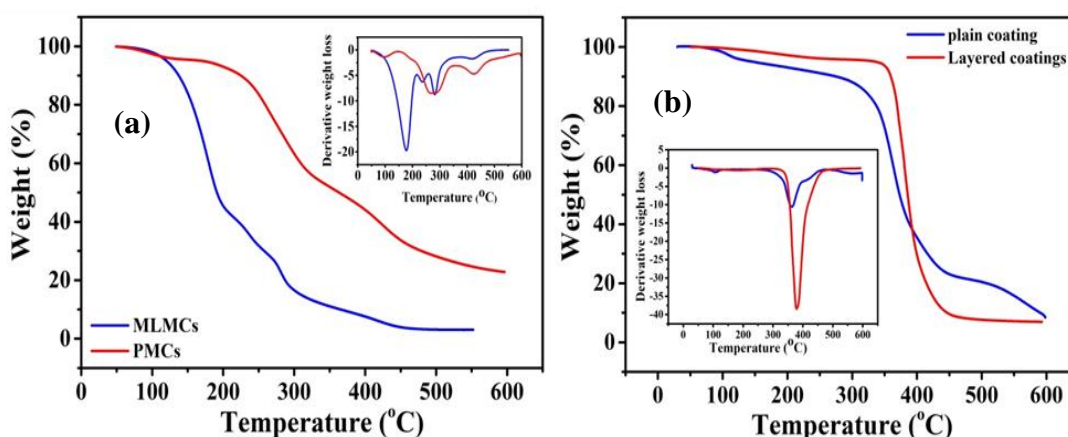


Figure 20: Thermal stability analysis (TGA) of (a) MLMCs [27] and PMCs (b) the plain and layered coatings

3.7 Measurement of self- releasing of DOC and PTU from MLUFMCs and PMCs in response to pH change

Fig. 21 shows the release of DOC from the MLUFMCs in response to pH change. MLUFMCs were dipped into 0.1 molar NaCl solution having five different pH values (2, 5, 7, 9, 11) and then UV-vis spectroscopy was under taken at each pH value for different time intervals (24, 48 and 72 h). After 24 h of immersion of MLUFMCs in the solution, no absorption peak was detected at any pH value (Fig. 21(a)). However, after 48 h (Fig. 21(b)) of immersion, the absorption peak at 280 nm in pH 2 indicates DOC release from the MLUFMCs. At this pH the NH_2 of DOC changes to NH_3^+

which facilitates the release of DOC. After 72 h (Fig. 21(c)) in pH 2, the intensity of the peak increased compared to 48 h, which demonstrates an increase of the amount of inhibitor released with time. Thus, the results obtained at pH 2 confirm that the release of the impregnated DOC in MLUFMCs is a time-dependent process. Furthermore, DOC release is pH sensitive, but the most efficient release was noticed only in acidic environment (pH 2).

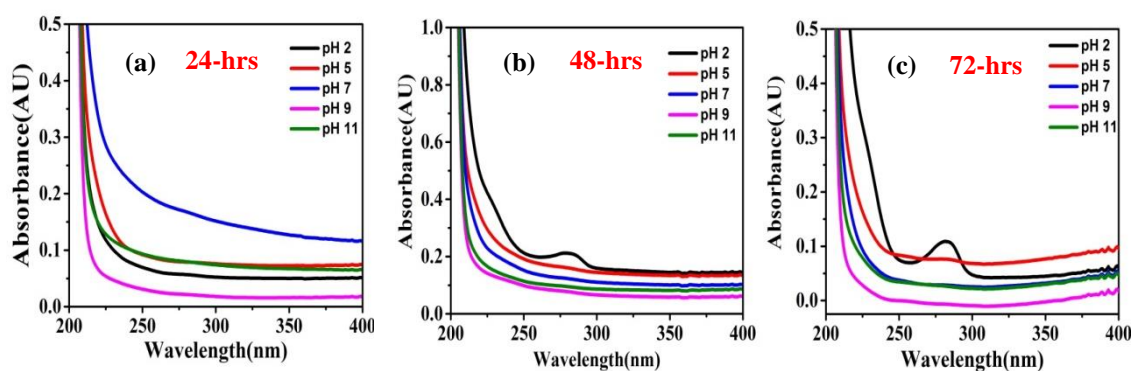


Figure 21: UV-vis spectra of the MLUFMCs immersed in 0.1 M NaCl solutions having various pH values after (a) 24 h (b) 48 h and (c) 72 h.

Furthermore for the second set of the capsules, UV-vis spectroscopy was also used to study the release behavior of the inhibitor from the multilayered microcapsules with different time intervals. The UV spectra were recorded after dipping the PMCs in 0.1 M NaCl solutions of pH 2, 5, 7, 9, 11 after different periods: 2, 24 and 48 h - figure 22. The absorbance intensity changes with pH after 24 and 48 h and as shown in the figure 22(b, c). The absorbance value at ~ 303 nm represents the protonation of phenylthiourea and hence confirmed the presence of inhibitor in solution. It can be noticed that the relative absorption peak intensity increased after 24 and 48 h (figure 22 (b, c)). Furthermore there was a more dominant absorption at pH 2, 9 and 11

compared to pH 5 and 7, which showed that the release of PTU seemed to occur preferentially in both acidic and alkaline medium. The intensity of the peaks increased with time, which evidenced the time dependent release behavior of the inhibitors from the PMCs.

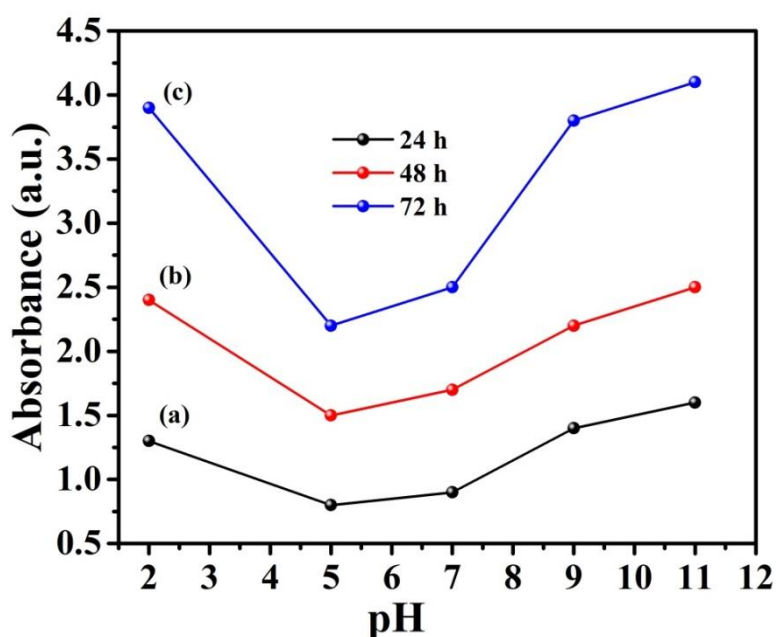


Figure 22: UV spectroscopy of polyelectrolyte multilayered microcapsules after (a) 24 h (b) 48 h (c) 72 h of the immersion in 0.1 M NaCl solution with different pH values.

3.8 Self-healing of smart coatings

Figure 23 shows the self-healing ability of SLSCs and PMLSCs. The coatings were subjected to controlled damage. In response to the mechanical damage (creation of a scratch in the coatings), the microcapsules present in the coating matrix are ruptured and release the self-healing agent (linalyl acetate), which polymerizes in air and heals

the scratch. Linalyl acetate has the ability to autoxidize when exposed to air, forming sensitizing hyperoxides as it contains oxidizable positions within its chemical structure. Hyperoxides, an epoxide and alcohol have been identified as oxidation products from linalyl acetate. However, 6,7-epoxy-3,7-dimethylocta-1,5-diene-3yl acetate is identified as the secondary oxidation product. A comparison of Figure 23 (a, d) indicates that after 24 h SLSCs have healed significantly, whereas the PMLSCs were partially self-healed. This observation suggests that the self-healing ability of SLSCs is superior to PMLSCs. This is due to the higher amount of self-healing agent (linalyl acetate) present in the UFMCs. It is pertinent to note that SLCs contain UFMCs which are encapsulated with linalyl acetate only, while the PMLSCs have linalyl acetate in the core and loaded dodecylamine in the layers as well. So, with the same weight percent of encapsulated UFMCs (5 wt. %) and MLUFMCs (5 wt. %), SLSCs have more amount of self-healing agent (linalyl acetate) when compared to PMLSCs (because of the only linalyl acetate as a core material in UFMCs) and thus shows better self-healing performance. These findings are consistent with previous results. However, it is worth to note that after 72 h, the PMLSCs have also been self-healed as shown in Figure 23 (e, f) demonstrating successful healing effect.

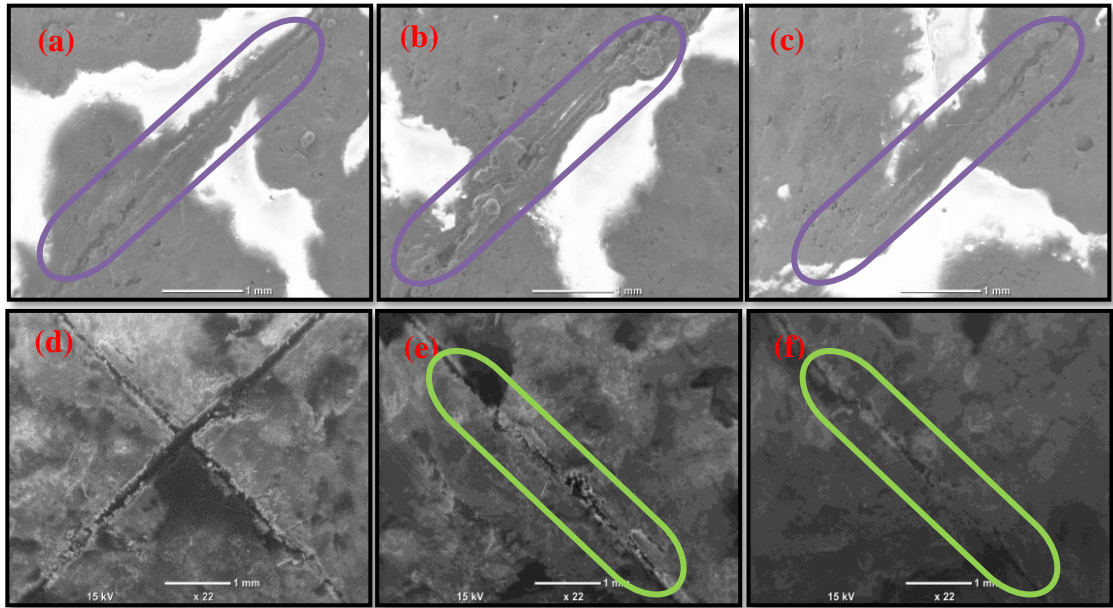


Figure 23: SEM images of the scratched samples (a, b, c) SLSCs after 24, 48 and 72 h. and (d, e, f) PMLSCs after 24, 42 and 72 h.

Also, the self-healing capability of the plain and layered coatings was evaluated by scanning electron microscopy- figure 24. The coatings were subjected to controlled mechanical damage by creating a 5 mm scratch. Under mechanical load, the microcapsules are ruptured and release the core species (linalyl acetate) into the damaged area. This agent is expected to polymerize forming a protective layer that restricts the contact of the substrate with the harsh corrosive environment. Linalyl acetate has the ability to oxidize under contact with air, hence forming hyperoxides, and epoxide. The SEM images of plain coatings (a, b and c) showed the time evolution of the healing process in the scratched area. After 24 h of damage, the scratch seemed healed in both plain and layered coating as shown in figure 24 (b, e). After 48 h, the images evidenced a stable coating healing.

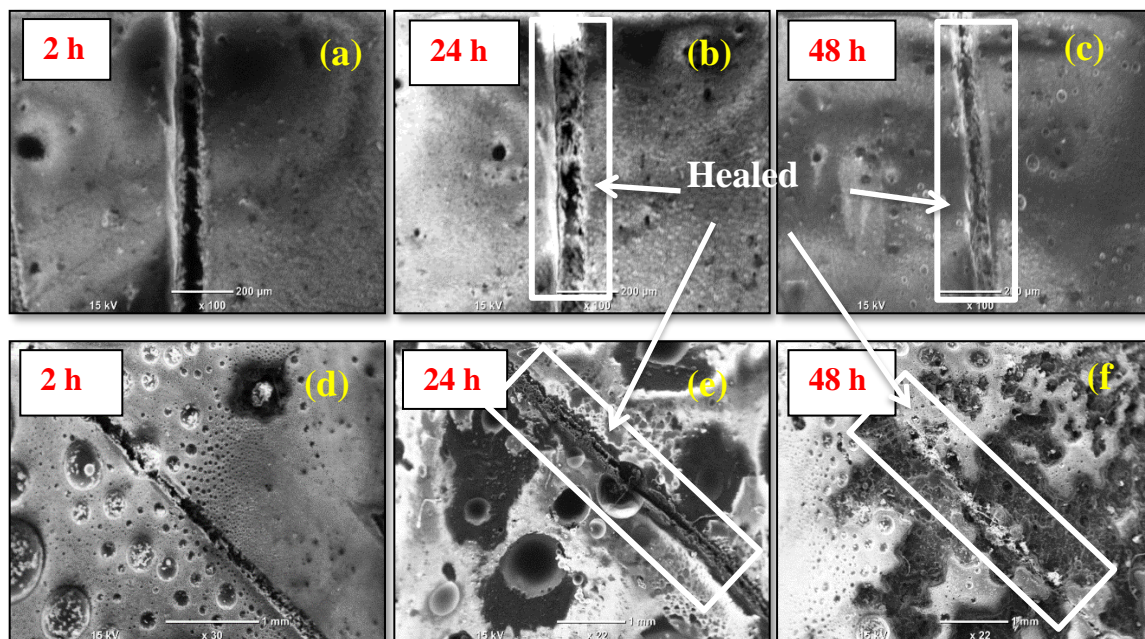


Figure 24: SEM images of the scratched samples (a, b, c) MLMCs and (d, e, f) PMCs after different time intervals.

3.9 Electrochemical Impedance Spectroscopic (EIS) of DOC samples

EIS analysis was performed to investigate the anti-corrosive and consequently the corrosion healing performance of the prepared coatings. The EIS measurements were carried out after the immersion of the scratched samples in 3.5 wt% NaCl solution for 2, 24 and 48 h at room temperature. Bode plots for PECs, SLSCs and PMLSCs are depicted in Figure 25.

Figure 25 show that EIS spectra have a similar shape. Therefore, all coatings seem to display an identical number of time constants that were fitted with an equivalent electric circuit of the two-time constants with mass-controlled diffusion-Figure 26. R_s is the solution resistance, R_{po} is the pore resistance in the intact parts of the coating,

R_{ct} represents the charge transfer resistance at the steel interface (pores and scratched areas). The constant phase elements related to double layer capacitance and coating capacitance are represented by CPE_{dl} and CPE_c , respectively. The Warburg diffusion element (W) illustrates the presence of mass transport. The combination of CPE_{dl} and R_{ct} was used to fit the low frequency time constant and can be assigned to the steel/coating interface. The high frequency time constant (CPE_{coat} and R_{po}) accounts for the barrier properties of the coated areas.

Table 2 contains the charge transfer resistance values acquired from fitting the measured EIS data of the coatings. Figure 25(a, b) and Table 1 reveal that after 2 h of immersion, the SLSCs and PMLSCs show higher values of R_{ct} i.e. 10.3×10^4 and $81.9 \times 10^3 \Omega cm^2$, respectively, compared to the PECs samples ($43.1 \times 10^3 \Omega cm^2$). The higher R_{ct} values of the SLSCs and PMLSCs indicate better corrosion protection of both coatings. This effect is probably related to rupture of the microcapsules during scratching and release of linalyl acetate that, in turn, is oxidized by the atmospheric oxygen, which results in healing the scratched area of the coating by formation of a stable film as explained above in section 3.8. However, the lower R_{ct} value of PMLSCs, as shown in Table 1, might be related to the complex layered structure of PLUFMCs, which slows down the release of linalyl acetate from the microcapsules and the inhibitor.

PECs sample shows a lower R_{ct} value of $20.6 \times 10^3 \Omega cm^2$ after 24 h (Figure 25c) compared to the corresponding value after 2 h, which keeps decreasing upon prolongation of the immersion time (up to 48 h) - Figure 25e and Table 2. This expected trend is due to continuous corrosion activity as no inhibitor or healing agent

is present. The R_{ct} value obtained for the SLSCs increases by about 67 % after 24 h immersion, while that of the PMLSCs rises by about 82 % (see Figure 25c and Table 2). The higher R_{ct} value for the coating containing the multilayered capsules indicates that the corrosion inhibitor and the self-healing agent encapsulated in the multilayers of the synthesized capsules were released as consequence of the scratch and local pH acidification caused by hydrolysis of iron ions released due to corrosion. It can be noticed that the PMLSCs show further increase in the R_{ct} value, with a major shift in the phase angle compared to the corresponding value after 24 h of immersion due to further release of corrosion inhibitor (dodecylamine) to the scratched area leading to inhibition of the corrosion activity. The higher R_{ct} value ($25.2 \times 10^6 \Omega \text{cm}^2$) can be attributed to effective release of inhibitor and simultaneous formation of the healing film.

The charge transfer resistance is increasing in the SLSCs and PMLSCs with time (from 2 h of immersion to 24 h) due to the release of dodecylamine as well as release of linalyl acetate, both forming protective species. The R_{ct} values showed further increase for the PMLSCs compared to SLSCs due to the double action of the PMLSCs coatings that comes from the polymer healing effect and corrosion inhibition of steel). In fact, the damaged area, even after healing by linalyl acetate still contains some micro defects and may not avoid totally the corrosion activity. Hence, after 24 h of the scratch the corrosion process slowly progresses, and the pH of the surrounding medium acidifies due to hydrolysis of Fe cations and effect that stimulates the release of dodecylamine from the polyelectrolyte layers. The results obtained in the present work are in line with the previous reported literature.

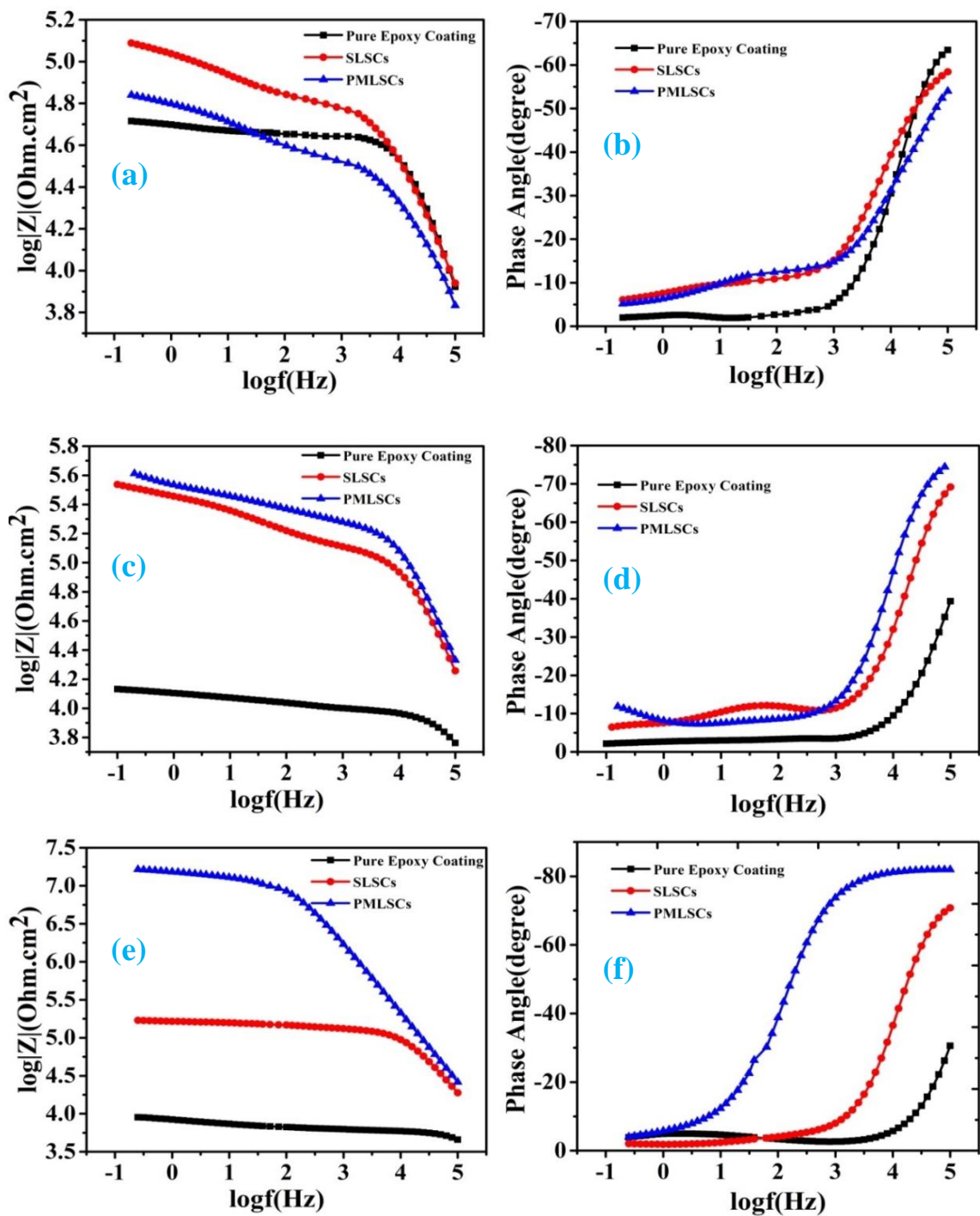


Figure 25: (a, c and e) Bode and (b, d and f) the corresponding phase angle plots for the scratched coated specimens with PECs (epoxy resin only), SLSCs (epoxy loaded with 5 wt% of the UFMCS) and PMLSCs (epoxy loaded with 5 wt% of the MLUFMCS) after immersion in

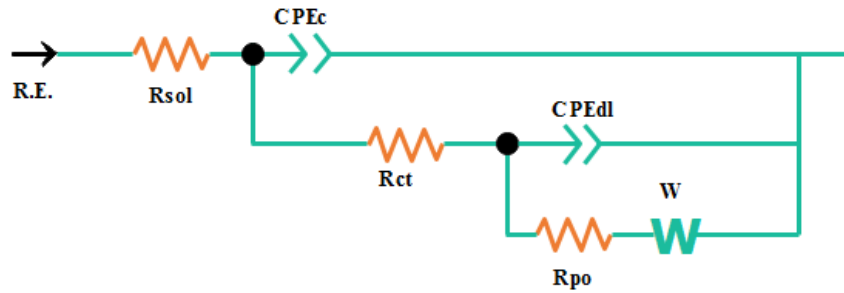


Figure 26: Electrochemical equivalent electric circuit obtained from fitting the impedance data.

Table 2: Electrochemical parameters obtained by fitting the measured impedance data shown in Figure 12 of the scratched coated specimens immersed in 3.5 wt.% NaCl solution.

Coatings	Time (h)	R_{ct} ($\Omega \cdot \text{cm}^2$)
PECs		43.1×10^3
SLSCs	2	10.3×10^4
PMLSCs		81.9×10^3
PECs		20.6×10^3
SLSCs	24	31.5×10^4
PMLSCs		46.8×10^4
PECs		10.8×10^3
SLSCs	48	12.2×10^4
PMLSCs		25.2×10^6

3.10 Electrochemical Impedance Spectroscopic (EIS) of PTU samples

EIS technique has been utilized as an influential technique for studying the corrosion performance of various numbers of applications such as material selection, corrosion inhibitors and coatings. Figure 27 represent the equivalent circuits (ECs), which are applied to analyze and fit the measured data. A two-time constant equivalent circuit, which is commonly used for analyzing electrodes undergoing simple coating layer, is depicted in Figure 27 (a). Intriguingly, a three-time constant equivalent circuit (Figure 27 (b)) which is used for electrodes with coatings and some other influences on the ions transfer and resistivity of the prepared layer on top. The parameters of the electrochemical reactions occurring at the metal/solution interface can be measured and calculated from the EIS Nyquist and bode plots, e.g., the solution resistance (R_s), pore resistance (R_{po}), constant phase elements (CPE), warburg diffusion coefficient (W), charge transfer resistance (R_1 and R_2).

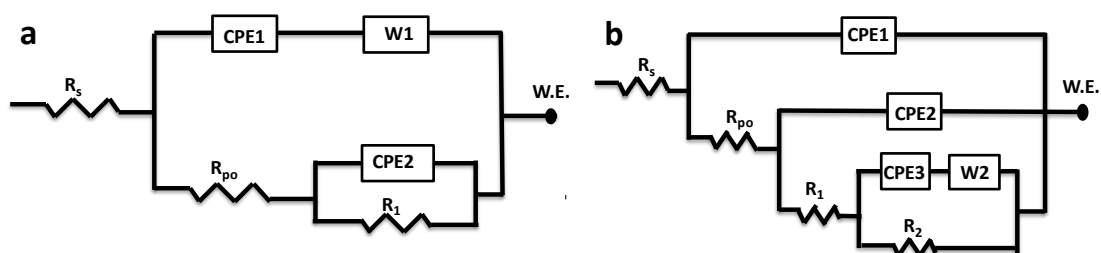


Figure 27: Electrochemical equivalent circuit used to fit the impedance data.

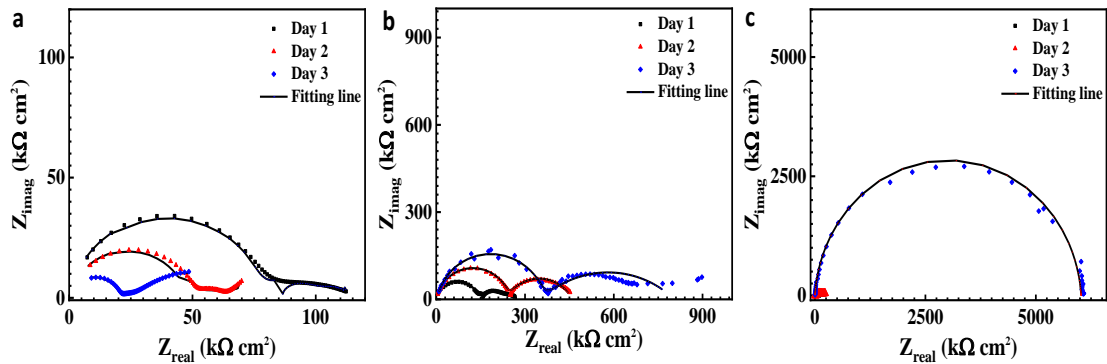


Figure 28: Nyquist plots for the measured EIS data (symbols) and their fittings (solid lines) using the EC shown in Figure 27 for different epoxy resin exposed in 3.5% NaCl solution for different exposure time a) neat coating, b) plain coating, and c) layered coatings

The fitted results of charge transfer resistances (R_1 and R_2), the constant phase elements (Y_1 and Y_2) and Warburg diffusion coefficient (W), are seen in Table 3. The obtained results show that the constant phase element decreases as the resistance values increase with the increasing number of layer or inhibitor composition, which are due to the increase in the thickness of the protecting layer on the metal/solution interface. It is obvious that the Nyquist and Bode plots for all the same coating material content has the same behavior after different exposure time. A comparison of the charge transfer resistance recorded data in Table 3 indicates the increasing corrosion inhibition behavior of mild steel with increasing layer content. It is obvious that the decrease of CPE values indicates an increase in the area or the thickness of the electrical double layer. EIS test was used to analyze the corrosion impeding quality of the coatings. The corrosion protection property of the coating is directly related to the impedance value of at low frequency. Higher the value at low frequency

better will be the corrosion protection capability and vice versa. Figure 29 shows the EIS spectra and the corresponding phase angle of the developed coatings.

Three types of steel coated samples were tested, one control sample which is blank epoxy coating and two test samples (UF and multilayered UF microcapsules coatings). For the test samples 4 wt % of the microcapsules were dispersed into the epoxy matrix and EIS test was conducted of the cured steel coated samples. Figure 29 (a) shows the EIS spectra, after the immersion of 2 hours of scratched coated samples. The scratched pure epoxy coating showed comparatively less resistance at low frequency. The UF microcapsules showed higher impedance than that of the layered microcapsules coating after 2 hours because of the complex structure and the multilayered microcapsules. The self-healing agent (linalyl acetate) is completely released in the damaged part in case of UF microcapsules while in that of multilayered microcapsules it takes time to release the complete core materials because of the deposited polyelectrolyte layers above the UF microcapsules. The low impedance of the multilayered microcapsules coating, after 2 hours also confirms that the corrosion inhibitor (PTU) is not released from the polyelectrolyte layers.

In figure 29 (c) , the EIS spectra of the scratched sample after 24 hours of the immersion in the NaCl represents that the corrosion impedance of multilayered UF microcapsules coating is higher than that of the UF microcapsules coating due the efficient release of PTU (inhibitor) and the core self-healing agent (linalyl acetate). The blank epoxy coating showed decrease in the impedance value at low frequency which clearly demonstrates the initiation of the corrosion process after 24 hours.

After 48 hours of the immersion, Figure 29(e) represents the EIS spectra of the scratched coatings. The multilayered UF microcapsules showed further increase in the impedance illustrating the effects of the releasing PTU on the resistance of corrosion process. The UF microcapsules coating showed a slight decrease in the impedance value which shows the diffusion of the corrosive species from the outside medium. This diffusion in the scratch area shows the discontinuity of the auto oxidized linalyl acetate in the damaged area.

Table 3: Electrochemical Impedance Parameters for different coatings in 3.5% NaCl

layer	Exposure time, days	R_s , $k\Omega$ cm^{-2}	R_{po} , $k\Omega$ cm^{-2}	Y_{po} $\times 10^{-6}$ $s^n \Omega^{-1}$ cm^{-2}	R_1 , $k\Omega$ cm^{-2}	$Y_1 \times 10^{-12}$ $s^n \Omega^{-1}$ cm^{-2}	R_2 , $k\Omega$ cm^{-2}	Y_2 $\times 10^{-3}$ $s^n \Omega^{-1}$ cm^{-2}	$W \times 10^{-6}$ $s^n \Omega^{-1}$ cm^{-2}
Epoxy	1 st	1.67	48.77	3.53	67.78	160.2	----	----	----
	2 nd	0.21	12.45	2.14	51.34	449.3	----	----	----
	3 rd	1.57	7.73	101.2	18.7	269.6	49.3	1.01	32.5
UFMCs	1 st	1.96	162.2	0.942	123.4	123.7	----	----	----
	2 nd	0.67	139.6	0.573	16.19	189.46	199.4	1.03	7.89
	3 rd	1.74	214.3	0.197	242	247.9	----	----	----
PLFMCs	1 st	0.34	95.2	1.71	94.88	342.1	179.1	1.51	0.193
	2 nd	0.99	347.9	624.9	83.98	868.8	2200	1.06	8.31
	3 rd	0.13	----	----	6025	164.7	----	----	----

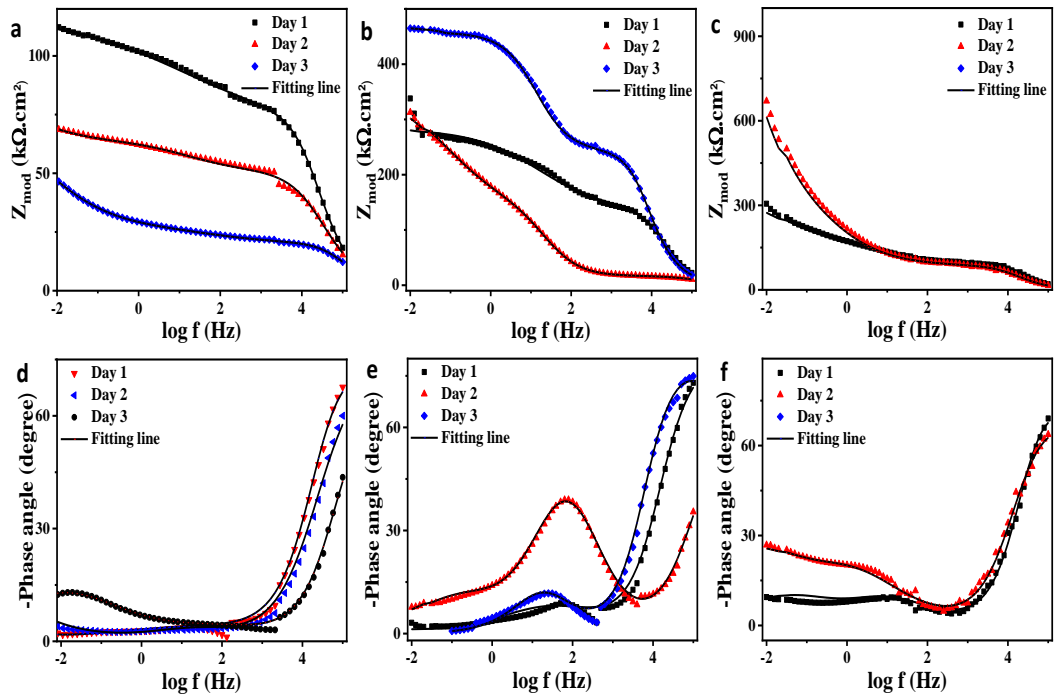


Figure 29: Bode plots for the measured EIS data (symbols) and their fittings (solid lines) using the EC shown in Figure 2 for for different epoxy resin exposed in 3.5% NaCl solution for different exposure time (a, b) pure epoxy resin, (c, d) single layer, and (e, f) multi-layer

A comparison of the anticorrosive properties of the coatings developed within this work with those already reported literature is presented in Table 4. The comparative analysis demonstrates that the coatings developed in the present work possess superior anti-corrosive performance, an effect that can be attributed to the novel chemistry of the polyelectrolyte multilayered urea formaldehyde microcapsules, selection of the selected inhibitors (DOC and PTU), self-healing agent (linalyl acetate) and their efficient release in response to the external stimuli. The two

protective mechanisms are independently and simultaneously occurring in the developed coatings and hence, increasing the corrosion protection performance of the smart coatings. The enhanced anticorrosion performance makes this composite coating an interesting option to protect steel components used in the oil and gas as well as other related industries.

Table 4: Comparison of the present coatings with the previous results in terms of corrosion impedance values.

S.No	Coatings	Immersion time	Rct	Reference	
1	Blank Epoxy	2 hr.	$4.3 \times 10^4 \Omega$	Present work	
		24 hr.	$2.0 \times 10^4 \Omega$		
		48 hr.	$1.0 \times 10^4 \Omega$		
	Epoxy with UF microcapsules	2hr.	$1.0 \times 10^5 \Omega$		
		24 hr.	$3.1 \times 10^5 \Omega$		
		48 hr.	$1.2 \times 10^5 \Omega$		
		Epoxy with multilayered microcapsules	2hr.		$8.1 \times 10^4 \Omega$
			24 hr.		$4.6 \times 10^5 \Omega$
		(UF/PEI/SPEEK/DOC/SPEEK/PEI)	48 hr.		$2.5 \times 10^7 \Omega$
(UF/PEI/SPEEK/PTU/SPEEK/PEI)	48hr	$6.0 \times 10^6 \Omega$			
2	Blank Epoxy	7 hr.	$1.4 \times 10^3 \Omega$	E.M. Fayyad et al [10]	
	Epoxy with UF microcapsules	7 hr.	$8.9 \times 10^4 \Omega$		

S.No	Coatings	Immersion time	Rct	Reference
3	Blank Epoxy	2 hr.	$7.5 \times 10^3 \Omega$	D. Abrantes et al [37]
		24 hr.	$4.7 \times 10^3 \Omega$	
	Epoxy with UF microcapsules	2 hr.	$1.9 \times 10^4 \Omega$	
		24 hr.	$1.2 \times 10^4 \Omega$	
	Epoxy with multilayered microcapsules (UF/PEI/PSS/BTZ/PSS/PEI)	2 hr.	$1.1 \times 10^4 \Omega$	
		24 hr.	$3.5 \times 10^4 \Omega$	
4	Blank Epoxy	24 hr.	$1.4 \times 10^5 \Omega$	X. Liu et al [41]
		48 hr.	$6.6 \times 10^4 \Omega$	
	Epoxy with CeO ₂ capsules	24 hr.		
		48 hr.	$4 \times 10^5 \Omega$	
			$7.4 \times 10^5 \Omega$	
5	Multilayered with benzotriazole (UF/PEI/PSS/benzotriazole/PSS/PEI)	48h	4.54×10^3	
6	CeO ₂ / benzotriazole /(PEI/PSS) ²	48h	3.33×10^4	

CHAPTER 4: CONCLUSIONS AND FUTURE RECOMMENDATIONS

4.1 Conclusion

In this thesis work, initially urea formaldehyde microcapsules (UFMCs) were synthesized with encapsulated self-healing agent (linalyl acetate). Novel multilayered microcapsules (PMLMCs) having self-healing specie as a core material and corrosion inhibitor entrapped in the layers were synthesized using layer by layer technique. Single layer smart coatings (SLSCs) and polyelectrolyte multilayered smart coatings (PMSCs) were prepared by reinforcing these microcapsules in the polymeric matrix and applying on carbon steel substrate, respectively. Two different corrosion inhibitors (dodecylamine and phenylthiourea) are used separately in the layered design of the multilayered microcapsules. It can be concluded that PMLSCs demonstrate improved thermal and superior anticorrosion properties compared to SLSCs. This enhancement can be attributed to the efficient release of the encapsulated self-healing species, linalyl acetate, and corrosion inhibitor (dodecylamine and phenylthiourea) entrapped in polyelectrolyte layers of the multilayered microcapsules. The healing effect of linalyl acetate was evidenced by the slow repair of scratches formed on the surface, while the inhibitive action of dodecylamine and phenylthiourea has been confirmed by the increased resistances determined by electrochemical impedance spectroscopy. Owing to the good thermal and enhanced anticorrosion properties, the novel multilayered microcapsules may be attractive for designing functional coatings for corrosion protection of steel parts.

4.2 Future Recommendations

In view of the current study about multilayered microcapsules, it proved to be a best alternative of using multiple containers in a single polymeric coating matrix. By using polyelectrolyte multilayer microcapsules, we can achieve hybrid function from a single micro container. Furthermore by using SPEEK in the current layers formulation with PEI, made it more polarized which confirms the adsorption of layers on the surface of UFMCs.

The future recommendations include the deposition of this multilayer formulation with different corrosion inhibition on other micro/nano containers and analyze their corrosion inhibition capability. We can also study the synergetic effect of the two corrosion inhibitors in a single nano container reinforced polymeric coatings instead of a self-healing and inhibition properties. One of the future goals can also be to analyze different polyelectrolyte materials (Polystyrene sulfonate, Sulfonated poly(ether ether ketone), Polyethyleneimine etc) in multilayer formulation and their effect of the structure of multilayer microcapsules.

REFERENCES

- [1] P. E. Philip A. Schweitzer, *Paint and Coatings: Applications and Corrosion Resistance*, 1st Editio. CRC press, 2005.
- [2] C. K. Lee, “Surface & Coatings Technology Corrosion and wear-corrosion resistance properties of electroless Ni – P coatings on GFRP composite in wind turbine blades,” vol. 202, pp. 4868–4874, 2008.
- [3] K. Ali *et al.*, “Synthesis and Performance Evaluation of Pulse Electrodeposited Ni-AlN Nanocomposite Coatings,” vol. 2018, 2018.
- [4] M. F. Montemor, “Surface & Coatings Technology Functional and smart coatings for corrosion protection: A review of recent advances,” *Surf. Coat. Technol.*, vol. 258, pp. 17–37, 2014.
- [5] R. W. and H. H. U. Revie, *CORROSION AND CORROSION CONTROL An Introduction to Corrosion Science and Engineering*, 4rth ed. A JOHN WILEY & SONS.
- [6] “NACE International ’ s IMPACT Breaks New Ground in the Study of Corrosion Management,” pp. 1–16.
- [7] E. Wang, Wei Xu, Likun Li, Xiangbo Yang, Yi An, “Self-healing properties of protective coatings containing isophorone diisocyanate microcapsules on carbon steel surfaces,” *Corros. Sci. Sci.*, vol. 80, pp. 528–535, 2014.
- [8] B. Soo, H. Cho, S. R. White, and P. V Braun, “Self-Healing Polymer Coatings,” pp. 645–649, 2009.
- [9] S. Lang and Q. Zhou, “Synthesis and characterization of poly(urea-formaldehyde) microcapsules containing linseed oil for self-healing coating

- development,” *Prog. Org. Coatings*, vol. 105, no. November, pp. 99–110, 2017.
- [10] E. M. Fayyad, M. A. Almaadeed, and A. Jones, “Encapsulation of tung oil for self-healing coatings in corrosion applications,” *Sci. Adv. Mater.*, vol. 7, no. 12, pp. 2628–2638, 2015.
- [11] J. M. Falcón, F. F. Batista, and I. V. Aoki, “Encapsulation of dodecylamine corrosion inhibitor on silica nanoparticles,” *Electrochim. Acta*, vol. 124, pp. 109–118, 2014.
- [12] S. T. Selvi, V. Raman, and N. Rajendran, “Corrosion inhibition of mild steel by benzotriazole derivatives in acidic medium,” *J. Appl. Electrochem.*, pp. 1175–1182, 2003.
- [13] J. Wang, A. Singh, M. Talha, X. Luo, X. Deng, and Y. Lin, “Electrochemical and Theoretical Study of Imidazole Derivative as Effective Corrosion Inhibitor for Aluminium,” *Int. J. Electrochem. Sci.*, vol. 13, pp. 11539–11548, 2018.
- [14] S. R. Whites, “Poly(Urea-Formaldehyde) Microencapsulation of Dicyclopentadiene,” no. 6, 2003.
- [15] D. Snihirova, S. V. Lamaka, and M. F. Montemor, “‘SMART’ protective ability of water based epoxy coatings loaded with CaCO₃microbeads impregnated with corrosion inhibitors applied on AA2024 substrates,” *Electrochim. Acta*, vol. 83, pp. 439–447, 2012.
- [16] P. Poornima Vijayan and M. A. S. A. Al-Maadeed, “TiO₂ nanotubes and mesoporous silica as containers in self-healing epoxy coatings,” *Sci. Rep.*, vol. 6, no. November, pp. 1–9, 2016.
- [17] E. Abdullayev and Y. Lvov, “Halloysite clay nanotubes for controlled release


- of protective agents Halloysite Clay Nanotubes for Controlled Release of Protective Agents,” vol. 2, no. September, 2015.
- [18] A. A. Antipov and G. B. Sukhorukov, “Polyelectrolyte multilayer capsules as vehicles with tunable permeability,” vol. 111, pp. 49–61, 2004.
- [19] A. Mechanics and A. Engineering, “In situ poly (urea-formaldehyde) microencapsulation of dicyclopentadiene,” vol. 20, no. 6, pp. 719–730, 2003.
- [20] V. V Tyagi, S. C. Kaushik, S. K. Tyagi, and T. Akiyama, “Development of phase change materials based microencapsulated technology for buildings : A review,” *Renew. Sustain. Energy Rev.*, vol. 15, no. 2, pp. 1373–1391, 2011.
- [21] B. B and B. Š, “Microencapsulation technology and its applications in building construction materials Tehnologija mikrokapsuliranja in njena uporaba v gradbenih materialih,” vol. 55, no. 3, pp. 329–344, 2008.
- [22] “Review on Micro-encapsulated Phase Change Materials (MEPCMs): Fabrication , Characterization and Applications,” vol. 15, no. 8, pp. 3813–3832, 2011.
- [23] H. Huang and X. D. Chen, “Microencapsulation Based on Emulsification for Producing Pharmaceutical Products : A Literature Review,” vol. 14, pp. 515–544, 2006.
- [24] N. V. N. Jyothi, P. M. Prasanna, S. N. Sakarkar, K. S. Prabha, P. S. Ramaiah, and G. Y. Srawan, “Microencapsulation techniques , factors influencing encapsulation efficiency,” vol. 27, no. 3, pp. 187–197, 2010.
- [25] Y. Deyrail, N. Zydowicz, and P. Cassagnau, “Polymer crosslinking controlled by release of catalyst encapsulated in polycarbonate micro-spheres,” vol. 45, pp. 6123–6131, 2004.

- [26] K. S. Mayya, A. Bhattacharyya, and J. Argillier, “Micro-encapsulation by complex coacervation : influence of surfactant †,” vol. 647, no. May 2002, pp. 644–647, 2003.
- [27] W. Lafayette, “Yoon Yeo , Namjin Baek , and Kinam Park * MICROENCAPSULATION METHODS,” pp. 213–230, 2001.
- [28] S. Fabien, “The Manufacture of Microencapsulated Thermal Energy Storage Compounds Suitable for Smart Textile,” vol. 2, no. 2005, 2006.
- [29] A. Jamekhorshid, S. M. Sadrameli, and M. Farid, “A review of microencapsulation methods of phase change materials (PCMs) as a thermal energy storage (TES) medium,” *Renew. Sustain. Energy Rev.*, vol. 31, pp. 531–542, 2014.
- [30] V. Palanivel, “Microencapsulation : A vital technique in novel drug delivery system,” no. May, 2014.
- [31] F. Salau and I. Vroman, “POLYMER Influence of core materials on thermal properties of melamine – formaldehyde microcapsules,” vol. 44, pp. 849–860, 2008.
- [32] P. Report, “Air-Suspension Technique,” no. August, pp. 451–454, 1959.
- [33] H. Sedighikamal, A. Biotech, R. Zarghami, and N. Mostoufi, “Sustained release coating of ibuprofen pellets at Wurster fluidization : statistical approach Sustained release coating of ibuprofen pellets at Wurster fluidization : statistical approach,” no. February, 2015.
- [34] S. Y. A. N. Cheng *et al.*, “Cosmetic textiles with biological benefits : Gelatin microcapsules containing Vitamin C,” pp. 411–419, 2009.
- [35] I. M. Martins, M. F. Barreiro, M. Coelho, and A. E. Rodrigues,


- “Microencapsulation of essential oils with biodegradable polymeric carriers for cosmetic applications,” *Chem. Eng. J.*, vol. 245, pp. 191–200, 2014.
- [36] E. N. Brown and N. R. Sottos, “In situ Poly (Urea-formaldehyde) Microencapsulation of Dicyclopentadiene,” *J. Microencapsul.*, vol. 20, no. 6, pp. 719–730, 2003.
- [37] D. Abrantes, I. C. Riegel-vidotti, M. Guerreiro, S. Ferreira, C. Eliana, and B. Marino, “Smart coating based on double stimuli-responsive microcapsules containing linseed oil and benzotriazole for active corrosion protection,” *Corros. Sci.*, vol. 130, no. April 2017, pp. 56–63, 2018.
- [38] D. G. Shchukin, M. Zheludkevich, K. Yasakau, S. Lamaka, M. G. S. Ferreira, and H. Möhwald, “Layer-by-layer assembled nanocontainers for self-healing corrosion protection,” *Adv. Mater.*, vol. 18, no. 13, pp. 1672–1678, 2006.
- [39] C. Tan, M. J. Selig, M. C. Lee, and A. Abbaspourrad, “Polyelectrolyte microcapsules built on CaCO₃scaffolds for the integration, encapsulation, and controlled release of copigmented anthocyanins,” *Food Chem.*, vol. 246, no. August 2017, pp. 305–312, 2018.
- [40] A. Khan *et al.*, “Synthesis and Properties of Polyelectrolyte Multilayered Microcapsules Reinforced Smart Coatings,” *J. Mater. Sci.*, vol. 54, no. 18, pp. 12079–12094, 2019.
- [41] X. Liu, C. Gu, Z. Wen, and B. Hou, “Improvement of active corrosion protection of carbon steel by water-based epoxy coating with smart CeO₂nanocontainers,” *Prog. Org. Coatings*, vol. 115, no. June 2017, pp. 195–204, 2018.

APPENDICES


APPENDIX A: Poster presentation



كلية الهندسة
College of Engineering
QATAR UNIVERSITY



TÉCNICO LISBOA



Graduate Students
Energy, Environment & Resource Sustainability

Synthesis and Properties of Polyelectrolyte Multilayered Microcapsules Reinforced Smart Coatings

Adnan Khan^{1,4}, Fareeha Ubaid¹, Eman M. Fayyad¹, Zubair Ahmed¹, R. A. Shakoor¹, M. F. Montemor², Ramazan Kahraman³

¹ Center of Advanced Materials (CAM), Qatar University, 2713 Doha, Qatar
² Centro de Química Estrutural (CQE), Instituto Superior Técnico, Universidade de Lisboa, Av. Rovisco Pais, 1049-001 Lisboa, Portugal
³ Department of Chemical Engineering, Qatar University, 2713 Doha, Qatar
⁴ Department of Mechanical and Industrial Engineering, Qatar University, 2713 Doha, Qatar
Corresponding author email: shakoor@qu.edu.qa

Abstract

The present research work focuses on the synthesis, characterization and properties of novel polyelectrolyte multilayered microcapsules used as smart additives in organic coatings for corrosion protection of steel parts. Urea formaldehyde microcapsules encapsulated with linalyl acetate (UFMCs), sensitive to mechanical stimulus, were synthesized by in situ emulsion polymerization technique. In the next step, dodecylamine (DOC), working as a pH stimulus corrosion inhibitor, was loaded into layers of polyelectrolyte molecules, polyethylenimine (PEI) and polyether ether ketone (PEEK). These were applied layer-by-layer over the microcapsules to form inhibitor containing multilayered urea formaldehyde microcapsules (MLUFMCs). In the next step, MLUFMCs (5.0 wt. %) and UFMCs (5.0 wt. %) were thoroughly dispersed into the epoxy resin and coated on cleaned steel. A comparison of the structural, thermal and anticorrosive properties indicates that coatings modified with multilayered capsules (PMLSCs) can be attributed to efficient release of the encapsulated self-healing agent and corrosion inhibitor from the MLUFMCs. Therefore epoxy coatings modified with the novel multilayered capsules may be attractive for corrosion protection of steel parts used in oil & gas and related industries.

Result and Discussion

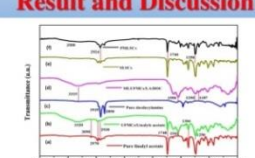


Fig. 1: FTIR spectra of the microcapsules and coatings (a, b) as synthesized UFMCs encapsulated with linalyl acetate and pure linalyl acetate (c, d) MLUFMCs and pure dodecylamine (e, f) PMLSCs and SLSCs.

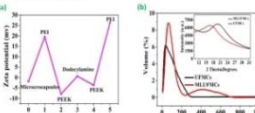


Fig. 2: (a) Zeta potential measurements, (b) Particle size analysis and Inset shows the XRD of the as synthesized microcapsules

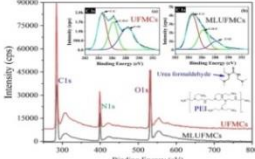


Fig. 3: XPS survey spectra of UFMCs and MLUFMCs samples

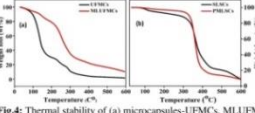


Fig. 4: Thermal stability of (a) microcapsules-UFMCs, MLUFMCs and (b) developed smart coatings-SLSCs and PMLSCs.

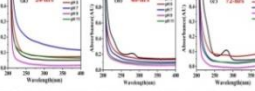


Fig. 5: UV-vis spectra of the MLUFMCs immersed in 0.1 M NaCl solutions having various pH values after (a) 24 h (b) 48 h and (c) 72h.

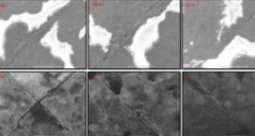


Fig. 6: SEM images of the scratched samples (a, b, c) SLSCs and (d, e, f) PMLSCs

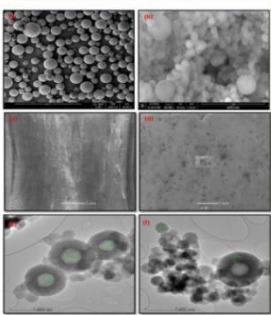


Fig. 7: FE-SEM analysis of microcapsules and smart coatings (a) UFMCs (b) MLUFMCs, (c) SLSCs, (d) PMLSCs and (e, f) HR-TEM of MLUFMCs.

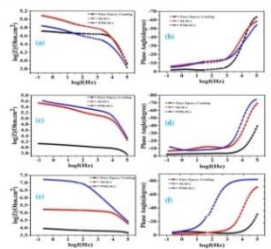
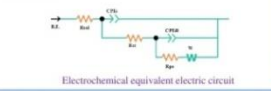



Fig. 8: (a, c and e) Bode and (b, d and f) the corresponding phase angle plots for the scratched coated specimens with PECS, SLSCs and PMLSCs

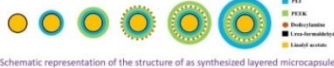


Electrochemical equivalent electric circuit

Experimental



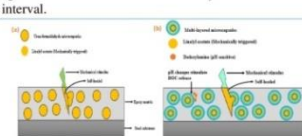
Schematic diagram of the experimental set up for the synthesis of encapsulated urea formaldehyde microcapsules



Schematic representation of the structure of as synthesized layered microcapsules

Preparation of Coatings

- Coatings containing UFMCs and MLUFMCs were prepared using 5.0wt% for direct comparison.
- The thickness of the coatings was 150µm approximately.
- The coatings were subjected to a controlled damage, self healing and corrosion resistance was analyzed after different time interval.




Schematic diagrams of smart coatings (a) SLSCs (b) PMLSCs

Conclusion

- Single layer smart coatings (SLSCs) and polyelectrolyte multilayered smart coatings (PMLSCs) were prepared.
- It can be concluded that PMLSCs demonstrate improved thermal and superior anticorrosion properties compared to SLSCs.
- This enhancement can be attributed to the efficient release of encapsulated self-healing agent, linalyl acetate, and corrosion inhibitor entrapped in polyelectrolyte layers from the MLUFMCs.

Acknowledgment

• This publication was made possible by the NPRP award (NPRP 9-080-2-039) from the Qatar National Research Fund (a member of The Qatar Foundation). The statements made herein are solely the responsibility of the authors.




APPENDIX B: Journal article 1

J Mater Sci (2019) 54:12079–12094

Metals & corrosion



Synthesis and properties of polyelectrolyte multilayered microcapsules reinforced smart coatings

Adnan Khan^{1,5}, Fareeha Ubaid¹, Eman M. Fayyad^{1,6}, Zubair Ahmad¹, R. A. Shakoor^{1,*} , M. F. Montemor², Ramazan Kahraman³, Said Mansour⁴, Mohammad K. Hassan¹, Anwarul Hasan⁵, and Aboubakr M. Abdullah¹

¹Center for Advanced Materials, Qatar University, 2713 Doha, Qatar

²Centro de Química Estrutural, Instituto Superior Técnico, Universidade de Lisboa, Av. Rovisco Pais, 1049-001 Lisboa, Portugal

³Department of Chemical Engineering, Qatar University, 2713 Doha, Qatar

⁴Qatar Energy and Environment Research Institute, Hamad Bin Khalifa University, Qatar Foundation, 34110 Doha, Qatar

⁵Department of Mechanical and Industrial Engineering, Qatar University, 2713 Doha, Qatar

⁶Physical Chemistry Department, National Research Centre, P.O. Box 12622, Dokki, Giza, Egypt

Received: 7 March 2019

Accepted: 4 June 2019

Published online:
17 June 2019

© The Author(s) 2019

ABSTRACT

The present research work focuses on the synthesis, characterization and properties of novel polyelectrolyte multilayered microcapsules used as smart additives in organic coatings for corrosion protection of steel parts. Urea formaldehyde microcapsules encapsulated with linalyl acetate (UFMCs), sensitive to mechanical stimulus, were synthesized by in situ emulsion polymerization technique. In the next step, dodecylamine, working as a pH stimulus corrosion inhibitor, was loaded into layers of polyelectrolyte molecules, polyethylenimine (PEI) and sulfonated polyether ether ketone (SPEEK). These were applied layer-by-layer over the microcapsules to form inhibitor containing multilayered urea formaldehyde microcapsules (MLUFMCs). In the next step, MLUFMCs (5.0 wt%) and UFMCs (5.0 wt%) were thoroughly dispersed into the epoxy resin and coated on cleaned steel. A comparison of the structural, thermal and anticorrosive properties indicates that coatings modified with multilayered capsules (PMLSCs) demonstrate good thermal stability, improved self-healing characteristics and higher corrosion resistance compared to the coating modified with urea formaldehyde microcapsules. The improved properties of PMLSCs can be attributed to efficient release of the encapsulated self-healing agent and corrosion inhibitor from the MLUFMCs. Therefore, epoxy coatings modified with the novel multilayered capsules may be attractive for corrosion protection of steel parts used in oil and gas and related industries.

Address correspondence to E-mail: shakoor@qu.edu.qa

<https://doi.org/10.1007/s10853-019-03761-9>

 Springer

Introduction

Corrosion is one of the primary concerns faced by many industries which cause significant financial damages, wastage of time, efforts and natural resources. In severe situations, corrosion damages may lead to safety threats as well [1]. One of the most effective ways to protect metallic parts from corrosion is by applying organic coatings. Different types of organic coatings have been developed and tested for anticorrosion applications, and it has been demonstrated that the protection depends on the presence of effective anticorrosion pigments and barrier layer efficacy. However, abrasion, micro-scratches, pores and pinholes contribute significantly to cause failures of the protective coatings [2]. During operation, once the barrier layer is disrupted due to any reason, the degradation of the coated metal progresses rapidly. The aforementioned problems can be mitigated and the coating anticorrosive performance can be further enhanced through the application of smart additives. Smart additives-containing coatings, also known as smart coatings, can sense local environmental changes and respond to those stimuli accordingly [3]. Smart coatings have been synthesized and studied by several research groups [4, 5]. Smart coatings can provide self-healing of the polymeric matrix [4, 6–8] or/and healing of the corrosion process [9–14]. Under specific stimulus conditions, the active agents stored into nano/micro-containers can be released to heal the coating or to inhibit corrosion activity. As an example, self-healing coatings containing film forming agents such as linseed oil [15, 16], tung oil [4], silanes [17] and epoxy [6] loaded in carriers can heal micro-scratches and defects by forming a stable film in the defective area [5, 7, 16, 18, 19].

The performance of smart coatings is highly influenced by the nature of the nano/micro-containers that work as storage reservoirs and that can sense certain stimuli [20, 21] such as mechanical load [17], temperature [22], light and pH gradients [7, 23] that are expected to tune the release of the active species. For example, polymerizable species released thanks to capsules rupture can react either with the coating matrix [8], water [24] or oxygen [9], depending on the nature and type of the active agent. The polymerization of the active agents in coating defects repairs the coating and prevents corrosion [8, 17].

Another important and reliable trigger is based on pH gradients [25, 26]. pH-sensitive containers loaded with corrosion inhibitors can be activated by local pH gradients associated with the corrosion activity and release the inhibitor into these active areas, protecting the metal. ZnO [10], SiO₂ nanoparticles [11], halloysite nanotubes [27, 28], TiO₂ nanotubes [29, 30] and others have been used as pH-sensitive carriers of corrosion inhibitors. As an advancement, the use of multiple containers sensitive to similar or distinct stimuli, in a single polymeric coating, has gained significant attention and claimed as more effective corrosion protection route [31, 32]. However, very recently, instead of using multiple containers, double-stimuli-responsive smart microcapsules have been reported as a novel route to mitigate corrosion, while reducing the cost of the protective coating [33].

In the present work, novel polyelectrolyte multilayered microcapsule, with double-stimuli response, is proposed as additives for epoxy coatings to enhance corrosion protection of steel. Urea-formaldehyde microcapsules loaded with linalyl acetate (self-healing agent) were synthesized by in situ emulsion polymerization (UFMCs). Linalyl acetate is released when mechanical stimulus, i.e., an artificial crack is created. Furthermore, dodecylamine, a corrosion inhibitor, was entrapped into the layers of polyelectrolyte materials (PEI and SPEEK), using the layer-by-layer technique to develop pH-sensitive multilayered urea formaldehyde microcapsules (MLUFMCs) [33–37]. The results evidence that coatings modified with MLUFMCs provided increased corrosion resistance. The improvement in corrosion resistance can be attributed to the chemistry of the novel multilayered formulation. In case of SPEEK, deposited as a polyelectrolyte layer, the degree of sulfonation is much higher; hence, the interaction between the polyelectrolyte layers deposited in the current study will be stronger as compared to other polyelectrolyte materials already reported in the literature. This strong interaction between the polyelectrolyte layers will facilitate the entrapment of inhibitor which will be clearly shown in the TEM images presented in the results. The autoxidation phenomenon of linalyl acetate with the atmospheric oxidation makes it more efficient and spontaneous to use a self-healing agent as compared to other self-healing materials already reported, i.e., linseed oil and tung oil, etc. Dodecylamine is an efficient corrosion inhibitor especially in the acidic

medium, and the sustained and controlled release of DOC, in response to an external stimuli, makes it effective to use in the current polyelectrolyte multilayered formulation.

Experimental section

Materials

All the required chemicals, which include urea, ammonium chloride, resorcinol, hydrochloric acid, sodium hydroxide, 37 wt% formaldehyde, ethylene-maleic anhydride copolymer (EMA), dodecylamine, ethanol, sulfonated polyether ether ketone (SPEEK), linalyl acetate and sodium chloride, were purchased from Sigma-Aldrich. Epofix resin along with diethylenetriamine employed as hardener for the resin, dimethylacetamide and polyethylenimine (PEI) were purchased from BDH Chemicals Ltd. Cleaned and polished carbon steel sheet was used as substrates.

Synthesis of urea formaldehyde microcapsules encapsulated with linalyl acetate (LA)

Urea formaldehyde microcapsules encapsulated with linalyl acetate were synthesized by in situ emulsion polymerization method as reported by Brown et al. [38]. A schematic diagram of the experimental set up is presented in Fig. 1. During this process, 200 ml of deionized water was mixed with 50 ml of aqueous solution of EMA (25 wt%). Later, 5.0 g urea, 0.5 g of ammonium chloride and 0.5 g of resorcinol were added to the solution and thoroughly mixed using an overhead mechanical stirrer to form a homogenous solution. The pH of the solution was adjusted at approximately 3.0 using NaOH and/or HCl. After maintaining the desired pH, 50 ml of linalyl acetate was added to the solution and left to stabilize for 10 min under continuous stirring at 400 rpm. This stirring resulted in homogeneous mixing of the ingredients. Then 13.0 g of aqueous formaldehyde (37.0 wt%) was added to the solution, and the temperature was slowly increased until it reached to 55 °C, leading to encapsulation of linalyl acetate into the urea formaldehyde. The temperature of the solution was kept constant during the entire encapsulation process using a temperature-controlled

water bath. After obtaining the desired encapsulation temperature (55 °C), the stirring speed was increased to 1000 rpm to obtain medium size of the urea formaldehyde microcapsules encapsulated with linalyl acetate (UFMCs). It is pertinent to mention here that size of UFMCs is highly influenced by the stirring speed. The continuous stirring of the solution for 4 h employing 1000 rpm at 55 °C resulted in a suspension containing UFMCs. The suspension was then vacuum-filtered to obtain UFMCs, which were thoroughly rinsed with water and dried at room temperature.

Synthesis of multilayered microcapsules impregnated with dodecylamine (DOC)

The layer-by-layer technique was used to coat layers of the polyelectrolytes SPEEK and PEI on the surface of the UFMCs. The positively charged polyelectrolyte PEI was first coated on the surface of the UFMCs by mixing 40 ml microcapsules suspension with 60.0 ml of PEI solution (2.0 mg ml^{-1}) for 10.0 min at 300 rpm. To remove the excess PEI, the mixture was centrifuged and then washed three times with distilled water. Then a negatively charged polyelectrolyte SPEEK layer was assembled on the positively charged polyelectrolyte PEI by adding 40 ml suspension of the above prepared microcapsules (microcapsule + PEI) to 60.0 ml of the SPEEK solution. The suspension was continuously stirred at 300 rpm for 10 min. Excessive amount of the SPEEK was removed through centrifuging process similar to the first layer. The SPEEK solution was formed by dissolving SPEEK in the dimethylacetamide using concentration of 2.0 mg ml^{-1} at room temperature. To completely absorb the SPEEK and to form a homogeneous solution, the mixture was stirred for 10.0 min at 300 rpm [39]. The third layer, composed of positively charged dodecylamine (DOC), was prepared by adding the 40.0 ml solution of above-synthesized microcapsules (microcapsules + PEI + SPEEK) with the 60.0 ml solution of dodecylamine (10.0 mg ml^{-1}), adjusting the pH to 3 and stirring the mixture for 20 min at 300 rpm. The fourth layer, SPEEK, and the fifth layer, PEI, were deposited on the shell of the microcapsules containing DOC, respectively, using the same procedure described earlier. Finally, polyelectrolyte multilayered urea formaldehyde microcapsules (MLUFMCs) were

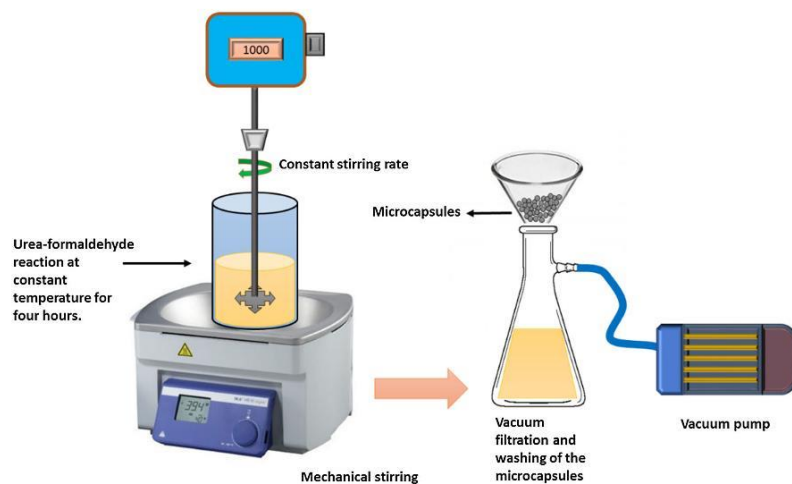


Figure 1 Schematic diagram of the experimental set up for the synthesis of encapsulated urea formaldehyde microcapsules (UFMCs).

obtained. The steps of synthesis of UFMCs are schematically shown in Fig. 2.

Preparation of coated specimens

Cleaned carbon steel specimens were ground using different SiC abrasive papers (180, 400, 800, 1000 and 1200 grits), washed with distilled water, degreased in acetone, washed again with distilled water and dried with air. For comparative purposes, three types of coatings were prepared using doctor blade technique; (1) pure epoxy coatings without any microcapsules referred as PEC (2) coatings containing UFMCs referred as SLSCs and (3) coatings containing MLUFMCs designated as PMLSCs. For a direct comparison purpose, 5.0 wt% of each type of microcapsules were uniformly dispersed in the epoxy, mixed with the hardener in the same stoichiometric ratio and finally sonicated for 10 min at room temperature to remove the air bubbles. Finally, coatings

of approximately 120 μm thickness were applied on cleaned carbon steel substrates using a doctor blade. The coated specimens were cured at room temperature for 24 h. The schematic diagrams of SLSCs and PMLSCs are shown in Fig. 3.

Characterization of microcapsules and coatings

The presence of polyelectrolyte layers, self-healing species and corrosion inhibitor in the microcapsules was confirmed through FTIR analysis. The analysis was carried out using the FTIR Frontier (PerkinElmer, Frontier, USA) instrument, and the spectra were recorded in the range of 4000 to 500 cm^{-1} . The charge of multilayers was determined employing zeta potential equipment (Malvern, Zeta sizer, Nano ZSP, USA).

The presence of polyelectrolyte layers on the surface of microcapsules and their chemical composition

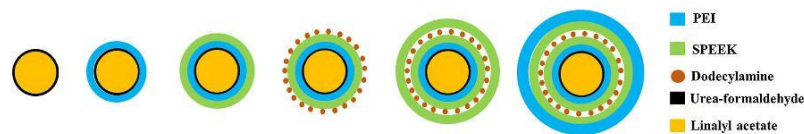


Figure 2 Schematic representation of the structure of as-synthesized layered microcapsules.

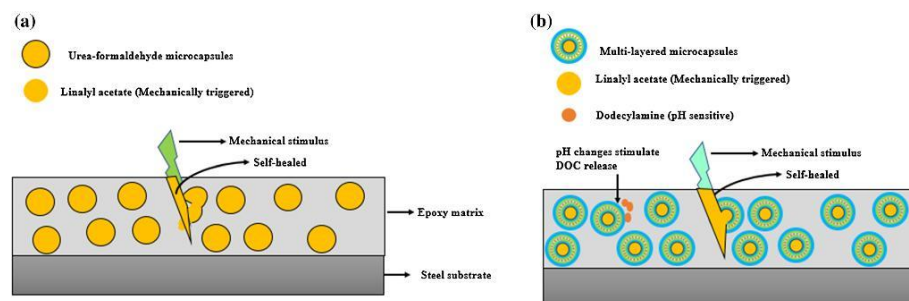


Figure 3 Schematic diagrams of smart coatings **a** modified with UFMCs referred to as SLSCs **b** modified with polyelectrolyte multilayered capsules (PMLSCs).

was further confirmed by XPS (AXIS Ultra DLD, Kratos, UK) employing monochromatic X-ray Source–Al K α source; the binding energy of C 1s (284.6 eV) was used as reference. To determine the elemental composition, XPS survey spectra were recorded in the binding energy range of 250 to 800 eV. High-resolution spectra were recorded for C 1s at an energy step size of 0.1 eV at pass energy of 10 eV.

The surface morphology of the synthesized microcapsules UFMCs and MLUFMCs was studied by a field emission scanning electron microscope (FE-SEM-Nova Nano-450, Netherland) and transmission electron microscopy (TEM, FEI, TALOS F200X, USA).

The particle size distribution of the prepared microcapsules was studied using particle size analyzer (Malvern, Master sizer 2000, Panalytical, USA).

The structural and phase analysis of microcapsules was performed through X-ray diffraction analysis using a PAN analytical X'pert Pro Cu (K α), with a scanning rate of 2° min⁻¹ and scanning angle ranging between 10° \leq 2 θ \leq 50°. A TGA synchronization analyzer (PerkinElmer, TGA 4000, USA) was used to analyze the thermal stability of the synthesized microcapsules and the developed coatings in the temperature range 30 °C to 600 °C employing heating rate of 20 °C min⁻¹.

Self-release of the inhibitor encapsulated in nanocontainers was carried out by conducting UV–Vis spectroscopic analysis (LAMBDA 650 UV/Vis Spectrophotometer, PerkinElmer, USA). During this test, small amount of MLUFMCs (0.2 g) was added to 0.1 M NaCl solution to form a suspension. The amount of the released DOC from the MLUFMCs

was measured as a function time at various pH values. The self-healing ability of smart coatings was evaluated using FE-SEM (FE-SEM-Nova Nano-450, Netherland).

The coatings were subjected to a controlled scratch following ASTM D1654 standard procedure and the scratch healing was recorded as a function of time. The corrosion resistance of coatings was studied by EIS in 3.5 wt% NaCl solution using a three-electrode electrochemical cell, using the coated steel sample as working electrode and a graphite rod and Ag/AgCl as counter and reference electrodes, respectively. The EIS analysis was carried out using a Gamry 3000 (30 K BOOSTER Potentiostat/Galvanostat/ZRA, USA). EIS experiments were conducted within a frequency range of 0.1 to 100 kHz, starting from the higher limit toward the lower one, at OCP, and the rms signal was 10 mV.

Results and discussion

FTIR analysis of microcapsules and coatings

FTIR analysis confirmed encapsulation of linalyl acetate in urea formaldehyde microcapsules and the loading of dodecylamine in the polyelectrolyte layers. Figure 4a, b shows the FTIR spectra of UFMCs and pure linalyl acetate. The broad absorption band at 3320 cm⁻¹ shows overlapping of the O–H bond and N–H bonds and can be ascribed to urea–formaldehyde. The O–H bond is shifted to the right side due to the strong C=O dipole force of encapsulated linalyl acetate in the UFMCs. The small sharp peak at

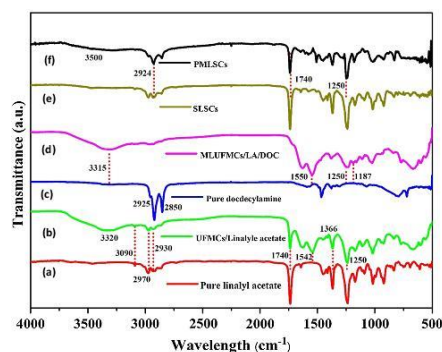


Figure 4 FTIR spectra of the microcapsules and coatings (a, b) as-synthesized UFMCS encapsulated with linalyl acetate and pure linalyl acetate (c, d) MLUFMCS and pure dodecylamine (e, f) PMLSCs and SLSCs.

3090 cm^{-1} represents the C–H bands, while peaks at 2970 cm^{-1} and 2930 cm^{-1} show the presence of C–H₃ and the sharp peak at 1740 cm^{-1} represents the carbonyl C=O bands, which can be associated with linalyl acetate and urea formaldehyde. All these bands confirm the presence of linalyl acetate. However, there is a new peak at 1542 cm^{-1} representing the N–H band and it accounts for the presence of urea–formaldehyde. Moreover, the peak at 1366 cm^{-1} also represents a C–H band with different vibration, while the peak at 1250 cm^{-1} corresponds to the C–N band. It can be noticed that the C–H and C–N vibrations are present in both UFMCS and pure linalyl acetate. The presence of corresponding distinctive absorption bands of N–H at 1542 cm^{-1} (urea formaldehyde), C=O at 1740 cm^{-1} (linalyl acetate) and C–N at 1250 cm^{-1} (linalyl acetate) in the UFMCS confirms efficient storage of linalyl acetate.

Figure 4c, d shows the FTIR spectra of pure dodecylamine (DOC) and MLUFMCS. The broad peak at 3315 cm^{-1} in the MLUFMCS spectrum and a minor sharp peak in the spectrum of pure DOC corresponds to the N–H bonding. The two sharp peaks at 2925 cm^{-1} and 2850 cm^{-1} represent the C–H bonds in DOC and MLUFMCS; however, the peak intensity is high in DOC because of the long C–H chain in the structure of DOC. The peaks present at 1550 cm^{-1} and 1187 cm^{-1} represent C=C and C–O bonds, respectively, which confirms the presence of SPEEK layer on the surface of MLUFMCS. Similarly, the peak at

1250 cm^{-1} can be ascribed to C–N band, which clearly demonstrates the existence of a PEI layer on the MLUFMCS. The presence of corresponding distinctive absorption bands of N–H at 3315 cm^{-1} (DOC), C=C at 1550 cm^{-1} and C–O band at 1187 cm^{-1} (SPEEK) and C–N at 1250 cm^{-1} (PEI) confirms the formation of MLUFMCS and efficient encapsulation of DOC. It is pertinent to note that C–N band at 1250 cm^{-1} overlaps with linalyl acetate as reported previously [40].

Figure 4e, f indicates the FTIR spectrum of PMLSCs and SLSCs. A comparison of FTIR spectra of PMLSCs, SLSCs, UFMCS and MLUFMCS confirms their identical nature. The multiple small peaks present at 2924 cm^{-1} represent the C–H bond and associated with DOC and MLUFMCS. The C=O bond at 1750 cm^{-1} represents the carbonyl C=O group which can be associated with linalyl acetate and urea form aldehyde. Moreover, the sharp peak at 1250 cm^{-1} represents the C–N bond that can be ascribed to urea form aldehyde, DOC and PEI. A small intensity peak at 3500 cm^{-1} indicates an N–H bond, which can be associated with urea form aldehyde, DOC and PEI. A close comparison of the FTIR spectra confirms encapsulation of linalyl acetate in UFMCS and DOC in MLUFMCS. Furthermore, FTIR spectra also confirms the presence of UFMCS and MLUFMCS in SLSCs and PMLSCs without evident side reactions.

Zeta potential measurements of microcapsules

To confirm the polarity of layers on the MLUFMCS, zeta potential of each layer was determined, and the

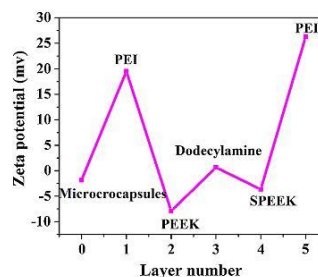


Figure 5 Zeta potential measurements of microcapsules. Layer number 0: microcapsules encapsulated with linalyl acetate (UFMCS) and layers 1–5, MLUFMCS having various polyelectrolyte layers.

results are presented in Fig. 5. It can be noticed that the zeta potential of the UFMCs is negative (~ -1.84 mV). However, when a PEI layer is formed on UFMCs the value of charge shifted to positive value ($\sim +20$ mV) which indicates that the PEI layer carries a positive charge and thus can be easily bonded to the UFMCs. Furthermore, adsorption of SPEEK layer on PEI shifts the charge toward negative value (~ -10.0 mV) confirming its negative polarity. Owing to negatively charged (from the $-\text{SO}_3$ group), the SPEEK layer can be easily bonded to the positively charged underneath PEI layer. Finally, shifting of the potential toward positive value ($\sim +1.0$ mV) due to DOC indicates that it can be easily encapsulated between the SPEEK layers. It can be noticed from Fig. 5 that the surface charge varies according to the deposited layer (PEI, SPEEK, DOC) confirming the adsorption of the corresponding layer. Furthermore, zeta potential is increased by the addition of PEI (cation) on the surface and it decreased with the deposition of SPEEK (anion). A slight increase in zeta potential is observed after the addition of DOC leading to the successful adsorption of DOC. The obtained zeta potential results are consistent with results reported elsewhere [33].

XPS analysis

The XPS survey spectra recorded in the binding energy range of 250 to 800 eV is shown in Fig. 6. XPS measurements with probe depths of up to 10 nm were performed. The major identified elements in the samples are carbon, oxygen and nitrogen. The presence of carbon, oxygen and nitrogen were expected from the chemical composition of the urea formaldehyde and polyethylenimine (PEI) in UFMCs and MLUFMCs, respectively. The high-resolution XPS spectra (C1s) for the UFMCs and MLUFMCs samples are also presented in inset (a) and (b) of Fig. 6, respectively. In C1s spectrum for the both type of samples, the peaks at 284.6 and 286.3 and 288.3 eV refer to C–C bond C–O bond and C=O bond, respectively [41]. The intensity of C–O and C=O bonds peaks in C1s spectrum have significantly been reduced after the adsorption of PEI on the surface of the microcapsules. The positions of the C–O and C=O are not very distinguishable in the encapsulated samples due to the peaks broadening. This indicated that the microcapsules have been encapsulated by the coated materials. As it is obvious from the molecular

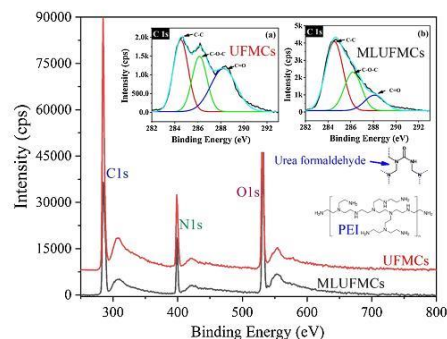


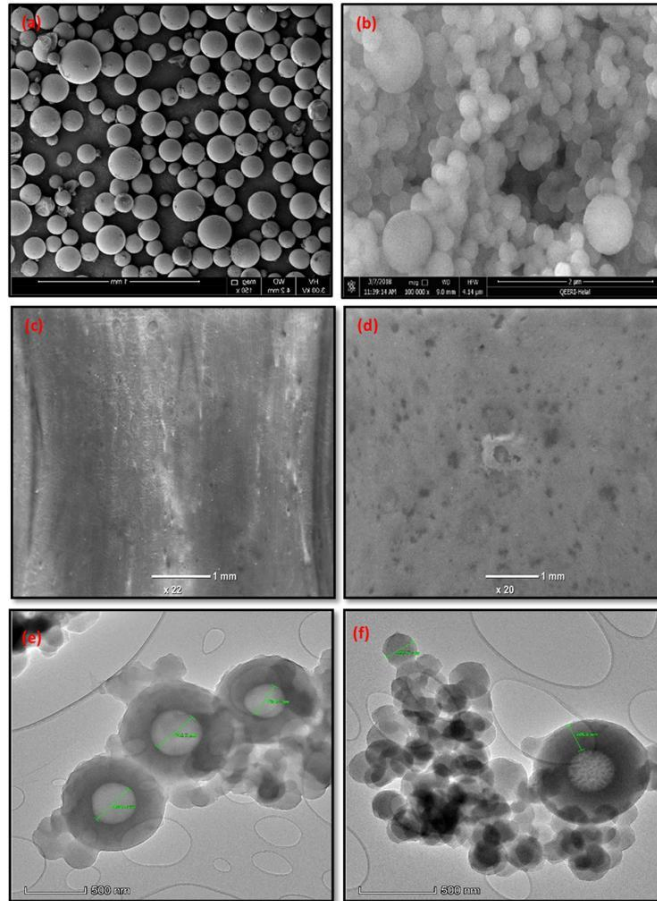
Figure 6 XPS survey spectra of UFMCs and MLUFMCs samples. Insets show the high-resolution XPS spectra C1s of the both UFMCs (a) and MLUFMCs (b) samples. Molecular structures of the urea formaldehyde and PEI are also given in the Figure.

structure of the PEI, it mainly consists of C–C chains and there is no clear existence of C–O and C=O bonds when compared to the urea formaldehyde.

FE-SEM/HR-TEM analysis of the encapsulated and multilayered microcapsules

Field emission scanning electron microscopy (FE-SEM) and high-resolution transmission electron microscopy (HR-TEM) analyses were conducted to study the morphology of the microcapsules (UFMCs, MLUFMCs) and the respective smart coatings (SLSCs, PMLSCs). Figure 7a shows the FE-SEM image of UFMCs. A spherical morphology of the UFMCs with mean diameter $36 \mu\text{m}$ is observed without any crack and porosity. Moreover, a rough surface and variation in the size of microcapsules can also be noticed. In the *in situ* polymerization, the size of the microcapsules depends on the stirring rate [4] and it becomes finer with increasing stirring rate due to high shear force. The rough exterior surface improves the adhesion of the microcapsules to the coating matrix. The complete dryness, high tensile strength and low water absorbing capability of the urea–formaldehyde has led to the formation of more visible and isolated UFMCs. Figure 7b shows the morphology of the MLUFMCs. These multilayered capsules have similar nodular morphology as UFMCs. A significant variation in the size of the

Figure 7 FE-SEM analysis of microcapsules and smart coatings **a** UFMCs **b** MLUFMCs, **c** SLSCs, **d** PMLSCs and **e, f** HR-TEM of MLUFMCs.



MLUFMCs capsules can also be noticed. A change in color may be related to the deposition of polyelectrolyte layers on the encapsulated UFMCs. However, a denser and more diffused structure is achieved in MLUFMCs as compared to UFMCs due to existence of multiple layers of polyelectrolyte materials. Figure 7c, d represents the structure of PMLSCs and SLSCs. It can be noticed that a dense, uniform, crack free and homogeneous structure is preserved in both kind of coatings. It can also be noticed that there are no pore and pin holes present in the coatings.

In order to have more insight of the developed MLUFMCs microcapsules, HR-TEM analysis was undertaken and the results are presented in Fig. 7e, f. It can be clearly noticed that well-defined multilayered nodular structure is preserved. The encapsulation of linalyl acetate and the presence of polyelectrolyte multilayers in MLUFMCs can be clearly noticed. The average core is ~ 350 nm, and the average thickness of polyelectrolyte multilayer is ~ 206 nm. The TEM analysis clearly confirms the formation of MLUFMCs. In TEM analysis, only

smaller-size microcapsules were focused to study morphological features. However, it is pertinent to note that the average particle size of the synthesized MLUFMCs is 65 μm as confirmed by our particle size analysis and discussed in the proceeding section.

Particle size and XRD analysis of the microcapsules

The particle size distribution of the microcapsules is further confirmed with particle size analyzer, and the results are shown in Fig. 8. It can be seen that the particle size of the UFMCs ranges from 0.01 to 500 μm . The majority of the UFMCs are made up of 10–63 μm , and the mean diameter of the UFMCs is found to be 36 μm . Our analysis indicates that the stirring rate of 1000 rpm has resulted in UFMCs having average size of 36 μm . Figure 8 also shows the particle size distribution of MLUFMCs. It can be seen that the mean diameter of MLUFMCs is about 65 μm . The increase in the diameter of MLUFMCs indicates the deposition of polyelectrolyte layers and the inhibitor on the surface of the UFMCs. Furthermore, size variation in MLUFMCs can also be noticed and it is found that majority of the MLUFMCs are made up of size in the range of 10 to 125 μm . The mean diameter of MLUFMCs is found to be 65 μm . These results are consistent with our TEM analysis.

In order to study the effect of polyelectrolyte layers and the surface of microcapsules and the structural analysis of UFMCs and MLUFMCs, XRD analysis was also conducted. Figure 8 inset shows the XRD spectra revealing the amorphous behavior of the UFMCs and MLUFMCs. The peak at 17.5° accounts

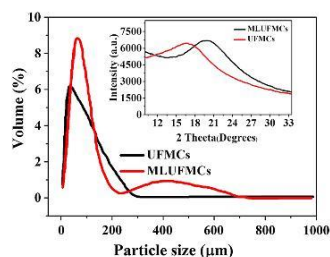


Figure 8 Particle size analysis of as-synthesized urea–formaldehyde microcapsules—UFMCs and multilayered urea–formaldehyde microcapsules—MLUFMCs. Inset shows the XRD of the UFMCs and MLUFMCs.

for the presence of urea–formaldehyde present as the shell material of UFMCs encapsulated with linalyl acetate. Another peak at 22° is observed, with higher intensity, which can be attributed to the deposited polyelectrolyte layers on the surface of UFMCs.

Thermal stability of the microcapsules and epoxy coatings

Thermal stability of encapsulated UFMCs, MLUFMCs, SLSCs and PMLSCs was analyzed using TGA, and the results are presented in Fig. 9 (a, b). It is seen that both UFMCs and MLUFMCs experience a gradual weight loss with increasing temperature up to 600 °C (Fig. 9a). The initial weight loss (50 to 80 °C) may be associated with the removal of the absorbed moisture in the microcapsules. In the next region, the UFMCs show complete weight loss up to 200 °C due to encapsulated linalyl acetate (B.P, 220 °C). However, the MLUFMCs exhibit better thermal stability which can be associated with the presence of high thermally stable polymeric structure (PEI and SPEEK) and dodecylamine. The drop around 200 °C could be due to the loss of sulfonic acid group of the SPEEK. These findings are consistent with previous studies [42]. Figure 9b shows the TGA spectra of the SLSCs and PMLSCs. Like microcapsules, there is small weight loss at the first stage (50 to 80 °C) for only the SLMCs, attributed to the presence of moisture in the coating. A comparison of Fig. 9a, b indicates that SLSCs and PMLSCs demonstrate better thermal stability compared to UFMCs, MLUFMCs which could be linked to the presence of polymeric matrices of the PEI and SPEEK and the long chain of dodecylamine.

Measurement of self-releasing of DOC from MLUFMCs in response to pH change

Figure 10 shows the release of DOC from the MLUFMCs in response to pH change. MLUFMCs were dipped into 0.1 molar NaCl solution having five different pH values (2, 5, 7, 9, 11) and then UV–Vis spectroscopy was undertaken at each pH value for different time intervals (24, 48 and 72 h). After 24 h of immersion of MLUFMCs in the solution, no absorption peak was detected at any pH value (Fig. 10a). However, after 48 h (Fig. 10b) of immersion, the absorption peak at 280 nm in pH 2 indicates DOC release from the MLUFMCs. At this pH, the NH_2 of

Figure 9 Thermal stability of **a** microcapsules—UFMCs, MLUFMCs and **b** developed smart coatings—SLSCs and PMLSCs.

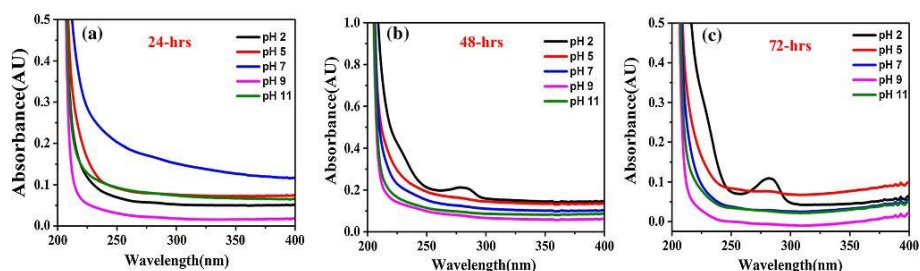
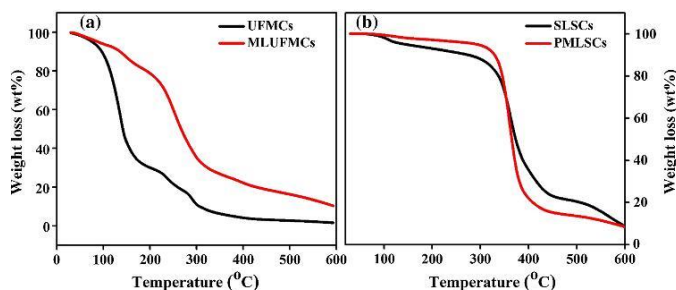


Figure 10 UV-Vis spectra of the MLUFMCs immersed in 0.1 M NaCl solutions having various pH values after **a** 24 h **b** 48 h and **c** 72 h.

DOC changes to NH_3^+ which facilitates the release of DOC. After 72 h (Fig. 10c) in pH 2, the intensity of the peak increased compared to 48 h, which demonstrates an increase in the amount of inhibitor released with time. Thus, the results obtained at pH 2 confirm that the release of the impregnated DOC in MLUFMCs is a time-dependent process. Furthermore, DOC release is pH sensitive, but the most efficient release was noticed only in acidic environment (pH 2).

Self-healing of smart coatings

Figure 11 shows the self-healing ability of SLSCs and PMLSCs. The coatings were subjected to controlled damage. In response to the mechanical damage (creation of a scratch in the coatings), the microcapsules present in the coating matrix are ruptured and release the self-healing agent (linalyl acetate), which polymerizes in air and heals the scratch. Linalyl acetate has the ability to auto-oxidize when exposed to air, forming sensitizing hyperoxides as it contains

oxidizable positions within its chemical structure. Hyperoxides, an epoxide and alcohol have been identified as oxidation products from linalyl acetate. However, 6,7-epoxy-3,7-dimethylocta-1,5-diene-3yl acetate is identified as the secondary oxidation product [43, 44]. A comparison of Fig. 11a, d indicates that after 24 h SLSCs have healed significantly, whereas the PMLSCs were partially self-healed. This observation suggests that the self-healing ability of SLSCs is superior to PMLSCs. This is due to the higher amount of self-healing agent (linalyl acetate) present in the UFMCs. It is pertinent to note that SLSCs contain UFMCs which are encapsulated with linalyl acetate only, while the PMLSCs have linalyl acetate in the core and loaded dodecylamine in the layers as well. So, with the same weight percent of encapsulated UFMCs (5 wt%) and MLUFMCs (5 wt%), SLSCs have more amount of self-healing agent (linalyl acetate) when compared to PMLSCs (because of the only linalyl acetate as a core material in UFMCs) and thus shows better self-healing performance. These findings are consistent with previous

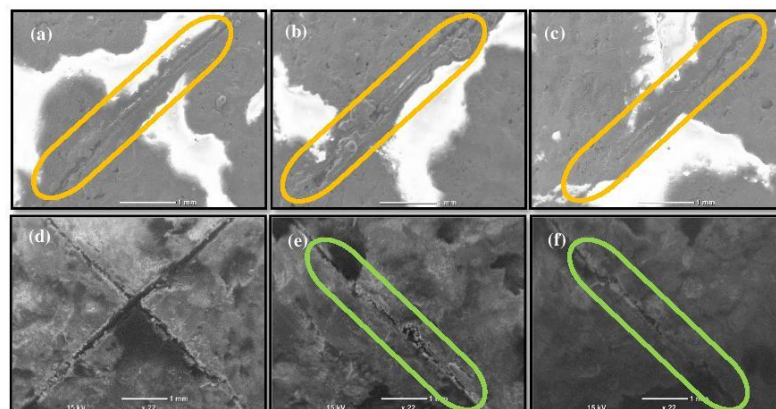


Figure 11 SEM images of the scratched samples (a, b, c) SLSCs after 24, 48 and 72 h. and (d, e, f) PMLSCs after 24, 42 and 72 h.

results [4, 45]. However, it is worth to note that after 72 h, the PMLSCs have also been self-healed as shown in Fig. 11e, f demonstrating successful healing effect.

Electrochemical Impedance Spectroscopy (EIS)

EIS analysis was performed to investigate the anti-corrosive and consequently the corrosion healing performance of the prepared coatings. The EIS measurements were carried out after the immersion of the scratched samples in 3.5 wt% NaCl solution for 2, 24 and 48 h at room temperature. Bode plots for PECs, SLSCs and PMLSCs are depicted in Fig. 12.

Figure 12 show that EIS spectra have a similar shape. Therefore, all coatings seem to display an identical number of time constants that were fitted with an equivalent electric circuit of the two-time constants with mass-controlled diffusion—Fig. 13. R_s is the solution resistance, R_{po} is the pore resistance in the intact parts of the coating, R_{ct} represents the charge transfer resistance at the steel interface (pores and scratched areas). The constant phase elements related to double layer capacitance and coating capacitance are represented by CPE_{dl} and CPE_c , respectively. The Warburg diffusion element (W) illustrates the presence of mass transport. The combination of CPE_{dl} and R_{ct} was used to fit the low-frequency time constant and can be assigned to the

steel/coating interface. The high-frequency time constant (CPE_{coat} and R_{po}) accounts for the barrier properties of the coated areas.

Table 1 contains the charge transfer resistance values acquired from fitting the measured EIS data of the coatings. Figure 12a, b and Table 1 reveal that after 2 h of immersion, the SLSCs and PMLSCs show higher values of R_{ct} , i.e., 10.3×10^4 and $81.9 \times 10^3 \Omega \text{cm}^2$, respectively, compared to the PECs samples ($43.1 \times 10^3 \Omega \text{cm}^2$). The higher R_{ct} values of the SLSCs and PMLSCs indicate better corrosion protection of both coatings. This effect is probably related to rupture of the microcapsules during scratching and release of linalyl acetate that, in turn, is oxidized by the atmospheric oxygen, which results in healing the scratched area of the coating by formation of a stable film as explained above in Sect. 3.8. However, the lower R_{ct} value of PMLSCs, as shown in Table 1, might be related to the complex layered structure of PLUFMCs, which slows down the release of linalyl acetate from the microcapsules and the inhibitor.

PECs sample shows a lower R_{ct} value of $20.6 \times 10^3 \Omega \text{cm}^2$ after 24 h (Fig. 12c) compared to the corresponding value after 2 h, which keeps decreasing upon prolongation of the immersion time (up to 48 h)—Fig. 12e and Table 1. This expected trend is due to continuous corrosion activity as no inhibitor or healing agent is present. The R_{ct} value obtained for the SLSCs increases by about 67% after 24 h immersion, while that of the PMLSCs rises by about 82%

Figure 12 (a, c, e) Bode and (b, d, f) the corresponding phase angle plots for the scratched coated specimens with PECs (epoxy resin only), SLSCs (epoxy loaded with 5 wt% of the UFMCs) and PMLSCs (epoxy loaded with 5 wt% of the MLUFMCs) after immersion in 3.5 wt% NaCl solution at room temperature for 2, 24 and 48 h, respectively.

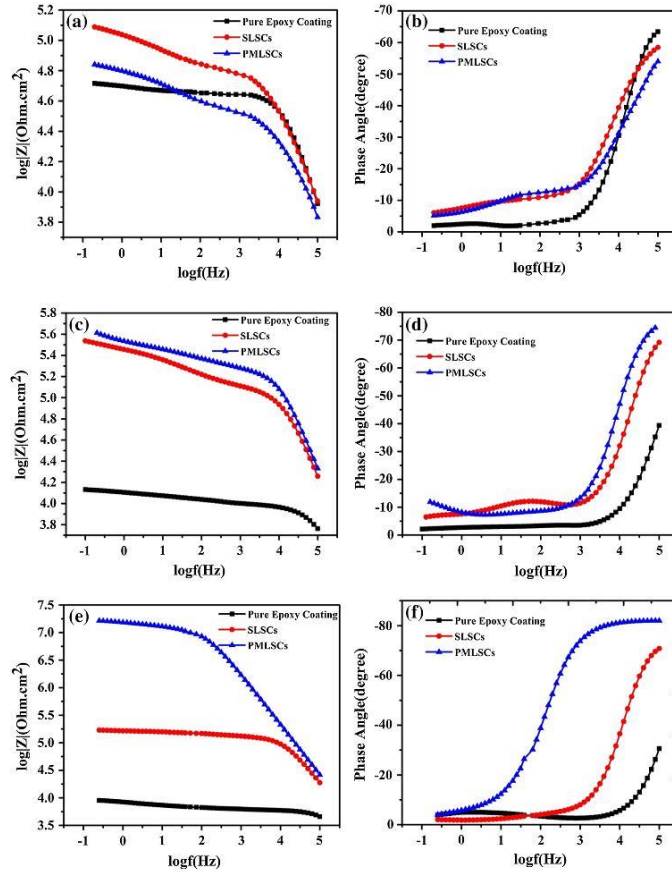
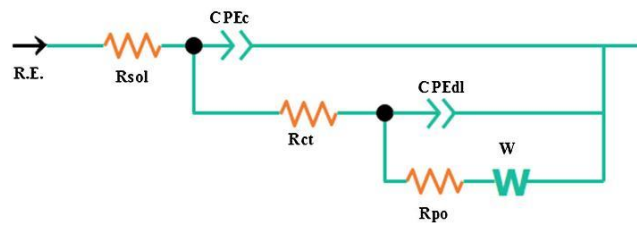


Figure 13 Electrochemical equivalent electric circuit obtained from fitting the impedance data.



(see Fig. 12c and Table 1). The higher R_{ct} value for the coating containing the multilayered capsules indicates that the corrosion inhibitor, and the self-healing

agent encapsulated in the multilayers of the synthesized capsules were released as consequence of the scratch and local pH acidification caused by

Table 1 Electrochemical parameters obtained by fitting the measured impedance data shown in Fig. 12 of the scratched coated specimens immersed in 3.5 wt% NaCl solution

Coatings	Time (h)	R_{ct} ($\Omega \text{ cm}^2$)
PECs	2	43.1×10^3
SLSCs		10.3×10^4
PMLSCs		81.9×10^3
PECs	24	20.6×10^3
SLSCs		31.5×10^4
PMLSCs		46.8×10^4
PECs	48	10.8×10^3
SLSCs		12.2×10^4
PMLSCs		25.2×10^6

hydrolysis of iron ions released due to corrosion. It can be noticed that the PMLSCs show further increase in the R_{ct} value, with a major shift in the phase angle compared to the corresponding value after 24 h of immersion due to further release of corrosion inhibitor (dodecylamine) to the scratched area leading to inhibition of the corrosion activity. The higher R_{ct} value ($25.2 \times 10^6 \Omega \text{ cm}^2$) can be attributed to effective release of inhibitor and simultaneous formation of the healing film.

The charge transfer resistance is increasing in the SLSCs and PMLSCs with time (from 2 h of immersion to 24 h) due to the release of dodecylamine as well as release of linalyl acetate, both forming protective species. The R_{ct} values showed further increase for the PMLSCs compared to SLSCs due to the double action of the PMLSCs coatings that comes from the polymer healing effect and corrosion inhibition of steel. In fact, the damaged area, even after healing by linalyl acetate, still contains some micro-defects and may not avoid totally the corrosion activity. Hence, after 24 h of the scratch the corrosion process slowly progresses, and the pH of the surrounding medium acidifies due to hydrolysis of Fe cations and effect that stimulates the release of dodecylamine from the polyelectrolyte layers. The results obtained in the present work are in line with the previous reported literature [33, 35].

A comparison of the anticorrosive properties of the coatings developed within this work with those already reported literature is presented in Table 2. The comparative analysis demonstrates that the coatings developed in the present work possess superior anti-corrosive performance, an effect that can be attributed to the novel chemistry of the polyelectrolyte multilayered urea formaldehyde

Table 2 Comparison of the present coatings with the previous results in terms of corrosion impedance values

S.No.	Coatings	Immersion time	R_{ct} (Ω)	Reference
1	Blank Epoxy	2 h.	4.3×10^4	Present work
		24 h	2.0×10^4	
		48 h	1.0×10^4	
	Epoxy with UF microcapsules	2 h	1.0×10^5	
		24 h	3.1×10^5	
		48 h	1.2×10^5	
	Epoxy with multilayered microcapsules (UF/PEI/SPEEK/DOC/SPEEK/PEI)	2 h	8.1×10^4	
		24 h	4.6×10^5	
		48 h	2.5×10^7	
2	Blank epoxy	7 h	1.4×10^3	Fayyad et al. [4]
	Epoxy with UF microcapsules	7 h	8.9×10^4	
3	Blank Epoxy	2 h	7.5×10^3	Abrantes et al. [33]
		24 h	4.7×10^3	
	Epoxy with UF microcapsules	2 h	1.9×10^4	
		24 h	1.2×10^4	
		2 h	1.1×10^4	
4	Epoxy with multilayered microcapsules (UF/PEI/PSS/BTZ/PSS/PEI)	24 h	3.5×10^4	Liu et al. [35]
		24 h	1.4×10^5	
	Blank epoxy	48 h	6.6×10^4	
		24 h	4×10^5	
		48 h	7.4×10^5	

microcapsules, selection of the selected inhibitor, self-healing agent and their efficient release in response to the external stimuli. The two protective mechanisms are independently and simultaneously occurring in the developed coatings and hence increasing the corrosion protection performance of the smart coatings. The enhanced anticorrosion performance makes this composite coating an interesting option to protect steel components used in the oil and gas as well as other related industries.

Conclusion

Single-layer smart coatings (SLSCs) and polyelectrolyte multilayered smart coatings (PMSCs) were prepared from urea formaldehyde capsules loaded with linalyl acetate and capsules loaded with linalyl acetate and containing dodecylamine, respectively. It can be concluded that PMLSCs demonstrate improved thermal and superior anticorrosion properties compared to SLSCs. This enhancement can be attributed to the efficient release of the encapsulated self-healing species, linalyl acetate and corrosion inhibitor (dodecylamine) entrapped in polyelectrolyte layers from the MLUFMCs. Owing to the good thermal and enhanced anticorrosion properties, the novel PMLSCs may be attractive for designing of functional coatings for corrosion protection of steel parts.

Acknowledgements

Open Access funding provided by the Qatar National Library. This publication was made possible by NPRP Grant 9-080-2-039 from Qatar National Research Fund (a member of the Qatar Foundation). Statements made herein are solely the responsibility of the authors. R. A. Shakoor would like to acknowledge the financial support of QU internal grant-QUCC-CAM-2018/2019-3 and the Core Labs, QEERI for their SEM and TEM imaging. M.F. Montemor thanks Fundação para a Ciência e a Tecnologia (FCT, Portugal) for financial support under the projects PEst-OE/QUI/UI0100/2013.

Compliance with ethical standards

Conflict of interest The authors declare that they have no conflict of interest.



Open Access This article is distributed under the terms of the Creative Commons Attribution 4.0 International License (<http://creativecommons.org/licenses/by/4.0/>), which permits unrestricted use, distribution, and reproduction in any medium, provided you give appropriate credit to the original author(s) and the source, provide a link to the Creative Commons license, and indicate if changes were made.

References

- [1] Philip A, Schweitzer PE (2005) Paint and coatings: applications and corrosion resistance, 1st edn. CRC Press, Boca Raton
- [2] Revie RW, Uhlig HH (2008) Corrosion and corrosion control corrosion and an introduction to corrosion science and engineering, 4th edn. Wiley, Hoboken
- [3] Montemor MF (2014) Functional and smart coatings for corrosion protection: a review of recent advances. *Surf Coat Technol* 258:17–37
- [4] Fayyad EM, Almaadeed MA, Jones A (2015) Encapsulation of tung oil for self-healing coatings in corrosion applications. *Sci Adv Mater* 7:2628–2638. <https://doi.org/10.1166/sam.2015.2583>
- [5] Shchukin DG, Zheludkevich M, Yasakau K et al (2006) Layer-by-layer assembled nanocontainers for self-healing corrosion protection. *Adv Mater* 18:1672–1678. <https://doi.org/10.1002/adma.200502053>
- [6] Safaei F, Khorasani SN, Rahnama H, Neisiany RE (2018) Progress in organic coatings single microcapsules containing epoxy healing agent used for development in the fabrication of cost efficient self-healing epoxy coating. *Prog Org Coatings* 114:40–46. <https://doi.org/10.1016/j.porgcoat.2017.09.019>
- [7] Shchukin DG, Möhwald H (2007) Self-repairing coatings containing active nanoreservoirs. *Small* 3:926–943. <https://doi.org/10.1002/sml.200700064>
- [8] White SR, Sottos NR, Geubelle PH et al (2001) Autonomic healing of polymer composites. *Nature* 409:794–797. <https://doi.org/10.1038/35057232>
- [9] Falcón JM, Batista FF, Aoki IV (2014) Encapsulation of dodecylamine corrosion inhibitor on silica nanoparticles. *Electrochim Acta* 124:109–118. <https://doi.org/10.1016/j.electacta.2013.06.114>
- [10] Kartsonakis IA, Danilidis IL, Pappas GS, Kordas GC (2010) Encapsulation and release of corrosion inhibitors into titania nanocontainers. *J Nanosci Nanotechnol* 10:5912–5920. <https://doi.org/10.1166/jnn.2010.2571>

- [11] Feng Y, Cheng YF (2017) An intelligent coating doped with inhibitor-encapsulated nanocontainers for corrosion protection of pipeline steel. *Chem Eng J* 315:537–551. <https://doi.org/10.1016/j.cej.2017.01.064>
- [12] Mahidashti Z, Shahrabi T, Ramezanzadeh B (2018) The role of post-treatment of an ecofriendly cerium nanostructure conversion coating by green corrosion inhibitor on the adhesion and corrosion protection properties of the epoxy coating. *Prog Org Coatings* 114:19–32. <https://doi.org/10.1016/j.porgcoat.2017.09.015>
- [13] Van Soestbergen M, Baukh V, Erich SJF et al (2014) Release of cerium dibutylphosphate corrosion inhibitors from highly filled epoxy coating systems. *Prog Org Coatings* 77:1562–1568. <https://doi.org/10.1016/j.porgcoat.2013.12.018>
- [14] Calado LM, Taryba MG, Carmezim MJ, Montemor MF (2018) *Corros Sci*. <https://doi.org/10.1016/j.corsci.2018.06.013>
- [15] Lang S, Zhou Q (2017) Synthesis and characterization of poly(urea-formaldehyde) microcapsules containing linseed oil for self-healing coating development. *Prog Org Coatings* 105:99–110. <https://doi.org/10.1016/j.porgcoat.2016.11.015>
- [16] Suryanarayana C, Rao KC, Kumar D (2008) Preparation and characterization of microcapsules containing linseed oil and its use in self-healing coatings. *Prog Org Coatings* 63:72–78. <https://doi.org/10.1016/j.porgcoat.2008.04.008>
- [17] Huang M, Zhang H, Yang J (2012) Synthesis of organic silane microcapsules for self-healing corrosion resistant polymer coatings. *Corros Sci* 65:561–566. <https://doi.org/10.1016/j.corsci.2012.08.020>
- [18] Soo B, Cho H, White SR, Braun PV (2009) Self-healing polymer coatings. *Adv mater*. <https://doi.org/10.1002/adma.200802008>
- [19] Liu X, Zhang H, Wang J et al (2012) Preparation of epoxy microcapsule based self-healing coatings and their behavior. *Surf Coat Technol* 206:4976–4980. <https://doi.org/10.1016/j.surfcoat.2012.05.133>
- [20] Wei H, Wang Y, Guo J et al (2015) Advanced micro/nanocapsules for self-healing smart anticorrosion coatings. *J Mater Chem A* 3:469–480. <https://doi.org/10.1039/c4ta04791e>
- [21] Shchukin DG, Grigoriev DO, Möhwald H (2010) Application of smart organic nanocontainers in feedback active coatings. *Soft Matter* 6:720–725. <https://doi.org/10.1039/b918437f>
- [22] Glinel K, Déjugnat C, Prevot M et al (2007) Responsive polyelectrolyte multilayers. *Colloids Surf A Physicochem Eng Asp* 303:3–13. <https://doi.org/10.1016/j.colsurfa.2007.02.052>
- [23] Lamaka SV, Shchukin DG, Andreeva DV et al (2008) Sol-gel/polyelectrolyte active corrosion protection system. *Adv Funct Mater* 18:3137–3147. <https://doi.org/10.1002/adfm.200800630>
- [24] Funke W (1997) Progress in organic coatings problems and progress in organic coatings science and technology. *Prog Org Coatings* 31:5–9. [https://doi.org/10.1016/S0300-9440\(97\)00013-1](https://doi.org/10.1016/S0300-9440(97)00013-1)
- [25] Andreeva DV, Fix D, Möhwald H, Shchukin DG (2008) Self-healing anticorrosion coatings based on pH-sensitive polyelectrolyte/inhibitor sandwichlike nanostructures. *Adv Mater* 20:2789–2794. <https://doi.org/10.1002/adma.200800705>
- [26] Snihirova D, Lamaka SV, Montemor MF (2012) “SMART” protective ability of water based epoxy coatings loaded with CaCO₃ microbeads impregnated with corrosion inhibitors applied on AA2024 substrates. *Electrochim Acta* 83:439–447. <https://doi.org/10.1016/j.electacta.2012.07.102>
- [27] Shchukin DG, Lamaka SV, Yasakau KA et al (2008) Active anticorrosion coatings with halloysite nanocontainers. *J Phys Chem C* 112:958–964. <https://doi.org/10.1021/jp076188r>
- [28] Lvov YM, Shchukin DG, Mohwald H, Price RR (2008) Halloysite clay nanotubes for controlled release of protective agents. *ACS Nano* 2:814–820
- [29] Mahulikar PP, Jadhav RS, Hundiwal DG (2011) Performance of polyaniline/TiO₂ nanocomposites in epoxy for corrosion resistant coatings. *Iran Polym J* 20:367–376
- [30] Balaskas AC, Kartsonakis IA, Tziveleka LA, Kordas GC (2012) Improvement of anti-corrosive properties of epoxy-coated AA 2024-T3 with TiO₂ nanocontainers loaded with 8-hydroxyquinoline. *Prog Org Coatings* 74:418–426. <https://doi.org/10.1016/j.porgcoat.2012.01.005>
- [31] Poomima Vijayan P, Al-Maadeed MASA (2016) TiO₂ nanotubes and mesoporous silica as containers in self-healing epoxy coatings. *Sci Rep* 6:1–9. <https://doi.org/10.1038/srep38812>
- [32] Montemor MF, Snihirova DV, Taryba MG et al (2012) Evaluation of self-healing ability in protective coatings modified with combinations of layered double hydroxides and cerium molybdate nanocontainers filled with corrosion inhibitors. *Electrochim Acta* 60:31–40. <https://doi.org/10.1016/j.electacta.2011.10.078>
- [33] Abrantes D, Riegel-vidotti IC, Guerreiro M et al (2018) Smart coating based on double stimuli-responsive microcapsules containing linseed oil and benzotriazole for active corrosion protection. *Corros Sci* 130:56–63. <https://doi.org/10.1016/j.corsci.2017.10.009>
- [34] Sonawane SH, Bhanvase BA, Jamali AA et al (2012) Improved active anticorrosion coatings using layer-by-layer assembled ZnO nanocontainers with benzotriazole. *Chem*

- Eng J 189–190:464–472. <https://doi.org/10.1016/j.ccej.2012.02.076>
- [35] Liu X, Gu C, Wen Z, Hou B (2018) Improvement of active corrosion protection of carbon steel by water-based epoxy coating with smart CeO₂ nanocontainers. *Prog Org Coatings* 115:195–204. <https://doi.org/10.1016/j.porgcoat.2017.10.015>
- [36] Tan C, Selig MJ, Lee MC, Abbaspourrad A (2018) Polyelectrolyte microcapsules built on CaCO₃ scaffolds for the integration, encapsulation, and controlled release of copigmented anthocyanins. *Food Chem* 246:305–312. <https://doi.org/10.1016/j.foodchem.2017.11.033>
- [37] Abu-Thabit NY, Hamdy AS (2016) Stimuli-responsive Polyelectrolyte Multilayers for fabrication of self-healing coatings—a review. *Surf Coatings Technol* 303:406–424. <https://doi.org/10.1016/j.surfcoat.2015.11.020>
- [38] Brown EN, Kessler MR, Sottos NR, White SR (2003) In situ poly (urea-formaldehyde) microencapsulation of dicyclopentadiene. *J Microencapsul* 20:719–730
- [39] Beck HN (1992) Solubility characteristics of poly (Etheretherketone) and poly (phenylene sulfide). *J Appl Polym Sci* 45:1361–1366
- [40] Cai J, Lin P, Zhu X, Su Q (2006) Comparative analysis of clary sage (*S. sclarea* L.) oil volatiles by GC-FTIR and GC-MS. *Food Chem* 99:401–407. <https://doi.org/10.1016/j.foodchem.2005.07.041>
- [41] Ahmad Z, Najeeb MA, Shakoor RA et al (2017) Instability in CH₃NH₃PbI₃ perovskite solar cells due to elemental migration and chemical composition changes. *Sci Rep* 7:15406–15414. <https://doi.org/10.1038/s41598-017-15841-4>
- [42] Liu X, Sheng X, Lee JK, Kessler MR (2009) Synthesis and characterization of melamine- urea-formaldehyde microcapsules containing ENB-based self-healing agents. *Macromol Mater Eng* 294:389–395. <https://doi.org/10.1002/mame.200900015>
- [43] Sköld M, Hagvall L, Karlberg A-T (2008) Autoxidation of linalyl acetate, the main component of lavender oil, creates potent contact allergens. *Contact Dermatitis* 58:9–14
- [44] Hagvall L, Berglund V, Christensson JB (2015) Air-oxidized linalyl acetate—an emerging fragrance allergen. *Contact Dermatitis* 2:216–223. <https://doi.org/10.1111/cod.12350>
- [45] Hatami Boura S, Peikari M, Ashrafi A, Samadzadeh M (2012) Self-healing ability and adhesion strength of capsule embedded coatings—micro and nano sized capsules containing linseed oil. *Prog Org Coatings* 75:292–300. <https://doi.org/10.1016/j.porgcoat.2012.08.006>

Publisher's Note Springer Nature remains neutral with regard to jurisdictional claims in published maps and institutional affiliations.

APPENDIX C: Journal article 2

Progress in Organic Coatings 137 (2019) 105319



Contents lists available at ScienceDirect

Progress in Organic Coatings

journal homepage: www.elsevier.com/locate/porgcoat



Designing and performance evaluation of polyelectrolyte multilayered composite smart coatings



Adnan Khan^{a,c}, Mostafa H. Sliem^a, Ayman Arif^b, Mohammed A. Salih^b, R.A. Shakoor^{a,*}, M.F. Montemor^c, Ramazan Kahraman^b, Said Mansour^d, Aboubakr M. Abdullah^a, Anwarul Hasan^{e,*}

^a Center for Advanced Materials (CAM), Qatar University, 2713 Doha, Qatar

^b Department of Chemical Engineering, Qatar University, 2713 Doha, Qatar

^c Centro de Química Estrutural (CQE), DEQ, Instituto Superior Técnico, Universidade de Lisboa, Av. Rovisco Pais, 1049-001 Lisboa, Portugal

^d Qatar Energy and Environment Research Institute, Hamad Bin Khalifa University, Qatar Foundation, 34110 Doha, Qatar

^e Department of Mechanical and Industrial Engineering, Qatar University, 2713 Doha, Qatar

ARTICLE INFO

Keywords:

Polyelectrolytes
Urea formaldehyde microcapsules
Coating
Corrosion inhibitor
Self-healing
Phenylthiourea

ABSTRACT

This work reports the synthesis of polyelectrolyte microcapsules and its effect on the anti-corrosion performance of polymeric coating applied on steel substrates. In situ polymerization technique was used for the synthesis of monolayered urea formaldehyde microcapsules loaded with linalyl acetate (MLMGs). These capsules can be broken upon mechanical stress, such as scratches or other forms of mechanical damage. To enhance corrosion protection, Phenylthiourea (PTU), a molecule sensitive to pH, was loaded between consecutive polyelectrolyte layers of polyethylenimine (PEI) and sulfonated polyether ether ketone (SPEEK) build on the surface of MLMGs using the layer by layer technique. This polyelectrolyte layered microcapsules (PMCs) carry linalyl acetate in its core and phenylthiourea entrapped between the outer layers. Both MLMGs and PMCs, in concentration of 6 wt%, were dispersed in the epoxy resin and the resulting formulation was used to coat steel plates. Experimental findings showed that epoxy coatings reinforced with PMCs demonstrate better thermal, self-healing and anti-corrosion properties. This improved performance can be attributed to the release of polymer healing and corrosion inhibiting species from the PMCs. The epoxy coatings modified with PMCs can serve as self healing coating for corrosion protection of steel parts used, for example, in the oil and gas industry.

1. Introduction

Corrosion is a serious deterioration phenomena for metallic components and leads to substantial economic loss and safety failures. It has been widely reported that 3–5% of the annual gross profit of a country is used to mitigate corrosion induced degradation of metallic parts [1]. Steel, in particular carbon steel, is very susceptible to corrosion in industrial or marine environments where different aggressive species can be found. To minimize the impact of corrosion steel can be protected with organic coatings, which act as passive barriers and constrain the contact of the metals with the corrosive environment [2]. However, defects formed in the coatings such as pores, pinholes, micro scratches and other damages may destroy the protective barrier, exposing the bare metal to the aggressive media [3]. The continuous supply of aggressive species, in the presence of oxygen and moisture promotes corrosion activity. Therefore, it is of utmost relevance to find

strategies to repair the damaged areas and to delay the corrosion-induced damages. In this sense, smart polymeric coatings modified with active agents, either freely dispersed or stored in micro or nano carriers that can impart self healing ability have been considered an attractive route to minimize corrosion damages [4]. Moreover, the use of carriers, sensitive to different stimulus, has been pin pointed as an important route to avoid unwanted interactions between the healing species and the host organic matrices [5–8].

Polymeric coatings modified with carriers where different species can be stored results in a composite coating that works as a smart protective system [9–11]. Recent literature is fertile in different solutions. For example, polymeric coatings have been modified with capsules loaded with self-healing agents like linseed oil, tung oil, dicyclo-petadiene, epoxy monomer, vegetable oil and silanes [12–16]. These species once released from the capsules, where they have been stored, can repair damaged areas in the coating, hindering the access of

* Corresponding authors.

E-mail addresses: shakoor@qu.edu.qa (R.A. Shakoor), ahasan@qu.edu.qa (A. Hasan).

<https://doi.org/10.1016/j.porgcoat.2019.105319>

Received 4 August 2019; Accepted 8 September 2019

0300-9440/© 2019 Elsevier B.V. All rights reserved.

aggressive species. In this case, the encapsulation strategy foreshadows the repair of the polymeric matrices. However, when the damages reach the bare metal, corrosion onset can be very fast and it is very relevant to have corrosion inhibitors that heal the corroding areas as well [5,17,18].

Therefore, different corrosion inhibitors such as dodecylamine [19], benzotriazole [20], methylthiourea [21], imidazole [22] have been loaded in different carriers and added into polymeric coatings to confer corrosion healing ability [12]. Different containers, sensitive to different stimulus, like mechanical damage, pH, light, electrochemical potential and others, have been proposed to carry the corrosion inhibitors as reviewed elsewhere [23].

Urea formaldehyde microcapsules have been widely used as containers for the storage of active species in polymeric matrices because their shell can be functionalised and made compatible with different host coatings [15,16,24–26]. Furthermore, these materials present high thermal stability and are robust enough to survive the different stages of coating formulation and application. However, a major limitation is that they are typically used to store only individual healing species and simultaneous healing of the coating and inhibition of active metal areas require the combination of distinct microcapsules or the loading of a certain type microcapsule with different species [23].

To avoid the use of different containers in the same epoxy matrix, the concept of multilayered hybrid urea formaldehyde microcapsules has been introduced as a novel strategy to bring into a coating different healing functionalities. This approach has already been attempted in previous work [27–31].

In this study, urea formaldehyde microcapsules loaded with linalyl acetate, as polymeric healing agent, were synthesized by in situ emulsion polymerization. The release of this species require the mechanical rupture of the capsule. Moreover, the urea formaldehyde microcapsules were used to synthesised double stimulus multilayered shells. The layer by layer technique was used to impregnate phenylthiourea (PTU) between consecutive layers of polyelectrolytes (PEI and SPEEK) to produce multilayered microcapsules. PTU is reported as an efficient corrosion inhibitor for steel and the good inhibition efficiency has been attributed to the S-containing groups that are preferential sites for adsorption on steel surface [32]. The experimental findings show that this novel multilayered microcapsules improve the anti corrosion protection performance of epoxy coatings applied on steel.

2. Experimental section

2.1. Materials and chemicals

Urea, ammonium chloride, resorcinol, hydrochloric acid, sodium hydroxide, 37 wt. % formaldehyde, ethylenemaleic anhydride copolymer (EMA), phenylthiourea (PTU), ethanol, sulfonated polyether ether ketone (SPEEK), linalyl acetate and sodium chloride, were purchased from Sigma-Aldrich and used without any further purification. Epon 815C along with the curing agent diethylthriamine, dimethylacetamide and polyethylenimine (PEI) were supplied by BDH chemicals. Carbon steel samples (30 × 30 × 1.0) grinded with silicon carbide papers and cleaned with ethanol were used as a substrate.

2.2. Urea formaldehyde microcapsules synthesis encapsulated with linalyl acetate

In situ polymerization (oil-in-water emulsion) was used for the synthesis of the monolayer urea formaldehyde microcapsules filled with linalyl acetate (MLMCs). Fig. 1 depicts the experimental approach. In this process 200 ml of deionized water were mixed with 50 ml of 2.5 wt. % aqueous solution of EMA copolymer in a beaker. The beaker was placed in a controlled temperature water bath to maintain the temperature. The mixture was stirred by the overhead mechanical stirrer, with a three bladed propeller placed above the bottom of the beaker.

Under slow agitation (about 200 rpm) 5.0 g of urea, 0.5 g of resorcinol and 0.5 g of ammonium chloride were added into the solution and dissolved to form a homogeneous mixture. The pH was maintained at 3.5 by the drop wise addition of hydrochloric acid (HCl) and sodium hydroxide (NaOH). After adjusting the pH, 50 ml of linalyl acetate were added to the solution, to form an oil-water emulsion that was stabilized for 15 min. After stabilization, 13 g of aqueous formaldehyde (37.0 wt. %) were added in the solution to obtain a 1:1.9 M ratio of formaldehyde to urea [33]. The mixture was covered with aluminum sheets and heated at the rate 3 °C min⁻¹ to reach the desired temperature of 55 °C. The stirring rate was increased to 1200 rpm to obtain fine sized MLMCs. After four hours under constant stirring and temperature, the mixture was separated and vacuum filtered. The obtained MLMCs were washed with deionized water and dried at room temperature for 48 h.

2.3. Synthesis of polyelectrolyte urea formaldehyde microcapsules loaded with phenylthiourea

The polyelectrolyte urea formaldehyde microcapsules (PMCs) were synthesized using layer by layer technique. The polyelectrolyte materials (SPEEK and PEI) were deposited on the surface of the MLMCs in consecutive steps to store the corrosion inhibitor between the layers. Thus, positively charged PEI was deposited on the surface of the original microcapsules by mixing 60 ml suspension of microcapsules with 90 ml of PEI solution (2 mg/ml). The mixture was stirred for 15 min (450 rpm) followed by centrifuging and washing with distilled water to remove the excess of PEI. The dried product (MLMCs/PEI) was then mixed with the negatively charged polyelectrolyte SPEEK solution (2 mg/ml) and stirred for 15 min at 450 rpm. The excess of the SPEEK was removed by centrifuging and washing with distilled water. The third layer was deposited by mixing 60 ml suspension of (MLMCs/PEI/SPEEK) with the 90 ml solution of phenylthiourea (10 mg/ml). The mixture was stirred at 450 rpm for 15 min and the pH was maintained at 3. The fourth and fifth layer (SPEEK and PEI) were deposited on the surface according to the previous procedure to produce the PMCs (MLMCs/PEI/SPEEK/PTU/SPEEK/PEI). Fig. 1 represents the schematics of the deposition of layer by layer on the surface of MLMCs.

2.4. Coating preparation

Three types of epoxy coatings were prepared and applied over the steel coupons by the doctor blade film applicator. (1) Control sample: i.e. the epoxy coating without microcapsules, referred as neat coating (2) the epoxy coating with MLMCs filled with linalyl acetate, referred as plain coating. And (3) the epoxy coatings with PMCs referred as layered coating.

Carbon steel specimens grinded with silicon carbide papers and cleaned with ethanol were used as a substrate. To prepare the coatings modified with capsules, 6 wt.% of each type of microcapsules were dispersed in the epoxy resin and stirred for 15 min. Curing agent in a stoichiometric ratio was mixed and finally the mixture was kept in low-pressure oven for 10 min to remove air bubbles. The epoxy mixture was applied on clean and grinded carbon steel specimen with doctor blade to obtain a uniform thickness of the coatings (300 μm). The epoxy coated specimens were cured at 37 °C for 48 h. According to ASTM D1654 standard, a manual scratch was made along the coatings using a scalpel. The scratch works as the mechanical load that breaks the microcapsules and forces the release of the linalyl acetate from the core of the microcapsules, to heal the coatings.

2.5. Characterization of microcapsules and coatings

The microcapsules were analyzed by FT-IR Frontier (PerkinElmer, Frontier, USA) instrument to confirm encapsulation of linalyl acetate and PTU. The spectra were recorded in the range 4000 to 500 cm⁻¹.

Zeta potential equipment (Malvern, Zeta sizer, Nano ZSP, USA) was

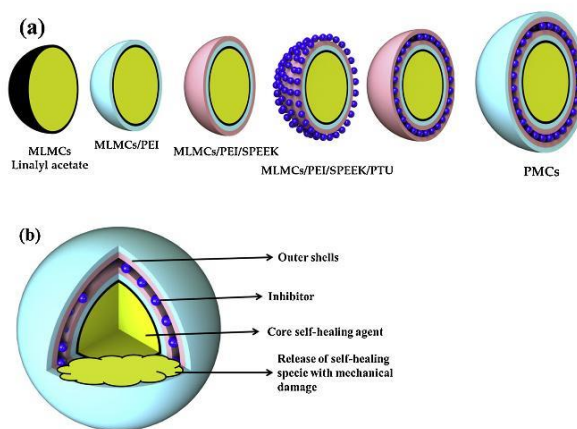


Fig. 1. (a) schematic representation of the synthesis of PMCs (b) profile of multilayers.

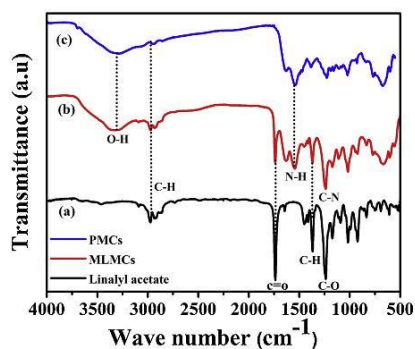


Fig. 2. FTIR spectra of the (a) linalyl acetate (b) MLMCs loaded with linalyl acetate (c) and PMCs.

used to confirm adsorption of PEI and PEEK, by determining the charge during layer by layer technique.

The size distribution of the as synthesized microcapsules was studied using a particle size analyzer (Malvern, Master sizer 2000, Analytical, USA).

XPS (AXIX Ultra DLD, Kratos, UK) using a monochromatic X-Ray Source - Al K α source was used to further confirm the adsorption of the polyelectrolyte layers of the surface of MLMCs and to detail its chemical composition. The binding energy of C 1s (284.6 eV) was used as reference. The energy resolution was 160 eV and the spatial resolution was 20 eV.

The surface morphology, size, shell thickness and other morphological features of the microcapsules were investigated by a field emission scanning electron microscope (FE-SEM-Nova Nano-450, Netherlands) and transmission electron microscopy (TEM, FEI, TALOS F200X, USA).

A TGA synchronization analyzer (PerkinElmer, TGA 4000, USA) was used to analyze the thermal stability of the microcapsules and modified epoxy coatings. The analysis was carried out in the temperature range from 40 °C to 600 °C at the heating rate of 20 °C/minute.

UV-vis spectroscopic analysis (LAMBDA 650 UV/Vis

Spectrophotometer, PerkinElmer, USA) was used to analyze the release of inhibitor from the PMCs. Various solutions with different pH were prepared and a small amount (0.1 g) of layered microcapsules were added to determine the release of the PTU at different pH and after different times. The coatings were controlled damaged as per the ASTM D1654 standard procedure, and the self-healing ability was analyzed as a function of time. FE-SEM (FE-SEM-Nova Nano-450, Netherlands) was used to assess the self-healing effect.

The EIS study was performed at open circuit potential (OCP) within frequency range 10 mHz to 100 KHz, with rms of 50 mV, using a GAMRY 3000 potentiostat (Gamry, Warminster, PA, USA). The coated steel plates were used as working electrodes, with an exposed area of 0.5 cm² and a platinum wire was used as counter electrode. A Ag/AgCl electrode was employed as reference. All electrochemical tests were carried out at controlled room temperature. Two scratches with 5 cm length were made on the cured epoxy coatings to study the self-healing effect. The coated specimens were exposed to a 3.5% NaCl solution for 60 min before the electrochemical tests. Tests were carried out after different exposure time 24, 48 and 72 h respectively. To ensure reproducibility each test was repeated three times in coated samples with similar scratched.

3. Result and discussions

3.1. FTIR analysis of the synthesized microcapsules

Fig. 2 depicts the FTIR spectra of (a) pure linalyl acetate, (b) MLMCs and (c) PMCs. Linalyl acetate spectrum shows several absorption peaks including the C–H bond stretching at 2972 cm⁻¹, and C=O ester bond at 1736 cm⁻¹, as well as the C=C bond at 1646 cm⁻¹ and C–OC–ester at 1250 cm⁻¹. The MLMCs spectrum presents the O–H peak around 3303.6 cm⁻¹, C–H stretching peak around 2964.76 cm⁻¹, as the amide C=O peak was observed at 1623.63 cm⁻¹. Finally the C–N and NH– peaks were found around 1232.43 cm⁻¹ and 1541–1631 cm⁻¹ respectively, and were assigned to bond formation in the MLMCs.

The mechanism behind MLMCs formation is the reaction of the acetate group with the hydroxyl methylene group of urea formaldehyde, which leads to the formation of an ester/ether bond. The formation of the ester/ether bonds is evidenced in the FTIR spectrum by the shift in the urea formaldehyde amide group to 1541–1631 cm⁻¹.

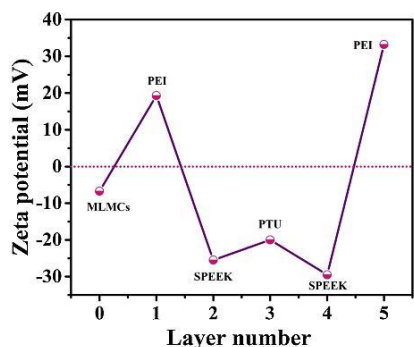


Fig. 3. Zeta potential value of the microcapsules. Layer 0: as synthesized MLMCs and layer 1–5, the different layers of the PMCs.

The change in the amide group is due to the change in polarity between the linalyl acetate and the urea formaldehyde bonds, confirmed by the shift in the N–H bond. The spectrum (c) representing the PMCs is similar to the one for MLMCs. The major differences can be observed in the frequency region where the C=O stretching peak responds. First, the elimination of the C=O in PMCs indicates the formation of new bonds, which can be explained by the successful layering with PEI, SPEEK and PTU. Other significant changes are the contents of O–H and the NH– peak intensity; the peak intensity of N–H after addition of polyelectrolyte layers to the MLMCs is clearly high. As for the hydroxyl content, the O–H content in the MLMCs is much lower than the O–H content in the PMCs, due to the consumption of hydroxyl after addition of the polyelectrolyte layers (SPEEK and PEI).

3.2. Zeta Potential analysis

The surface charge of the microcapsules was studied to confirm adsorption of the polyelectrolyte layers and the layer by layer design of the PMCs. Fig. 3 presents the zeta potential of each layer of the PMCs. It is noticed that the zeta potential of the as synthesized MLMCs is negative (\square -6.7 mV). After deposition of PEI the zeta potential shifted to positive values (\square 19.3 mV), which confirmed the bonding of the MLMCs with the polycation PEI. Furthermore because of the sulphonic group in SPEEK, the zeta charge shifted to the negative value (\square -25.5 mV). In addition due to the difference in the specific charge and molar mass of PTU compared to the polyanion SPEEK, the zeta potential slightly increased (\square -20 mV) after adsorption of the PTU layer. The valence electrons in PTU hold the $-\text{SO}_3$ group of the SPEEK and thus ensure the loading of PTU between the two polyanion layers. Finally the zeta potential was dramatically shifted to positive values (\square 33.2 mV) after the deposition of the new PEI layer. The results are in agreement with results reported elsewhere [27,31,34].

3.3. XPS analysis

To confirm the adsorption of the polyelectrolyte layers on the surface of the MLMCs, XPS characterization was carried out as shown in the Fig. 4. The XPS spectra of the MLMCs and PMCs show the presence of carbon, nitrogen and oxygen which correspond to the structure of the urea-formaldehyde and PEI + SPEEK (outer layer in PMCs) and the respective quantification is depicted in Table 1.

The XPS spectra of C1s on the surface of microcapsules (MLMCs and PMCs) is shown in Fig. 4 (a,b). For MLMCs the main peak was fitted with three peaks placed at 284.9 eV, 286.6 eV and 288.5 eV assigned to

the binding energies of C–C, COC and CO–= on the surface of MLMCs. In PMCs the fitting peaks are shown at 284.8 eV, 286.3 eV and 288.0 eV which were assigned to the same species observed for the MLMCs surface. Since XPS is a surface analysis technique, there is a clear difference in the concentration at the surface of the microcapsules which accounts for the adsorption of polyelectrolyte layers on the MLMCs. The XPS results showed only the outer small portion of the PMCs layers (mainly consist of PEI and SPEEK) because of the short mean free path of photoelectrons. The contents of carbon increased in the PMCs surface (PEI + SPEEK) from 55.2% to 69.19%, which reflect the complex carbon chain structure of PEI and SPEEK. Nitrogen and Oxygen showed a decrease in the PMCs. Fig. 4 (c, d) represents the nitrogen peak and both MLMCs and PMCs showed only the binding energy of C–N H₂. Moreover O1s is shown in Fig. 4 (e, f) for both microcapsules. The O1s spectra showed that the binding energy of C–O and CO= were dominant.

3.4. FE-SEM/HR-TEM analysis

Fig. 5 depicts the structural and morphological study of the as synthesized MLMCs and PMCs. Fig. 5(a) shows the MLMCs and reveals the presence of micro sized spherical beads with a slightly rough outer surface, according to previous results [27]. Fig. 5(b) is the wall thickness of the broken MLMCs. The average wall thickness is about 712 nm with a smooth inner surface [35]. The thickness of the wall depends on the stirring rate and the time of polymerization reaction during the syntheses of the MLMCs. By prolonging the time of polymerization reaction it is expected to achieve thicker wall microcapsules with higher mechanical strength [36].

Fig. 5(b, c) depict the SEM images of PMCs, that present various sizes, in line with the particle size analysis. The morphology of the PMCs is also spherical with more compaction compared to MLMCs. The surface morphology of the PMCs was also studied by TEM to clarify the presence of the multilayers (polyelectrolyte and inhibitor) on the surface of MLMCs. Fig. 5(e, f) depicts the TEM analysis, which clearly showed the deposited polyelectrolyte layers on the surface of the MLMCs in agreement with previous results [37]. The average thickness of the deposited polyelectrolyte is about 350 nm. The images clearly demonstrate the core microcapsules with an average size of about 620 nm. The detail discussion about the size distribution of the microcapsules is made in the proceeding sections. Fig. 5(g–j) represent the elemental mapping of the surface of MLMCs which showed that carbon, nitrogen and oxygen are the primary elements present in the MLMCs.

3.5. Particle size analysis of the microcapsules

Fig. 6 indicate the particle size study of MLMCs and PMCs, using particle size analyzer. The MLMCs were in the range of 0.01 μm –500 μm . The average size of the capsules observed was 37 μm . The majority of the particle lies in the range of 4 μm –63 μm (volumes %) while there was only 10 vol % of capsules in the size range of 125 μm –250 μm . The analysis indicates that most of the particles are in the lower range which reflects the high stirring rate which further split the linalyl acetate into smaller pieces resulting in smaller microcapsules. Fig. 7 also shows the particle size distribution of the PMCs. The mean size observed was about 68 μm . The particles are in the range of 0.01–2000 μm but the majority of the microcapsules were present in 4–125 μm (77.79 vol %). Only 4.39 vol % of the PMCs lies in the range of 1000–2000 μm . The increase in the mean diameter of the PMCs indicates the successful adsorption on the surface of MLMCs. The insets in Fig. 6 present the variation in the size of microcapsules. It is worth to note that the TEM images shown above focuses only the smallest PMCs.

3.6. Thermal stability of the microcapsules and epoxy coatings

The thermal stability of the MLMCs and PMCs added into the epoxy

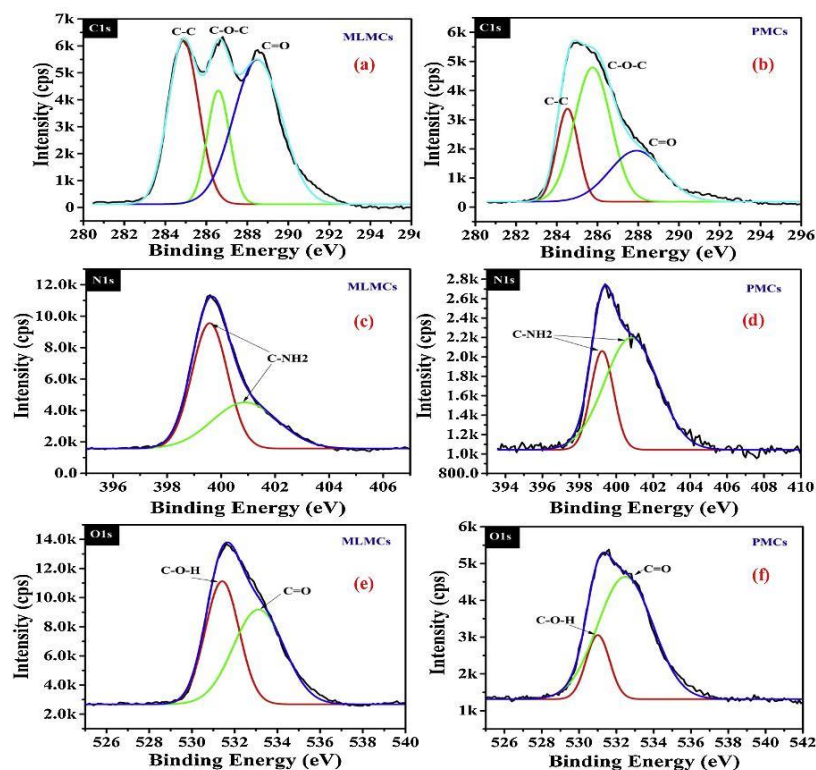


Fig. 4. XPS survey spectra of MLMCs and PMCs samples: (a, b) C 1s, (c, d) N 1s, (e, f) O 1s.

Table 1
The elemental analysis of MLMCs and PMCs.

Elements	MLMCs (%)	PMCs (%)
C 1s	55.52 ± 2%	69.22 ± 2%
N 1s	23.25 ± 2%	19.64 ± 2%
O 1s	21.24 ± 2%	11.24 ± 2%

coatings were analyzed by TGA (Fig. 8(a, b)). Fig. 7(a) indicate that there is a gradual weight loss in both the MLMCs and PMCs with the increasing temperature (up to 600 °C). The complete weight loss in the MLMCs spectra observed was from 130 °C to around 270 °C which can be associated with the shell of urea-formaldehyde (200 °C) and the encapsulated linalyl acetate (B.P 220 °C). The PMCs display improved thermal stability because of the highly thermally stable polyelectrolyte materials (PEI and SPEEK) [38]. The first stage (100 °C to 230 °C) showed a minor weight loss which can associate with the decomposition of impregnated phenylthiourea (157 °C) and core linalyl acetate (220 °C). The second stage (270 °C to 420 °C) was attributed to the adsorbed polyelectrolyte materials [27]. The inset in Fig. 7(a) shows the peaks of the derivative weight loss of both the MLMCs and PMCs. Fig. 7(b) shows the TGA spectra for the plain and layered coatings. Like the microcapsules, the layered coating exhibited better thermal stability compared to the plain coating. Both the coatings are thermally stable

and showed negligible weight loss till 400 °C, which can be attributed to the highly thermally stable epoxy resin matrix. The peaks of the derivative weight loss of the coatings can be seen in the inset of Fig. 7(b).

3.7. Release behavior of phenylthiourea with pH variation

UV-vis spectroscopy was used to study the release behavior of the inhibitor from the multilayered microcapsules with different time intervals. The UV spectra were recorded after dipping the PMCs in 0.1 M NaCl solutions of pH 2, 5, 7, 9, 11 after different periods: 2, 24 and 48 h (Fig. 8). The absorbance intensity changes with pH after 24 and 48 h and as shown in the Fig. 8(b, c). The absorbance value at ~ 303 nm represents the protonation of phenylthiourea and hence confirmed the presence of inhibitor in solution. It can be noticed that the relative absorption peak intensity increased after 24 and 48 h (Fig. 8(b, c)). Furthermore there was a more dominant absorption at pH 2, 9 and 11 compared to pH 5 and 7, which showed that the release of PTU seemed to occur preferentially in both acidic and alkaline medium. The intensity of the peaks increased with time, which evidenced the time dependent release behavior of the inhibitors from the PMCs.

3.8. Self-healing of the coatings

The self-healing capability of the plain and layered coatings was

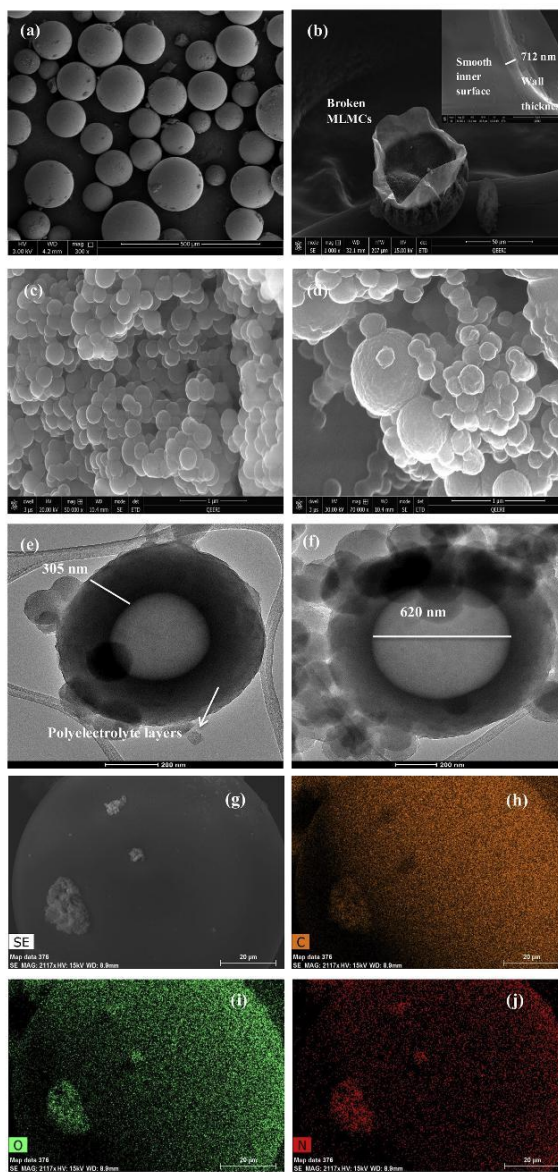


Fig. 5. The structural and morphological study of the synthesized microcapsules (a, b) SEM of the UF microcapsules (b, c) the SEM of the multilayered microcapsules (d, e) TEM of the multilayered microcapsules. (f, g, h, i) elemental mapping of MLMCs.

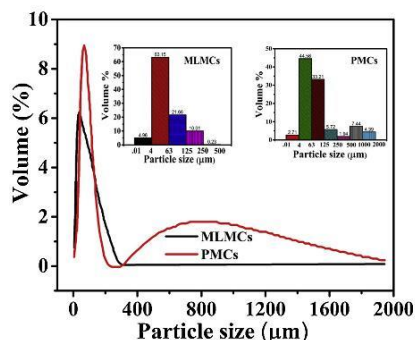


Fig. 6. Particle size analysis of MLMCs and PMCs.

evaluated by scanning electron microscopy- Fig. 9. The coatings were subjected to controlled mechanical damage by creating a 5 mm scratch. Under mechanical load, the microcapsules are ruptured and release the core species (linalyl acetate) into the damaged area. This agent is expected to polymerize forming a protective layer that restricts the contact of the substrate with the harsh corrosive environment. Linalyl acetate has the ability to oxidize under contact with air, hence forming hyperoxides, and epoxide. The SEM images of plain coatings (a, b and c) showed the time evolution of the healing process in the scratched area. After 24 h of damage, the scratch seemed healed in both plain and layered coating as shown in Fig. 9(b, e). After 48 h, the images evidenced a stable coating heal

3.9. Electrochemical impedance spectroscopy (EIS)

The corrosion protection of the modified coatings was studied by electrochemical impedance spectroscopy. The impedance spectra were fitted using the equivalent circuits as depicted in Fig. 10. The two-time constant equivalent circuit, which is commonly used for coated steel, is depicted in Fig. 10a. However, a three-time constant equivalent circuit, Fig. 10b was also necessary to fit some of the experimental results. A Warburg, accounting for mass transfer-controlled processes was also included to simulate the low frequency response [39,40]. The parameters extracted from fitting of the experimental results are the solution resistance (R_s), pore resistance (R_{po}), constant phase elements (CPE), Warburg diffusion coefficient (W), charge transfer resistance (R_1 in circuit a) and R_2 in circuit b). In the equivalent circuit b) the resistor R_1 corresponds to formation of an interfacial layer with properties different from those of coating and bare metal [41,42]. The fitted results of charge transfer resistances (R_1 and R_2), the admittance of the constant phase elements (Y_1 and Y_2) and Warburg diffusion coefficient

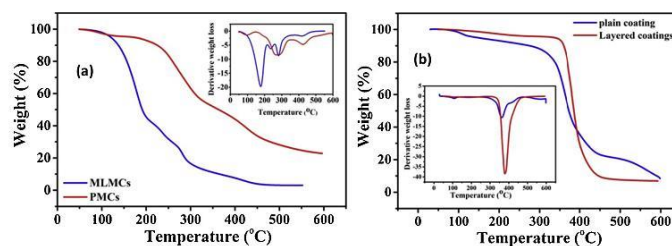


Fig. 7. Thermal stability analysis (TGA) of (a) MLMCs [27] and PMCs (b) the plain and layered coatings.

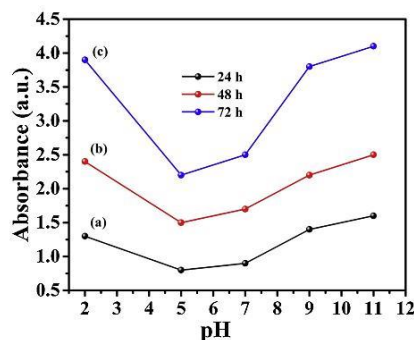


Fig. 8. UV spectroscopy of polyelectrolyte multilayered microcapsules after (a) 24 h (b) 48 h (c) 72 h of the immersion in 0.1 M NaCl solution with different pH values.

(W), are depicted in Table 2. The obtained results show that the constant phase element decreased as the resistance values increased, with the increasing number of layers or inhibitor composition, which are due to the increase in the thickness of the protective layer on the metal/solution interface. The EIS plots for all the same coating material content displayed identical behavior after different exposure time [43].

Fig. 11 shows the EIS spectra, after the immersion of the scratched coated samples for different exposure times: 24, 48 and 72 h. The scratched neat coating showed lower resistance at low frequency. The plain coating showed higher impedance than the layered coating after 24 h because of the multilayered microcapsules. The self-healing agent (linalyl acetate) is completely released in the damaged part in the plain coating, while in the layered coating it took some time to release the complete core materials because of the deposited polyelectrolyte layers above the MLMCs. The low impedance of the layered coating, after 24 h also confirmed that the corrosion inhibitor (PTU) is not released from the polyelectrolyte layers.

A comparison of the charge transfer resistances in Table 2 suggested a decrease of the corrosion activity in the multilayered coating. The admittance of the CPE was similar for the plain and multilayered coatings. The evolution of the low frequency resistance, which can be assigned to the charge transfer resistance and therefore reflects the corrosion activity increased for one order of magnitude over the time in the multilayered coating, indicating that the scratch previously formed has been inhibited. For the plain and layered coating, the spectra were fitted with three-time constants and the intermediate resistance (R_1) increased over the time suggesting that a more protective interfacial layer has been formed. The coating without additives revealed a decreasing pore resistance and a decreasing charge transfer resistance

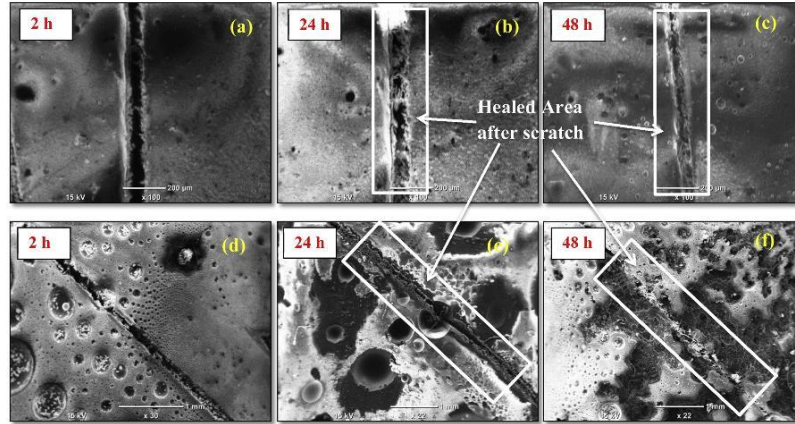


Fig. 9. SEM images of the scratched samples (a, b, c) MLMCs and (d, e, f) PMCs after different time intervals.

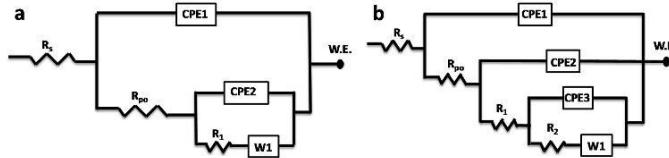


Fig. 10. Electrochemical equivalent circuit used to fit the impedance data.

Table 2
EIS parameters for neat coatings, plain coatings and layered coatings in 3.5% NaCl at room temperature.

Coating	Exposure time, days	R_s , k Ω cm ²	R_{po} , k Ω cm ²	$V_{coat} \times 10^{-6} \Omega^{-1} s^{\alpha} cm^{-2}$	R_1 , k Ω cm ²	$V_1 \times 10^{-6} \Omega^{-1} s^{\alpha} cm^{-2}$	R_2 , k Ω cm ²	$V_2 \times 10^{-6} \Omega^{-1} s^{\alpha} cm^{-2}$	$W \times 10^{-6} \Omega^{-1} s^{\alpha} cm^{-2}$
Neat	1 st	1.67	48.77	33.53	67.78	0.16	—	—	—
	2 nd	0.21	12.45	72.14	51.34	0.27	—	—	—
	3 rd	1.57	7.73	101.2	18.7	0.45	49.3	1.01	1.05
Plain	1 st	1.34	12.56	0.145	120.6	0.28	139.8	2.41	0.61
	2 nd	1.41	66.98	0.102	163.9	0.21	151.9	2.05	1.14
	3 rd	2.34	82.27	0.038	248.9	0.16	259.7	1.01	1.46
Layered	1 st	0.34	95.2	1.71	94.88	0.34	179.1	1.51	0.193
	2 nd	0.12	151.4	1.539	46.4	2.47	1142	1.43	6.89
	3 rd	0.99	347.9	624.9	83.98	868.8	2200	1.06	8.31

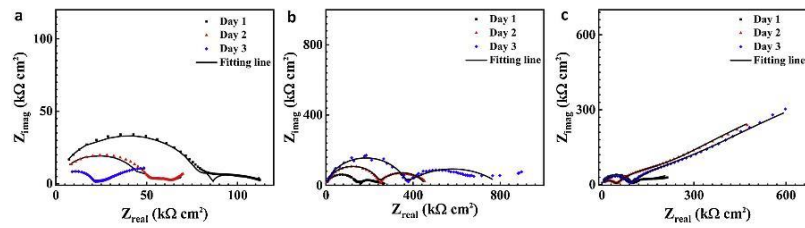


Fig. 11. Experimental Nyquist plots and respective fittings (solid lines) for different coatings immersed in 3.5% NaCl solution for different exposure times a) neat coating, b) plain coating, and c) layered coatings.

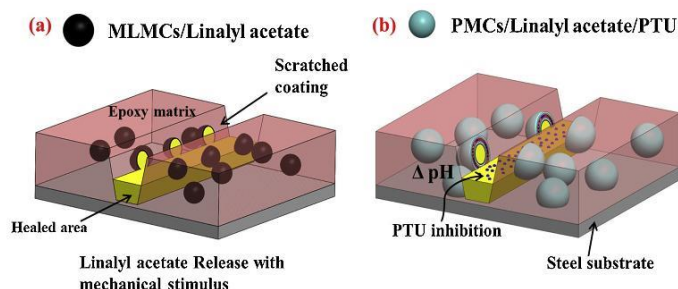


Fig. 12. Protective mechanism of the self-healing coatings; (a) plain coating (b) layered coating.

Table 3

Comparison of the coatings in current study with the already reported literature in terms of anti-corrosive properties.

S.No	Type of container	Coatings formulation	Immersion time (h)	R_{ct} (Ω cm ²)	References
1	Urea formaldehyde microcapsules	Multilayered with phenylthiourea (UF/PEI/SPEEK/PTU/SPEEK/PEI)	48	2.20×10^6	Current study
2	Urea formaldehyde microcapsules	Multilayered with benzotriazole (UF/PEI/PSS/benzotriazole/PSS/PEI)	48	4.54×10^3	[31]
3	CeO ₂ nano-containers	CeO ₂ / benzotriazole /(PEI/PSS) ₂	48	3.33×10^4	[30]

accounting for its increased corrosion activity. The EIS measurements suggest that in scratched coatings the presence of loaded microcapsules reduced the corrosion activity in good agreement with previous findings [27].

The R_{po} and R_2 impedance values of the layered coating are higher than the plain one, which confirm the protective effect of PTU. Moreover, the R_2 for the layered coating did not show a noticeable increase in the first days of immersion but it increased one order of magnitude in the second and the third days of immersion compared to the plain coating. This might be ascribed to the release of PTU [44,45]. The Warburg impedance in the low frequency range showed increased values after two days of immersion. Fig. 12 shows the proposed protective mechanism of the self-healing coatings.

Table 3 compares the impedance values of the current work and the studies already reported in the literature. It can be noticed that the smart coatings developed in the current work current demonstrate superior anti-corrosive properties.

4. Conclusion

Mono layered microcapsules (MLMCs) and Polyelectrolyte multi-layered microcapsules (PMCs) were prepared and used as additives to modify epoxy coatings for corrosion protection of steel. It is concluded that the modified coatings show improve thermal and anticorrosive performance. The enhanced corrosion protection can be attributed to the release of the self-healing agent (linalyl acetate) stored in the core of the capsules and corrosion inhibitor (Phenylthiourea) stored between layers. The loaded corrosion inhibitor in the layered system improves corrosion protection compared to the plain coating. The healing effect of linalyl acetate was evidenced by the slow repair of scratches formed on the surface, while the inhibitive action of phenylthiourea has been confirmed by the increased resistances determined by electrochemical impedance spectroscopy.

Declaration of Competing Interest

Authors declare no conflict of interest.

Acknowledgements

This publication was made possible by NPRP Grant 9–080-2-039 from Qatar National Research Fund (a member of the Qatar Foundation). Statements made herein are solely the responsibility of the authors. R. A. Shakoor would like to acknowledge the financial support of QU internal grant-QUCG-CAM-2018/2019-3 and the Core Labs, QEERI for their SEM and TEM imaging. M.F. Montemor thanks Fundação para a Ciência e a Tecnologia (FCT, Portugal) for financial support under the projects PEst-OE/QUI/UI0100/2019.

References

- [1] R.W. H.H.U. Revie, *Corrosion and Corrosion Control An Introduction to Corrosion Science and Engineering*, 4th ed., A JOHN WILEY & SONS, 2019 n.d.
- [2] S.B. Lyon, R. Bingham, D.J. Mills, *Advances in corrosion protection by organic coatings: what we know and what we would like to know*, *Prog. Org. Coat.* 102 (2017) 2–7, <https://doi.org/10.1016/j.porgcoat.2016.04.030>.
- [3] M. Ahmadzadeh, T. Shahrabi, M. Izadi, I. Mohammadi, S.M. Hoseini, A. Barnoush, *Calcereous scales deposited in the organic coating defects during artificial seawater cathodic protection: effect of zinc cations*, *J. Alloys Compd.* (2019) 744–755, <https://doi.org/10.1016/j.jallcom.2019.01.096>.
- [4] T.M.T.D. Tuan Anh Nguyen, T.H. Nguyen, T.L. Pham, X.S. Hoang Thai, *Application of Nano-SiO₂ and Nano-Fe₂O₃ for protection of steel rebar in chloride contaminated concrete: epoxy nanocomposite coatings and nano-modified mortars*, *J. Nanosci. Nanotechnol.* 17 (2017) 427–436, <https://doi.org/10.1166/jnn.2017.12396>.
- [5] M.F. Montemor, *Surface & coatings technology functional and smart coatings for corrosion protection: a review of recent advances*, *Surf. Coat. Technol.* 258 (2014) 17–37, <https://doi.org/10.1016/j.surfcoat.2014.06.031>.
- [6] S.E. Karekar, U.D. Bagale, S.H. Sonawane, A. Bharat, D.V. Pinjari, *A smart coating established with encapsulation of Zinc Molybdate centred nanocontainer for active corrosion protection of mild steel: release kinetics of corrosion inhibitor*, *Compos. Interfaces* 6440 (2018) 1–24, <https://doi.org/10.1080/09276440.2018.1439631>.
- [7] X. Liu, Y. Cheng, W. Wang, F. Liu, B. Hou, *Application of 1D attapulgite as reservoir with benzotriazole for corrosion protection of carbon steel*, *Mater. Chem. Phys.* 205 (2018) 292–302, <https://doi.org/10.1016/j.matchemphys.2017.11.038>.
- [8] K.A. Zahidah, S. Kakooei, M.C. Ismail, P.B. Raja, *Halloysite nanotubes as nano-container for smart coating application: a review*, *Prog. Org. Coat.* 111 (2017) 175–185, <https://doi.org/10.1016/j.porgcoat.2017.05.018>.
- [9] H. Garate, M. Bianchi, L.I. Pietrasanta, S. Goyanes, N.B. D'Accorso, *High-energy dissipation performance in epoxy coatings by the synergistic effect of carbon nanotube/block copolymer conjugates*, *ACS Appl. Mater. Interfaces* 9 (2017) 930–943, <https://doi.org/10.1021/acsami.6b13212>.
- [10] L. Tang, J. Whalen, G. Schutte, C. Weder, *Stimuli-responsive epoxy coatings*, *ACS Appl. Mater. Interfaces* 1 (2009) 688–696, <https://doi.org/10.1021/am800199u>.
- [11] M. Odarczenko, D. Thakare, W. Li, K. Yang, S. Tang, S.P. Venkateswaram, N.R. Sottos, S.R. White, *Self-protecting epoxy coatings with anticorrosion*

- microcapsules, *ACS Omega* 3 (2018) 14157–14164, <https://doi.org/10.1021/acsomega.8b01950>.
- [12] M.F. Montemor, C. Vicente, I.S. Técnico, Functional Self-Healing Coatings: A New Trend in Corrosion Protection by Organic Coatings, Elsevier, 2018, <https://doi.org/10.1016/B978-0-12-409547-2.13442-0>.
- [13] H. Abdipour, M. Rezaei, F. Abbasi, Progress in Organic Coatings Synthesis and characterization of high durable linseed oil-urea formaldehyde micro / nano-capsules and their self-healing behaviour in epoxy coating, *Prog. Org. Coat.* 124 (2018) 200–212, <https://doi.org/10.1016/j.porgcoat.2018.08.019>.
- [14] H. Li, Y. Cui, Z. Li, Y. Zhu, H. Wang, Progress in Organic Coatings Fabrication of microcapsules containing dual-functional tung oil and properties suitable for self-healing and self-lubricating coatings, *Prog. Org. Coat.* 115 (2018) 164–171, <https://doi.org/10.1016/j.porgcoat.2017.11.019>.
- [15] R.P. Ollier, M.E. Penoff, V.A. Alvarez, Microencapsulation of epoxy resins: optimization of synthesis conditions, *Colloids Surf. A Physicochem. Eng. Asp.* 511 (2016) 27–38, <https://doi.org/10.1016/j.colsurfa.2016.09.081>.
- [16] E.N. Brown, N.R. Sottos, In situ poly (urea-formaldehyde) microencapsulation of Dicyclopentadiene, *J. Microencapsul.* 20 (2003) 719–730.
- [17] B. Qian, M. Michailidis, M. Bilton, T. Hobson, Z. Zheng, D. Shchukin, Electrochimica Acta Tannic complexes coated nanocontainers for controlled release of corrosion inhibitors in self-healing coatings, *Electrochim. Acta* 297 (2019) 1035–1041, <https://doi.org/10.1016/j.electacta.2018.12.062>.
- [18] M.L. Zheludkevich, J. Tedim, M.G.S. Ferreira, Electrochimica Acta “Smart” coatings for active corrosion protection based on multi-functional micro and nanocontainers, *Electrochim. Acta* 82 (2012) 314–323, <https://doi.org/10.1016/j.electacta.2012.04.095>.
- [19] J.M. Falcón, F.F. Batista, I.V. Aoki, Encapsulation of dodecylamine corrosion inhibitor on silica nanoparticles, *Electrochim. Acta* 124 (2013) 109–118, <https://doi.org/10.1016/j.electacta.2013.06.114>.
- [20] S.T. Selvi, V. Raman, N. Rajendran, Corrosion inhibition of mild steel by benzotriazole derivatives in acidic medium, *J. Appl. Electrochem.* (2003) 1175–1182.
- [21] M.K. Awad, Semiempirical investigation of the inhibition efficiency of thiourea derivatives as corrosion inhibitors, *J. Electroanal. Chem.* 567 (2004) 219–225, <https://doi.org/10.1016/j.jelechem.2003.12.028>.
- [22] J. Wang, A. Singh, M. Talha, X. Luo, X. Deng, Y. Lin, Electrochemical and theoretical study of imidazole derivative as effective corrosion inhibitor for aluminium, *Int. J. Electrochem. Sci.* 13 (2018) 11539–11548, <https://doi.org/10.20964/2018.12.44>.
- [23] M.F. Montemor, Hybrid nanocontainer-based smart self-healing composite coatings for the protection of metallic assets, *Smart Compos. Coatings Membr.* Elsevier Ltd, 2016, pp. 183–210, <https://doi.org/10.1016/B978-1-78242-283-9.00007-5>.
- [24] B. Yogyakarta, Mechanism of microencapsulation with urea-formaldehyde polymer rochmadi, Agus Prasetya and wahyu hasokowati department of chemical engineering, faculty of engineering, Am. J. Appl. Sci. 7 (2010) 739–745.
- [25] H. Ullah, K. Azizi, Z.B. Man, M.B. Che, Synthesis and characterization of urea-formaldehyde microcapsules containing functionalized polydimethylsiloxanes, *Procedia Eng.* 148 (2016) 168–175, <https://doi.org/10.1016/j.proeng.2016.06.519>.
- [26] H.H. Noh, J.K. Lee, Microencapsulation of self-healing agents containing a fluorescent dye, *Express Polym. Lett.* 7 (2013) 88–94, <https://doi.org/10.3144/expresspolymlett.2013.8>.
- [27] A. Khan, F. Ubaid, E. Fayyad, Z. Ahmad, P. Abdul Shakoor, F. Montemor, R. Kahruman, S. Mansour, M. Hassan, A. Hasan, A. Abdullah, Synthesis and properties of polyelectrolyte multilayered microcapsules reinforced smart coatings, *J. Mater. Sci.* 54 (2019) 12079–12094, <https://doi.org/10.1007/s10853-019-03761-9>.
- [28] S.H. Sonawane, B.A. Bhanvase, A.A. Jamali, S.K. Dubey, S.S. Kale, D.V. Pinjari, R.D. Kulkarni, P.R. Gogate, A.B. Pandit, Improved active anticorrosion coatings using layer-by-layer assembled ZnO nanocontainers with benzotriazole, *Chem. Eng. J.* 189–190 (2012) 464–472, <https://doi.org/10.1016/j.cej.2012.02.076>.
- [29] C. Tan, M.J. Selig, M.C. Lee, A. Abbaspourrad, Polyelectrolyte microcapsules built on CaCO₃ scaffolds for the integration, encapsulation, and controlled release of copigmented anthocyanins, *Food Chem.* 246 (2018) 305–312, <https://doi.org/10.1016/j.foodchem.2017.11.033>.
- [30] X. Liu, C. Gu, Z. Wen, B. Hou, Improvement of active corrosion protection of carbon steel by water-based epoxy coating with smart CeO₂ nanocontainers, *Prog. Org. Coat.* 115 (2018) 195–204, <https://doi.org/10.1016/j.porgcoat.2017.10.015>.
- [31] D. Abrantes, I.C. Riegel-vidotti, M. Guerreiro, S. Ferreira, C. Eliana, B. Marino, Smart coating based on double stimuli-responsive microcapsules containing linseed oil and benzotriazole for active corrosion protection, *Corros. Sci.* 130 (2018) 56–63, <https://doi.org/10.1016/j.corsci.2017.10.009>.
- [32] I. Dehri, M. Erbil, Organic sulphur-containing compounds as corrosion inhibitors for mild steel in acidic media: correlation between inhibition efficiency and chemical structure, *Appl. Surf. Sci.* 236 (2004) 155–164, <https://doi.org/10.1016/j.apsusc.2004.04.017>.
- [33] S.P. Sanghvi, J.G. Nair, Effect of viscosity and interfacial tension on particle size of cellulose acetate trimellitate microspheres, *J. Microencapsul.* 9 (1991) 215–227, <https://doi.org/10.3109/02652049109021238>.
- [34] D.G. Shchukin, M. Zheludkevich, K. Yasakau, S. Lamaka, M.G.S. Ferreira, H. Möhwald, Layer-by-layer assembled nanocontainers for self-healing corrosion protection, *Adv. Mater.* 18 (2006) 1672–1678, <https://doi.org/10.1002/adma.200502053>.
- [35] G. Kurt Çömlekçi, S. Ulutan, Encapsulation of linseed oil and linseed oil based alkyl resin by urea formaldehyde shell for self-healing systems, *Prog. Org. Coat.* 121 (2018) 190–200, <https://doi.org/10.1016/j.porgcoat.2018.04.027>.
- [36] E.N. Brown, M.R. Kessler, N.R. Sottos, S.R. White, In situ poly(urea-formaldehyde) microencapsulation of dicyclopentadiene, *J. Microencapsul.* 20 (2003) 719–730, <https://doi.org/10.1080/0265204031000154160>.
- [37] M.M. De Villiers, D.P. Otto, S.J. Strydom, Y.M. Lvov, Introduction to nanocoatings produced by layer-by-layer (LbL) self-assembly, *Adv. Drug Deliv. Rev.* 63 (2011) 701–715, <https://doi.org/10.1016/j.addr.2011.05.011>.
- [38] Y. Shi, R.A. Weiss, Sulfonated poly(ether ether ketone) ionomers and their high temperature shape memory behavior, *Macromolecules* 47 (2014) 1732–1740, <https://doi.org/10.1021/ma500119k>.
- [39] A. Samara, A.M. Abdullah, K.A. Mahmood, Controlling the biocorrosion of sulfate-reducing Bacteria (SRB) on carbon steel using ZnO/Chitosan nanocomposite as an eco-friendly biocide, *Corros. Sci.* 148 (2018) 397–406, <https://doi.org/10.1016/j.corsci.2018.12.028>.
- [40] M.H. Silem, M. Arifi, A.B. Radwan, E.M. Fayyad, M.F. Shibl, F.E. Heskal, M.A. Aboubakar, AEO7 surfactant as an eco-friendly corrosion inhibitor for carbon steel in HCl solution, *Sci. Rep.* 9 (2019) 1–16.
- [41] E. Wang, Wei Xu, Likun Li, Xiangbo Yang, Yi An, Self-healing properties of protective coatings containing isophorone diisocyanate microcapsules on carbon steel surfaces, *Corros. Sci. Sci.* 80 (2014) 528–535.
- [42] M.L. Zheludkevich, M.G.S. Ferreira, On the application of electrochemical impedance spectroscopy to study the self-healing properties of protective coatings, *Electrochem. Commun.* 9 (2007) 2622–2628, <https://doi.org/10.1016/j.elecom.2007.08.012>.
- [43] P.C. Okonkwo, M.H. Sliem, R.A. Shakoor, A.M.A. Mohamed, A.M. Abdullah, Effect of temperature on the corrosion behavior of API X120 pipeline steel in H₂S environment, *J. Mater. Eng. Perform.* 26 (2017) 3775–3783, <https://doi.org/10.1007/s11665-017-2834-0>.
- [44] M. Behzadnasab, S.M. Mirabedini, M. Esfandeh, R.R. Farnood, Progress in Organic Coatings Evaluation of corrosion performance of a self-healing epoxy-based coating containing linseed oil-filled microcapsules via electrochemical impedance spectroscopy, *Prog. Org. Coat.* 105 (2017) 212–224, <https://doi.org/10.1016/j.porgcoat.2017.01.006>.
- [45] F. Kuang, T. Shi, J. Wang, F. Jia, Microencapsulation technology for thiourea corrosion inhibitor, *J. Solid State Electrochem.* (2009) 1729–1735, <https://doi.org/10.1007/s10008-009-0803-8>.